Reference copy

USCG-74-5

REPORT NO. CG-D-86-75
TASK NO.4204.2/3

THE DEVELOPMENT OF AN EXPERIMENTAL AIRBORNE LASER REMOTE SENSOR FOR OIL DETECTION AND CLASSIFICATION IN SPILLS

J. F. Fantasia
H. C. Ingrao

FEBRUARY 1975
FINAL REPORT

Prepared for
U.S. DEPARTMENT OF TRANSPORTATION
UNITED STATES COAST GUARD
OFFICE OF RESEARCH AND DEVELOPMENT
Washington DC 20590

Technical Report Documentation Page

1. Report No.	2. Government Accession No.	3. Recipient's Catalog No.
CG-D-86-75		

4. Title and Subtitle	5. Report Date
THE DEVELOPMENT OF AN EXPERIMENTAL AIRBORNE LASER REMOTE SENSOR FOR OIL DETECTION AND CLASSIFICATION IN SPILLS	February 1975
	6. Performing Organization Code
	8. Performing Organization Report No. DOT-TSC-USCG-74-5
7. Author(s) John F. Fantasia, Hector C. Ingrao	
9. Performing Organization Name and Address U.S. Department of Transportation Transportation Systems Center Kendall Square Cambridge MA 02142	10. Work Unit No. (TRAIS) 4204.2/3
	11. Contract or Grant No. PPA NO. CG-03
	13. Type of Report and Period Covered Final Report
12. Sponsoring Agency Name and Address U.S. Department of Transportation United States Coast Guard Office of Research and Development Washington DC 20590	14. Sponsoring Agency Code

15. Supplementary Notes

16. Abstract A study and measurements program to determine the feasibility of using laser-excited oil fluorescence as a means of detecting and classifying oils in spills in the marine environment was undertaken at the DOT/Transportation Systems Center. The study consisted of an analysis of the fluorescence properties of oils and oil slicks on the sea surface, and a theoretical analysis of the remote fluorometry of oil spills. As a result of this study a laboratory and field measurements program was undertaken. Laboratory measurements were made of 29 crude and refined oils commonly transported in the marine environment. These measurements included API gravity, fluorescence and reflectance spectra, fluorescence coefficient and fluorescence lifetimes. Similar measurements were made with a laboratory model of an N_2 laser oil spill remote sensor that was designed and built at TSC and installed at Point Allerton, Hull, Massachusetts. Results of these measurements showed that, under certain conditions, oil spill detection and classification can be made in the marine environment. A program was undertaken for further development of this technique. As part of the program the Experimental Remote Oil Detection and Classification (ERODAC) system was developed. After laboratory tests the ERODAC was field tested onboard a helicopter. The field tests showed that the ERODAC, under certain conditions, is capable of remotely detecting and classifying oils in spills.

17. Key Words	18. Distribution Statement
• Oil Spill • Remote Sensing Pollution • Fluorescense • Laser Application	DOCUMENT IS AVAILABLE TO THE PUBLIC THROUGH THE NATIONAL TECHNICAL INFORMATION SERVICE, SPRINGFIELD, VIRGINIA 22161

19. Security Classif. (of this report)	20. Security Classif. (of this page)	21. No. of Pages	22. Price
Unclassified	Unclassified	166	

Form DOT F 1700.7 (8-72) Reproduction of completed page authorized

PREFACE

This report documents the TSC program to develop an Experimental Remote Oil Detection and Clasification Sensor (ERODAC). The report deals with the oil fluoresence laboratory measurements, development of the ERODAC, and its field tests. Two appendices are attached to this report documenting the contributions of two contractors to this program, the Perkin-Elmer Corporation and the Charles Stark Draper Laboratory. Inclusion of these appendices was deemed justifiable because the work they document was reported only to TSC and did not have public dissemination.

This work was sponsored by the U.S. Coast Guard, Environmental and Transportation Technology Division, Pollution Prevention Projects Branch, 400 Seventh Street S.W., Washington, D.C., Lt. Allen Maurer, USCG Project Officer.

The optical-mechanical portion of the experimental airborne laser oil spill remote sensing system was designed and fabricated by the Perkin-Elmer Corporation of Norwalk, Connecticut, based on TSC specifications and under TSC Contract No. DOT-TSC-373. The Optical Multichannel Analyzer was designed and fabricated by the Charles Stark Draper Laboratory, based on TSC specifications and under TSC Contract No. DOT-TSC-350.

The two 3.4 kva converters were on loan from the National Aviation Facilities Experimental Center, Federal Aviation Administration, Atlantic City, N.J. Aircraft installation of the system was performed by the Naval Air Development Center (NADC), Engineering Design Division, Rotary Wing Branch, Warminister, Pennsylvania.

We are grateful to the following individuals supporting the project:

Dr. Thomas Hard, TSC, for his contribution in the early analysis, studies, laboratory measurements and field tests at Point Allerton, Massachusetts.

Mr Michael F. Cartwright, TSC, for his recommendations, guidance and review of the physical design of the system, especially regarding considerations on the system/aircraft interfaces and the operational environment.

Mr. Vincent Early, TSC, for his technical assistance in the laboratory and during the experimental model system flight tests.

Mr. Harry Ceccon and Dr. Horace W. Furomoto, TSC, for the basic design of the laboratory model Nitrogen laser.

Mr. Duncan H. Sprague, C.S. Draper Laboratories, for flight test assistance in the operation and maintenance of the Optical Multi-Channel Spectrum Analyzer.

Cmdr. D. Bennie, USN, and the flight crew of the NADC helicopter for their flight support. Also, the Sikorsky Aircraft Division team for their ground support, lead by Mr. Harry Stahlcup.

The Commanding Officers and crews of the USCG Cutters Cape Cross, Cape George and Cape Horn for their sea support.

We also wish to acknowledge the following commands and organizations for their support during the system field tests: U. S. Coast Guard Headquarters (overall program responsibility); Commander, U. S. Naval Air Development Center, Warminster PA (aircraft and support); Commander, First U. S. Coast Guard District (surface vessels and controlled oil spills); U. S. Coast Guard Research and Development Center, Groton CT (shipboard test observer); Commander, U. S. Naval Air Station, South Weymouth MA (base of operations).

TABLE OF CONTENTS

LIST OF ILLUSTRATIONS

LIST OF ILLUSTRATIONS (CONT'D)

LIST OF ILLUSTRATIONS (CONT'D)

LIST OF ILLUSTRATIONS (CONT'D)

LIST OF ILLUSTRATIONS (CONT'D)

LIST OF ILLUSTRATIONS (CONT'D)

LIST OF TABLES

SYMBOL DEFINITIONS AND UNITS

SYMBOL OR ABBREVIATION	UNIT OF TERM
a	ampere
Å	Angstrom
API	American Petroleum Institute
°C	degree Celsius
cm	centimeter
Hz	Hertz
km	kilometer
km h^{-1}	kilometer per hour
kva	kilovoltampere
l	liter
m	meter
ma	milliampere
mm	millimeter
mrad	milliradian
ms	millisecond
mv	millivolt
N_2	nitrogen
nm	nanometer
nm mm^{-1}	linear dispersion
ns	nanosecond
pps	pulse per second
t_f	fluorescence lifetime
torr	Torricelli
μs	microsecond
UV	ultraviolet
W	Watt
Δt	Laser pulsewidth
ε_0	fluorescence coefficient
λ_p	peak wavelength
λ_l	wavelength, laser

1. INTRODUCTION

There are many techniques for the remote sensing of oil spills in the marine environment, operating in different portions of the electromagnetic spectrum from the ultraviolet to the microwave region. These techniques have been implemented by either passive or active systems, represented by microwave radiometers, radar mappers, aerial photographic cameras, infrared thermographs and low light level television systems. All these systems can detect oil spills under a particular set of conditions (sea state, day or night, weather conditions, visibility) suited to each individual technique. However, none of these systems are able to adequately identify or classify the type of oil. To correct this deficiency an airborne remote sensing system based on laser stimulated oil fluorescence was developed at the U. S. Department of Transportation, Transportation Systems Center, Cambridge, Massachusetts.

1.1 OBJECTIVES

In July 1970 an Oil Spill Surveillance System program was undertaken at the U. S. Department of Transportation, Transportation Systems Center, Cambridge, Massachusetts at the request of the U. S. Coast Guard, Office of Research and Development.

The program had the following objectives:

- Determine the feasibility of using laser-excited oil fluorescence as a means of detecting and classifying oils in spills;
- Develop an experimental airborne laser remote sensor (ERODAC) for oil detection and classification of oils in spills;
- Install the experimental system in an aircraft and perform field tests in a marine environment.

1.2 TECHNICAL APPROACH

To accomplish the above objectives, a study and measurements program was undertaken. The study consisted of the analysis of the fluorescence emission properties of oil and oil slicks on the sea surface, and a theoretical analysis of the remote fluorometry of oil spills. As a result of this study, a measurements program was performed including laboratory and field measurements. Laboratory measurements were made of 29 crude and refined oils (see Table 1) commonly transported in the marine environment. These measurements included the American Petroleum Institute (API) gravity, fluorescence spectra, fluorescence coefficient and fluorescence lifetime of each sample. The values measured are given in Table 2, and shown in Figures 1 through 4.

Figure 1 gives the wavelengths of maximum fluorescence emission of the TSC oil samples as measured with a 128 response* photomultiplier tube. These wavelengths are indicated by vertical bars over the linear wavelength scale. Figure 2 presents the fluorescence coefficients of the TSC oil samples (on a logarithmic scale) versus their wavelength of maximum emission. The maximum wavelengths are measured with a 128 response photomultiplier tube; the excitation wavelength was 337 nm. Note that oils with high fluorescence coefficients emit at shorter wavelengths. The oils in Table 2 and Figures 2, 3 and 4 are designated by letters and a suffix. For proper identification of the oils see Table 1. Figure 3 gives the API gravity of the TSC oil samples versus wavelengths of fluorescence emission. The maximum wavelengths are as measured with a 128 response; the excitation wavelength was also 337 nm. We can observe that oils with lower API gravities exhibit spectra with peaks at longer wavelengths.

Figure 4 gives the fluorescence lifetime of the TSC oil samples versus wavelengths of peak fluorescence emission. For these measurements the excitation source was a pulsed N_2 laser (4 ns pulse width). The wavelengths are as measured with a 128 response photomultiplier tube. We can observe that oils with longer wavelength

*For details on the 128 response see "RCA Photo-multiplier Manual, Theory, Design and Application," RCA Technical Series PT-61. Harrison NJ, 07029

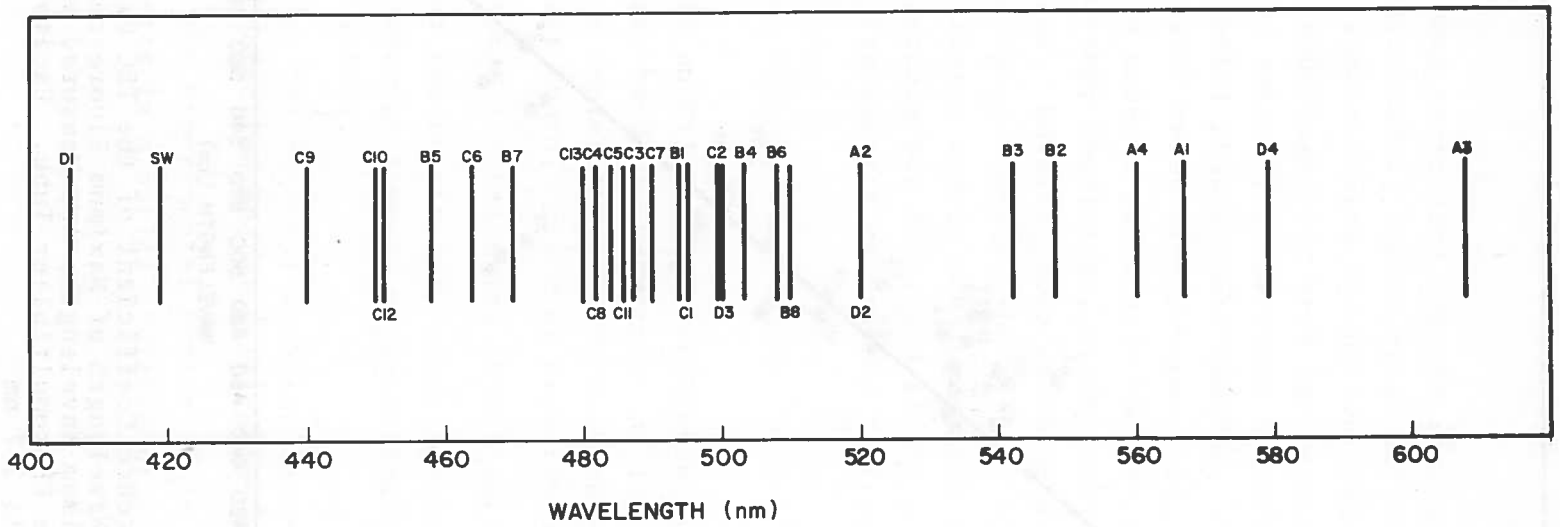

Figure 1. Wavelength of Maximum Fluorescence Emission of TSC Oil Samples as Measured with a 128 Response Photomultiplier Tube

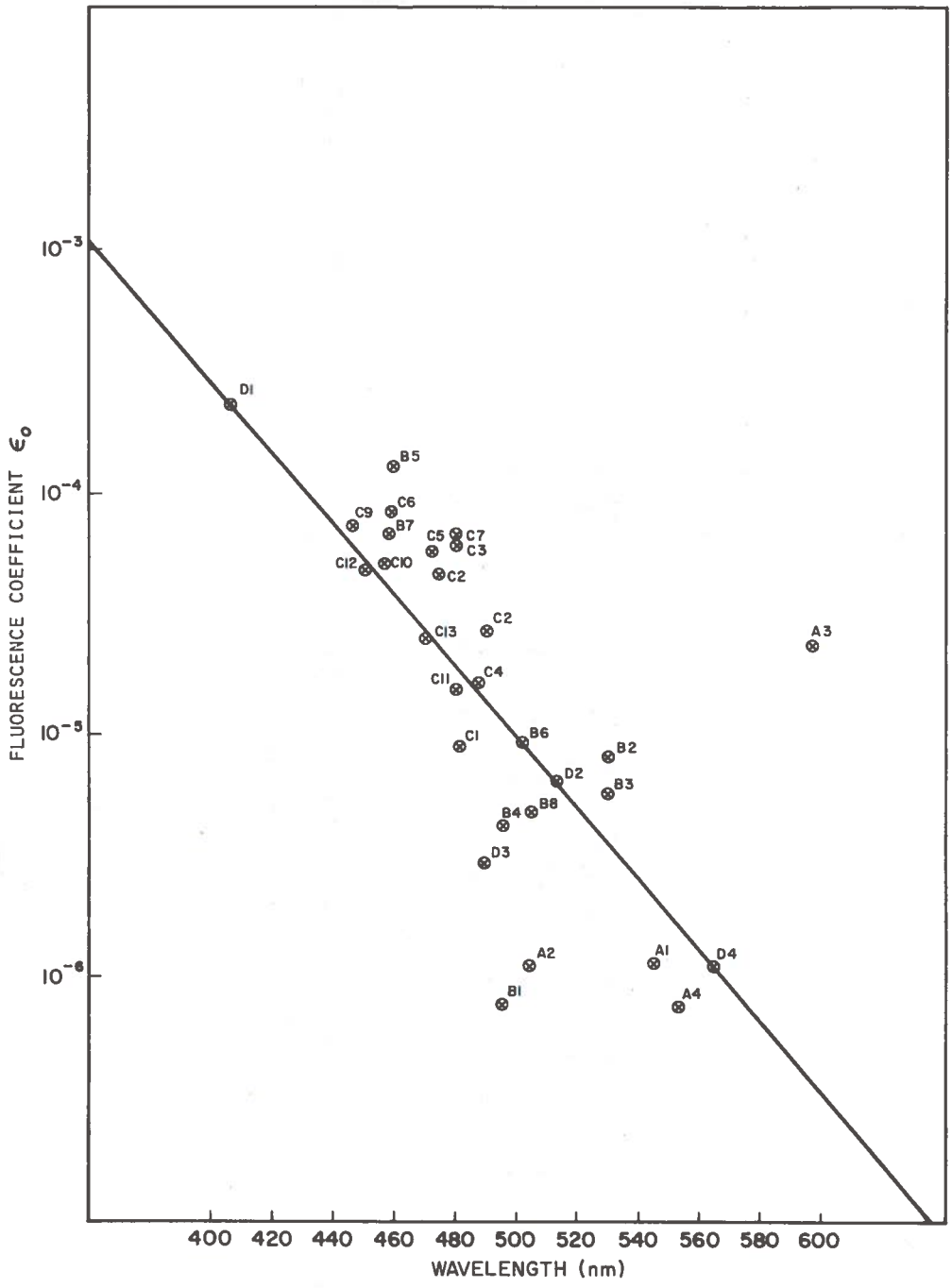

Figure 2. Fluorescence Coefficient of the TSC Oil Samples Versus Wavelength of Maximum Fluorescence Emission. The Maximum Wavelengths Are Measured with a 128 Response Photomultiplier Tube. Excitation Wavelength is 337 nm

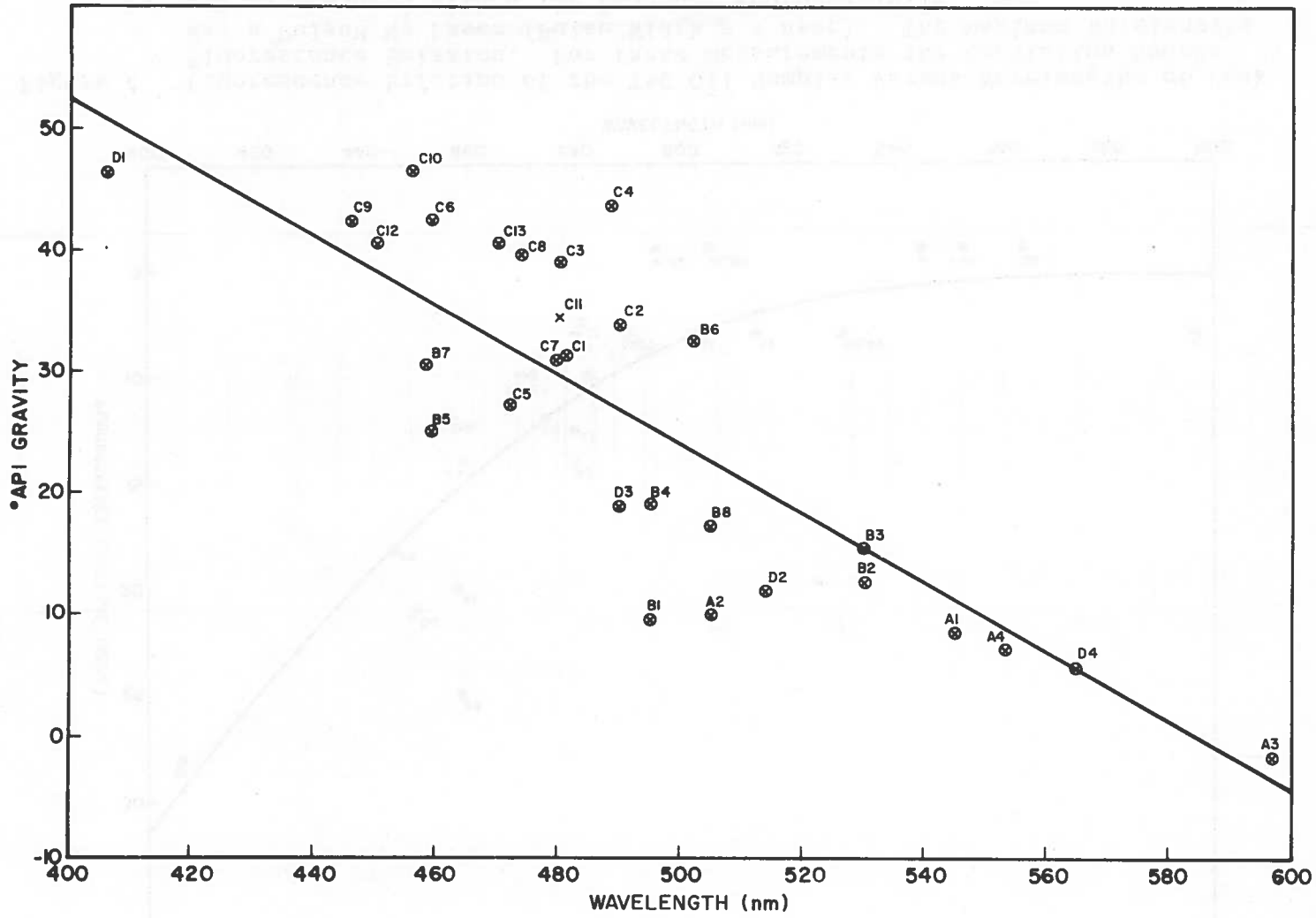

Figure 3. API Gravity of the TSC Oil Samples Versus Wavelength of Maximum Fluorescence Emission. The Maximum Wavelengths Are as Measured with a 128 Response Photomultiplier Tube. Excitation Wavelength is 337 nm.

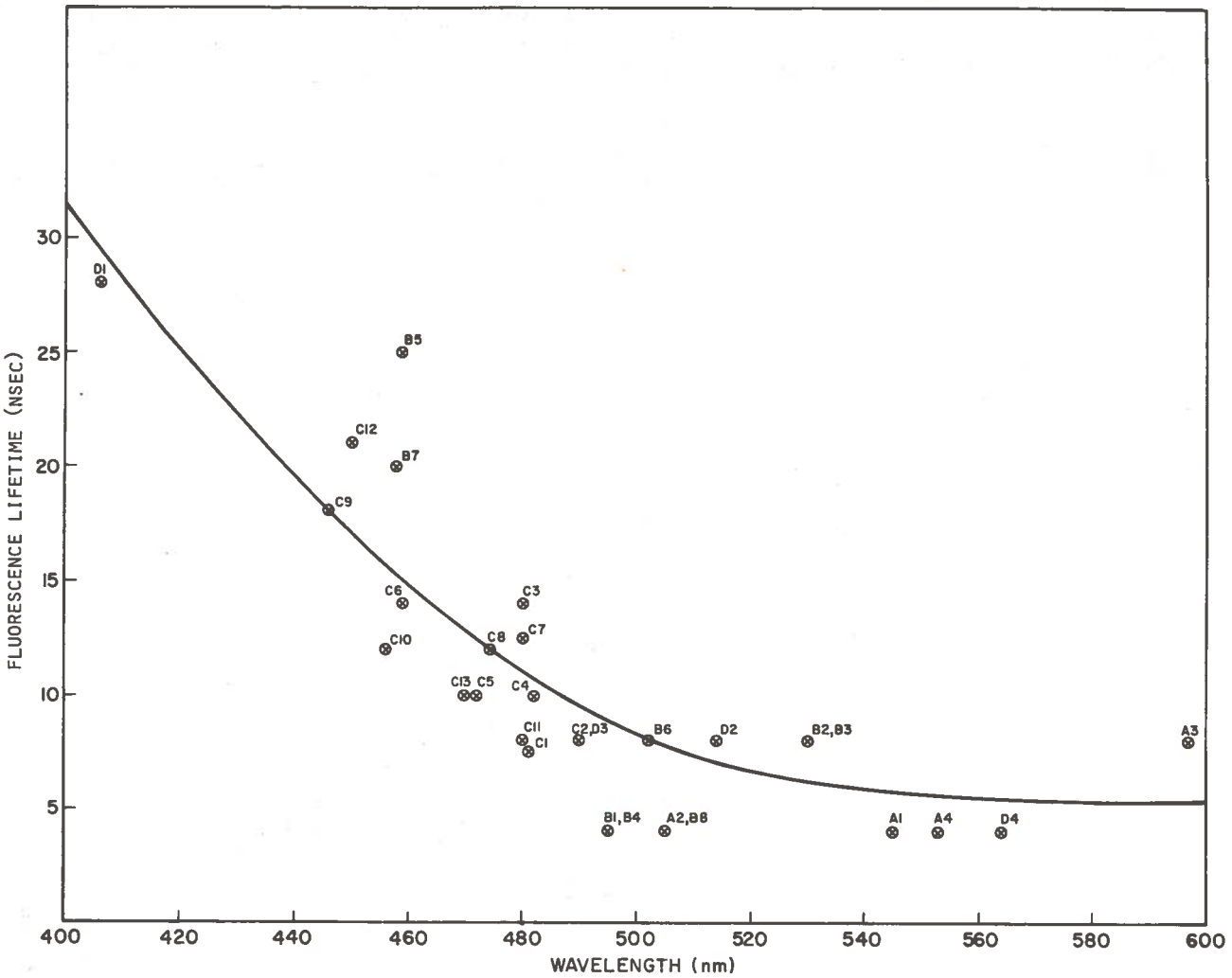

Figure 4. Fluorescence Lifetime of the TSC Oil Samples Versus Wavelengths of Peak Fluorescence Emission. For these Measurements the Excitation Source Was a Pulsed N_2 Laser (Pulse Width = 4 nsec). The Maximum Wavelengths are as measured with a 128 Response Photomultiplier Tube.

TABLE 1. CODING, DESCRIPTION, AND COMPANY SOURCE OF THE OIL SAMPLES USED AT TSC TO DETERMINE FEASIBILITY OF THE ERODAC

Sample A1 - Asphalt - ex Midcontinent crude flashed residual stock blended with Cutter Stock. Penetration Grade - 100/120 °API Gravity 8.7 Shell Oil Company	Sample B4 - Heavy Crude - Foreign - Lagunillas (Venezuela) - not refined - °API Gravity 19.2 Humble Oil & Refining Co.
Sample A2 - Asphalt - 180/2.00 Penetration Grade - °API Gravity 10.0 Chevron Oil Company	Sample B5 - Heavy Crude - Domestic - Jackson Miranda (Gulf Coast) - °API Gravity 25.0 Getty Oil Company
Sample A3 - Heavy Residuum (Delaware Refinery) - Bunker C - °API Gravity -1.7 Getty Oil Company	Sample B6 - Heavy Crude - Domestic - Hawkins (Texas) - not refined - °API Gravity 32.6 Humble Oil & Refining Co.
Sample A4 - Asphalt - Bayway Refinery - Virgin bottoms from vacuum distillation - Penetration Grade - 85/100 °API Gravity 7.2 Humble Oil & Refining Co.	Sample B7 - Heavy Crude - Domestic - Barbers Hill (Texas) - °API Gravity 30.3 Atlantic Richfield Company
Sample B1 - Heavy Crude - Foreign - °API Gravity 9.9 Chevron Oil Company	Sample B8 - Heavy Crude - Foreign - Lagunillas (Venezuela) - °API Gravity 17.4 Atlantic Richfield Company
Sample B2 - Heavy Crude - Domestic - Southern California - Asphaltic- °API Gravity 12.8 - not refined Shell Oil Company	Sample C1 - Light Crude - Foreign - Ceuta (Venezuela) - °API Gravity 31.3 Getty Oil Company
Sample B3 - Heavy Crude - Foreign -Guape (Trinidad) - °API Gravity 15.5 Getty Oil Company	Sample C2 - Light Crude - Domestic - West Texas Sour (Texas) - °API Gravity 33.9 Getty Oil Company
	Sample C3 - Light Crude - Foreign - Abu Dhabi (Persian Gulf) - not refined - °API Gravity 39.0 Shell Oil Company

TABLE 1. CODING, DESCRIPTION, AND COMPANY SOURCE OF THE OIL SAMPLES USED AT TSC TO DETERMINE FEASIBILITY OF THE ERODAC (CONTINUED)

Sample C4 - Light Crude - Domestic - Alabama - mixed base - not refined - °API Gravity 43.7 Shell Oil Company	Sample C11 - Light Crude - Foreign - °API Gravity 34.6 Chevron Oil Company
Sample C5 - Light Crude - Domestic - Perkins Crude - (Lake Charles, La.) - °API Gravity 27.1 Cities Service Oil Company	Sample C12 - Light Crude - Domestic - Southwest, Texas - °API Gravity 40.6 Atlantic Richfield Company
Sample C6 - Light Crude - Foreign - North Zeta (Venezuela) - not refined - °API Gravity 42.5 Humble Oil & Refining Co.	Sample C13 - Light Crude - Foreign - Zueitina (Libya) - °API Gravity 40.6 Atlantic Richfield Company
Sample C7 - Light Crude - Domestic - °API 31.0 Chevron Oil Company	Sample D1 - Refined Fuel Oil - Lake Arthur Condensate - °API Gravity 46.3 Cities Service Oil Company
Sample C8 - Light Crude - Domestic - North Texas - °API Gravity 39.9 Continental Oil Company	Sample D2 - Low Sulphur Fuel Oil (Bunker) - African Crude - Bottoms cut from atmospheric distillation - °API Gravity 10.2 Humble Oil & Refining Co.
Sample C9 - Light Crude - Domestic - Kingfisher (Oklahoma) - °API Gravity 42.3 Continental Oil Company	Sample D3 - Low Sulphur #6 Fuel Oil - °API Gravity 19.0 Chevron Oil Company
Sample C9 - Light Crude - Domestic - Kingfisher (Oklahoma) - °API Gravity 42.3 Continental Oil Company	Sample D4 - No. 6 Fuel Oil - Thermal cracked residual stock - ex Midcontinent - ° API Gravity 5.7 Shell Oil Company
Sample C10 - Light Crude - Domestic - Sweden (Texas) - not refined - °API Gravity 46.5 Humble Oil & Refining Co.	

TABLE 2. °API GRAVITY, WAVELENGTH OF MAXIMUM FLUORESCENCE EMISSION. FLUORESCENCE COEFFICIENT AND FLUORESCENCE LIFETIMES OF THE OIL SAMPLES ANALYZED AT TSC

TSC OIL SAMPLE*	°API GRAVITY	WAVELENGTH OF MAXIMUM FLUORSCENT EMISSION λ_p (nm)	FLUORESCENCE COEFFICIENT AT $\varepsilon_o \lambda p$ **	FLUORESCENT LIFETIME t_f (ns)***
A3	-1.7	597	$2.31X10^{-4}$	10
D4	5.7	565	$1.84X10^{-5}$	9
A4	7.2	553	$7.77X10^{-6}$	9
A1	8.7	545	$1.38X10^{-5}$	9
B1	9.9	495	$7.66X10^{-6}$	9
A2	10.0	505	$1.09X10^{-5}$	9
D2	10.2	514	$6.48X10^{-5}$	10
B2	12.8	530	$8.09X10^{-5}$	10
B3	17.4	505	$4.76X10^{-5}$	9
B8	15.5	530	$5.77X10^{-5}$	10
D3	19.0	490	$2.98X10^{-5}$	10
B4	19.2	495	$4.18X10^{-5}$	9
B5	25.0	459	$1.28X10^{-3}$	19
C5	27.1	472	$5.72X10^{-4}$	11
B7	30.3	458	$6.74X10^{-4}$	16
C7	31.0	480	$6.72X10^{-4}$	12
C1	31.3	481	$8.97X10^{-5}$	10
B6	32.6	502	$9.38X10^{-5}$	10
C2	33.9	490	$2.67X10^{-4}$	10
C11	34.6	480	$1.53X10^{-4}$	10
C3	39.0	480	$6.04X10^{-4}$	13
C8	39.9	474	$4.62X10^{-4}$	12
C12	40.6	450	$4.77X10^{-4}$	17
C13	40.6	470	$2.50X10^{-4}$	17
C9	42.3	446	$7.32X10^{-4}$	15
C6	42.5	459	$8.40X10^{-4}$	13
C4	43.7	487	$1.62X10^{-4}$	11
D1	46.3	406	$2.28X10^{-3}$	21
C10	46.5	456	$5.14X10^{-4}$	12

*See Table 1 for oil designations.

**ε_o is defined as the ratio of the fluorescent emission power in a 7 nm bandwidth, at the given wavelength, to the excitation power at 337 nm.

***Measurements using a pulsed N_2 - Laser (λ = 337 nm, pulse width = 4 nsec) as the excitation source.

maximum emission have lower lifetimes and are compatible with the laser pulse width. A synopsis of the above data shows a clear pattern. For heavy oils, such as the TSC samples A_1, A_4, and D_4 the peak fluorescence emission is toward the longer wavelengths; they have low fluorescence coefficients and short lifetimes. Similarly, for the medium and light weight oils the characteristic shift is opposite to that of the heavy oils. To demonstrate the feasibility of remote detection and classification of oils a laboratory model of a laser oil spill remote sensor was developed at TSC. A schematic of the laboratory system which, after in-house tests, was mounted in the dock house of the USCG Station at Point Allerton, Hull, Massachusetts is shown in Figure 5. By means of a flat mirror the field of view of the remote sensor was directed from the dock house to the water surface. An oil-slick retainer, consisting of a rubber inner tube supporting a stiff polyethylene cylinder, was placed in the water below the mirror. This arrangement was provided to contain the oil spill.

Figure 6 shows the fluorescence emission (amplitude) of sea water and a TSC oil sample (C_5). These two signals show the ability of the system to detect oil spilled in a sea environment under controlled conditions. Data similar to that shown in Figure 6 were obtained in the laboratory with the same remote sensor, using two bandpass filters with a band pass of 30 nm centered at 433 nm and 533 nm. The ratios of the fluorescence emission at these two wavelengths were obtained and are given in Table 3. Such a ratio is the simplest form of spectral comparison that can be made, yet it provided discrimination between different oils.

TABLE 3. REMOTE CLASSIFICATION OF OILS BY THE RATIO OF FLUORESCENT EMISSION AT TWO WAVELENGTHS

TSC OIL SAMPLE *	FLUORES EMISSION AT 433 nm TO FLUORES EMISSION AT 533 nm	OIL °API GRAVITY
B2	0.7	12.8
C5	1.1	27.1
B7	1.4	30.3
C9	1.7	42.3
D1	5.4	46.3

*See Table 1 for oil designations.

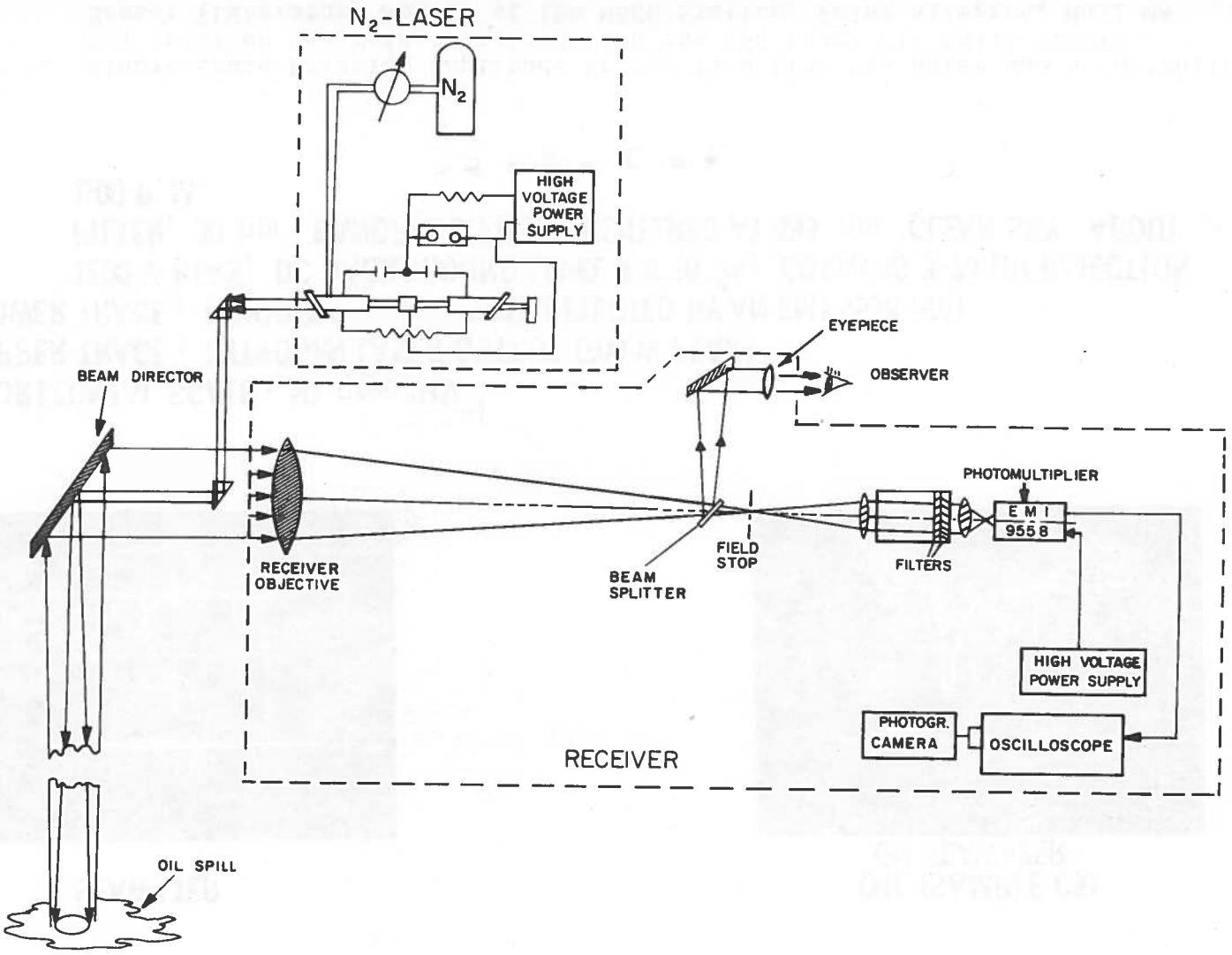

Figure 5. Schematic of the Laboratory Model of the TSC Laser Oil Spill Remote Sensor

FIELD EXPERIMENT, PT. ALLERTON USCG STATION, 11 MAY 1971

SEAWATER

OIL (SAMPLE C5)
ON SEAWATER

HORIZONTAL SCALE : 50 nsec DIV^{-1}
UPPER TRACE : NITROGEN LASER OUTPUT (700 W PEAK)
LOWER TRACE : FLUORESCENCE SIGNAL DETECTED BY AN EMI 9558 PMT
1200 V BIAS; DC BACKGROUND LEVEL 4 X 10^{-5}A; CORNING 3-74 UV REJECTION FILTER; 30 nm BANDPASS FILTER CENTERED AT 433 nm. CLEAR SKY, ABOUT 1:00 P.M.

Figure 6. Fluorescence Emission Amplitude Versus Time from Sea Water and a Controlled Oil Spill on Sea Water Obtained with the TSC Laser Oil Spill Remote Sensor (Laboratory Model) at the USCG Station, Point Allerton, Hull MA

2. EXPERIMENTAL AIRBORNE LASER REMOTE SENSOR FOR OIL DETECTION AND CLASSIFICATION (ERODAC)

2.1 DESIGN CRITERIA

Based on the results of our initial work on the remote fluorometry of oil spills, an analysis of airborne operational and environmental system requirements was performed. Out of this analysis and through consideration of hardware availability, a set of design criteria evolved. The criteria led to a preliminary system design and subsequently to the establishment of the subsystems specifications. On the basis of these specifications, procurements were carried out.

2.2 DESCRIPTION

The major subsystems are the optical transmitter, the optical receiver, the signal processor and display. The schematic of the ERODAC is given in Figure 7 and ERODAC characteristics are presented in Table 4.

2.2.1 Optical Transmitter

The optical transmitter consists of a N_2 laser, modulator, beam forming module, N_2 supply, vacuum pump, cooling system and power supply.

The laser is an AVCO Model C5000 (337.1 nm) emitting pulses 10 ns wide and at a rate of 500 pps. The cross section of the laser beam at the source is 0.32 cm by 5.1 cm. A beam forming module is used to reduce the full angle divergence to 1.3 mrad by 12.6 mrad. The beam forming module has a micrometer adjustment which permits shape adjustments within certain limits, but at the expense of laser output power. Laboratory tests of the laser beam forming system indicate that the beam divergence can be reduced to 12.6 mrad by 1.3 mrad with a 54% power loss, and to 3.5 mrad by 1.3 mrad with a 74% power loss. The laser uses a continuous flow of N_2 gas. A vacuum pump is used in conjunction with the bottled laser N_2 supply to initially purge the system of air and subsequently maintain

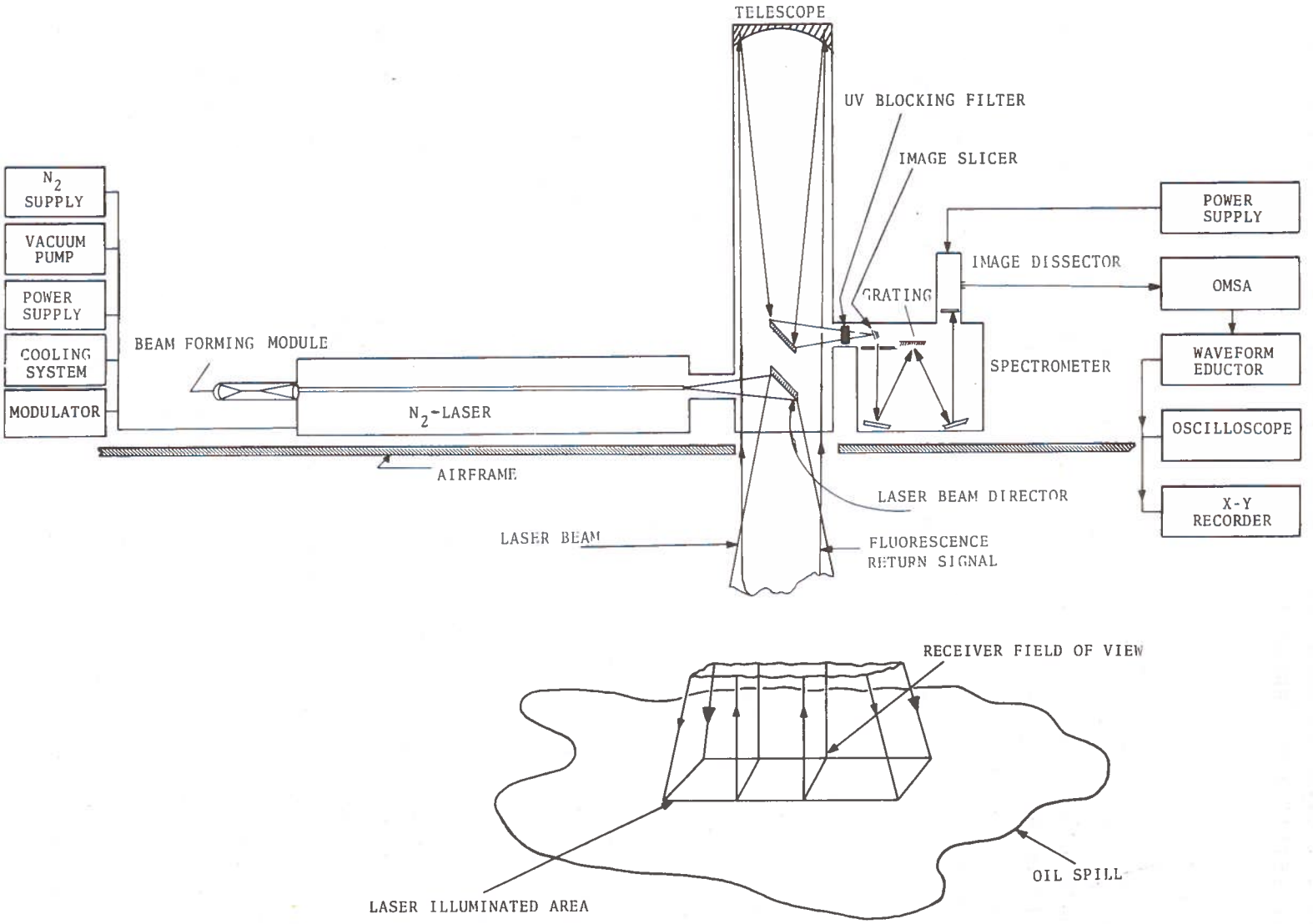

Figure 7. Schematic of the TSC Experimental Remote Oil Detection and Classification System (ERODAC) for the Detection and Classification of Oils in Spills

TABLE 4. ERODAC CHARACTERISTICS

SYSTEM

Transmitter

Laser	Pulsed N_2
Wavelength	337 nm
Pulsewidth	10 nsec
Peak Power	10^5 W
Repetition Rate	0 to 500 pps
Beam	
shape	rectangular
divergence	See Appendix A

Receiver (See Appendix A)

Telescope	Newtonian
Aperture	33 cm
f-number	4.7
Dispersive system	Ebert-Fastie
Grating blaze	450 nm
Linear dispersion	17.5 nm mm^{-1}
f-number	4.7
Bandwidth	10 nm
Detector type	image dissector
Spectral response	S-20
Spectral resolution	matched to spectrometer

TABLE 4. ERODAC CHARACTERISTICS (CONTINUED)

Signal Data Processing and Display (see Appendix B)

Signal Analyzer	Optical Multichannel Spectral Analyzer
Mode of operation	Detection and Classification
Data format	Fluorescence spectra
Spectra scan time	70 ms
Number of Spectral channels	35
Channel width	10 nm
Display	Oscilloscope/Photographic Camera X-Y recorder

a N_2 flow at 17 torr. A circulating mixture of glycol and water from a refrigerated cooling unit (Electro-Impulse Model RU-75LT) maintains a laser temperature of 4° C. Power for the laser is derived from a high voltage a.c. to d.c. power converter. Operating between 8 and 9kv, the laser requires 90 to 100 ma.

The laser output is directed down onto an area of the sea surface directly below the aircraft by means of several 45° flat dielectrically coated mirrors.

2.2.2 Optical Receiver

The optical receiver consists of a telescope, UV blocking filter, image slicer, spectrometer and image dissector. The telescope, with a Newtonian configuration, has a 33 cm clear aperture primary mirror and a 13 by 18 cm 45° secondary mirror. The focal length is 156 cm and the aperture ratio is f/4.7. A UV blocking filter is normally used at the output of the telescope to block the emitted laser pulse from being back-reflected into the spectrometer. However, with the blocking filter removed, the system can be calibrated for wavelength and range by measuring the laser pulse return in the second order at 674.2 nm.

The telescope is coupled to the spectrometer through an image slicer which is used to enhance the throughput of the system. The slicer consists of three front surfaced mirrors which are uniquely mounted to transpose an essentially square image into one long narrow strip of equal area matching the entrance slit of the spectrometer.

The spectrometer is an Ebert-Fastie type, and has a wavelength range of 350.0 to 700 nm in the first order. A replica gating of 295 grooves per mm blazed for 450.0 nm gives a reciprocal linear dispersion of 17.5 nm mm^{-1}. With this dispersion the 350 nm range subtends 20 mm at the output of the spectrometer. The calculated spectral bandwidth per channel is 10 nm at 450 nm with a 0.57 mm entrance slit width. The aperture ratio is f/4.7 matching the receiver telescope.

2.2.3 Signal Processor and Display

The signal processing and display unit consists of the image dissector (mounted at the output of the spectrometer), the Optical Multi-channel Spectral Analyzer (OMSA) (for details, see Appendix B) which includes the drive and control circuits for the image dissector, a waveform eductor, dual trace oscilloscope and X-Y recorder. The image dissector scans the spectral image produced by the spectrometer and the optical multi-channel analyzer processes the content of the image into a usable form for display and/or computer analysis. A basic guideline in designing the OMSA was the provision of maximum flexibility in gain, range gate width, detection channels, detection thresholds, etc. Operating and monitoring controls for these variables are provided.

The output of the spectrometer is focused onto the photocathode of an image dissector (ITT Model F4011RP) with an S-20 spectral response. It has ten stages of electron multiplication and is magnetically focused and deflected. The dissector has an aperture slit 6 mm by 0.57 mm resulting in a spectral bandpass of 10 nm. The amplified signal received from the image dissector is first converted into digital form for ease of handling. All the manipulations of the signal, i.e., noise subtraction, averaging, etc., are done in digital form. After the processing is complete, the digital signal is reconverted into analogue form and provided as an output. Digital outputs are also available. The analogue signal is fed to a waveform eductor (PAR Model TDH-9/99) where it is averaged to enhance the signal-to-noise ratio before being displayed or recorded. The associated noise is reduced by signal averaging.

The output of the waveform eductor is displayed on a dual channel oscilloscope (Tektronix Model R475) as a fluorescence spectrum with vertical displacement representing amplitude and horizontal displacement representing wavelength. The spectra are recorded by a camera (Tektronic Oscilloscope Model C30-AP) and/or an X-Y recorder (Hewlett Packard Model 2D-2).

2.2.4 Power Converters and Nitrogen Supply

The system configuration used during the laboratory tests differs from that which was flown, mainly in the addition of two 400 to 60 H_z power conversion units to facilitate operation from the aircraft 400 Hz supply. In the laboratory all a.c. power requirements at 60 Hz were satisfied from the line. Nitrogen at all times was provided from a standard cylinder.

2.3 THEORY OF OPERATION

The ERODAC operates in any of three selected modes: calibration, detection and classification. The principle of operation of these three modes may be followed by referring to the Appendix B. The operating modes discussed herein presume an overall preinstallation system alignment and calibration, and describe the normal sequence of operations for each successive mission.

2.3.1 Calibration Mode

The calibration function is executed prior to detection and classification to identify any change in performance of the system.

The calibration function makes it possible to determine that reasonable levels of transmitted and received signals are available, and that the spectrometer to image dissector interface has not been physically or electronically deregistered.

Wavelength calibration is effected by the observation of the second order (674.2 nm) N_2 Laser line. The ERODAC is capable of observing a wavelength spectrum from 350 nm to 700 nm. The ERODAC spectral image dissector divides the spectrum into 35 channels, each 10 nm wide. In the operational calibration mode, only one of the channels is of interest and this is dialed in on the console "band selector" by the operator. The image dissector tube electromagnetic deflection circuits are driven to a location corresponding to where the received spectral image should be.

When the laser is transmitting and the second order is detected and processed, it should appear as an "amplitude" readout on the fluorescence meter located on the OMSA front panel. The signal

level should then be peaked for maximum amplitude by adjusting the horizontal beam deflection positioning controls located at the rear of the image dissector housing. The indicated signal level, peaked as described, should result in an optimum calibration, and the system is ready to perform the detection function.

2.3.2 Detection Mode

The ERODAC first measures the stimulated laser fluorescence of the water without an oil spill. Two of the thirty channels are selected and identified as Channel A and Channel B (a channel is a spectral resolution element). (See Figure 8.) Threshold level is then obtained as follows: The ERODAC selects Channel A. When the channel is selected, the laser is commanded to fire and the ERODAC follows a time sequence (see Appendix B, Figure B-5). At a time determined by the distance to the target a range gate is opened for 500 nsec. The output of the range gate contains background noise plus any fluorescence stimulated by the laser energy striking the target. The peak amplitude of this signal plus noise is detected and held in a peak detector and hold circuit, where an analog to digital conversion is done on the contents and the result is stored. Again the range gate is opened for 500 nsec, and a sample of the background noise is taken. This noise is detected and also held in the peak detector and hold circuit for the analog to digital conversion. The noise is now subtracted from the signal plus noise, detected on the first opening of the range gate, and the difference stored as Channel A signal. Now the ERODAC selects Channel B and the laser is again fired with the above sequence repeated. The resulting information is stored as Channel B signal. This procedure is repeated and the digital representation of Channel A and B are accumulated in storage registers for a period of time and an average of each register is determined and displayed to the operator. When the operator determines he has a representation of a clean water amplitude level, he will set these values plus some safety margin above the average thresholds for Channels A and B respectively. Subsequent laser pulses and signal processing follow the same sequence as above

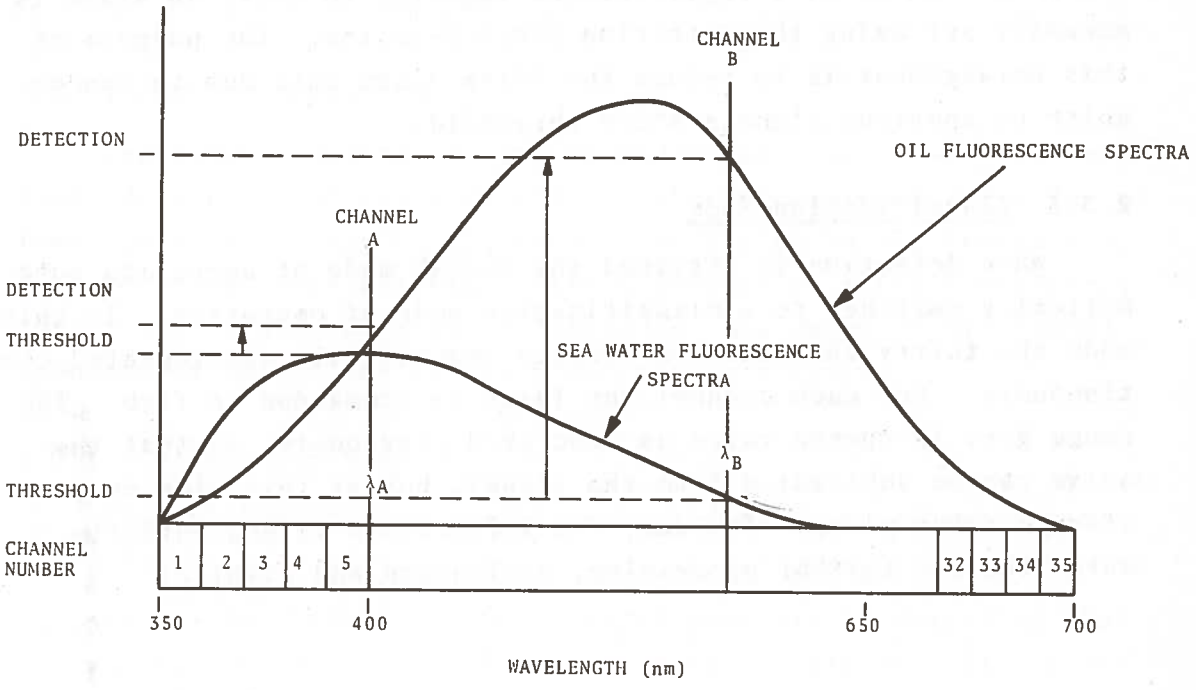

Figure 8. Representation of the Detection Mode of Signal Processing. Two of the 35 Signal Processing Channels, Designated A and B, and Corresponding to λ_A and λ_B, are First Calibrated for Sea Water Fluorescence. The Calibration Establishes the Threshold Levels. Oil Spill "Detection" Occurs When the Signal Level in Both Channels Exceeds the Thresholds a Predetermined Number of Times.

except that the digital representations of the signals are not stored but compared to their respective thresholds. If the difference exceeds the threshold, a register is incremented by one. If a pre-programmed number of consecutive registrations is exceeded from either Channel A or Channel B, it is possible that an oil spill has been detected and an alarm is generated. The number of consecutive registrations required to cause an alarm is manually set using the Detection Event Selector. The purpose of this arrangement is to reduce the false alarm rate due to random noise or spurious signals above threshold.

2.3.3 Classification Mode

When detection is obtained the ERODAC mode of operation automatically switches to a classification mode of operation. In this mode the thirty channels are stepped sequentially and repeated continuously. For each channel the laser is commanded to fire. The range gate is opened twice as described previously, so that the noise can be subtracted from the signal, but at this time no storage takes place. Instead, the information is sequentially outputted for further processing, evaluation and display.

3. ERODAC LABORATORY TESTING

The final phase in the development of the ERODAC included the assembly, integration, checkout and laboratory testing of the various system components previously described. This was accomplished at TSC in the Vertical Optical Test Facility (VOTF), a large silo type structure (9m in diameter by 18m in height) originally constructed for large astronomical mirror development (NASA-ERC). This development phase facilitated familiarization with the operation of the ERODAC under simulated altitude conditions, calibration of the system, acquisition of oil sample signatures and specifications of interfaces for aircraft installation.

3.1 LABORATORY INSTALLATION

There were three basic requirements that had to be satisfied in a facility adequate to accomplish the final development phase: a controlled environment free of atmospheric obscuration, a sufficiently long simulated altitude signal path length, and control of background illumination (day/night). The conveniences of access to power, shop facilities and ancillary instrumentation to implement operations, maintenance and modifications normal to an experimental model system development were also invaluable. The VOTF satisfied these requirements. The experiment was configured as shown in Figure 9 and is described in detail as follows: A wood-frame structure was built as a platform for mounting the system above an existing floor well (1.5m deep by 4.5m in diameter) where the oil samples being examined were placed in shallow stainless steel trays. The platform was constructed primarily to facilitate the mechanics of implementing the requirement for a long (38m) optical path between the down looking transmitter/receiver and the irradiated oil samples. A folded optical path system of mirrors was used to achieve the long path measurement. Short path (8m) measurements were made by removing one of the mirrors and viewing the samples in the well directly.

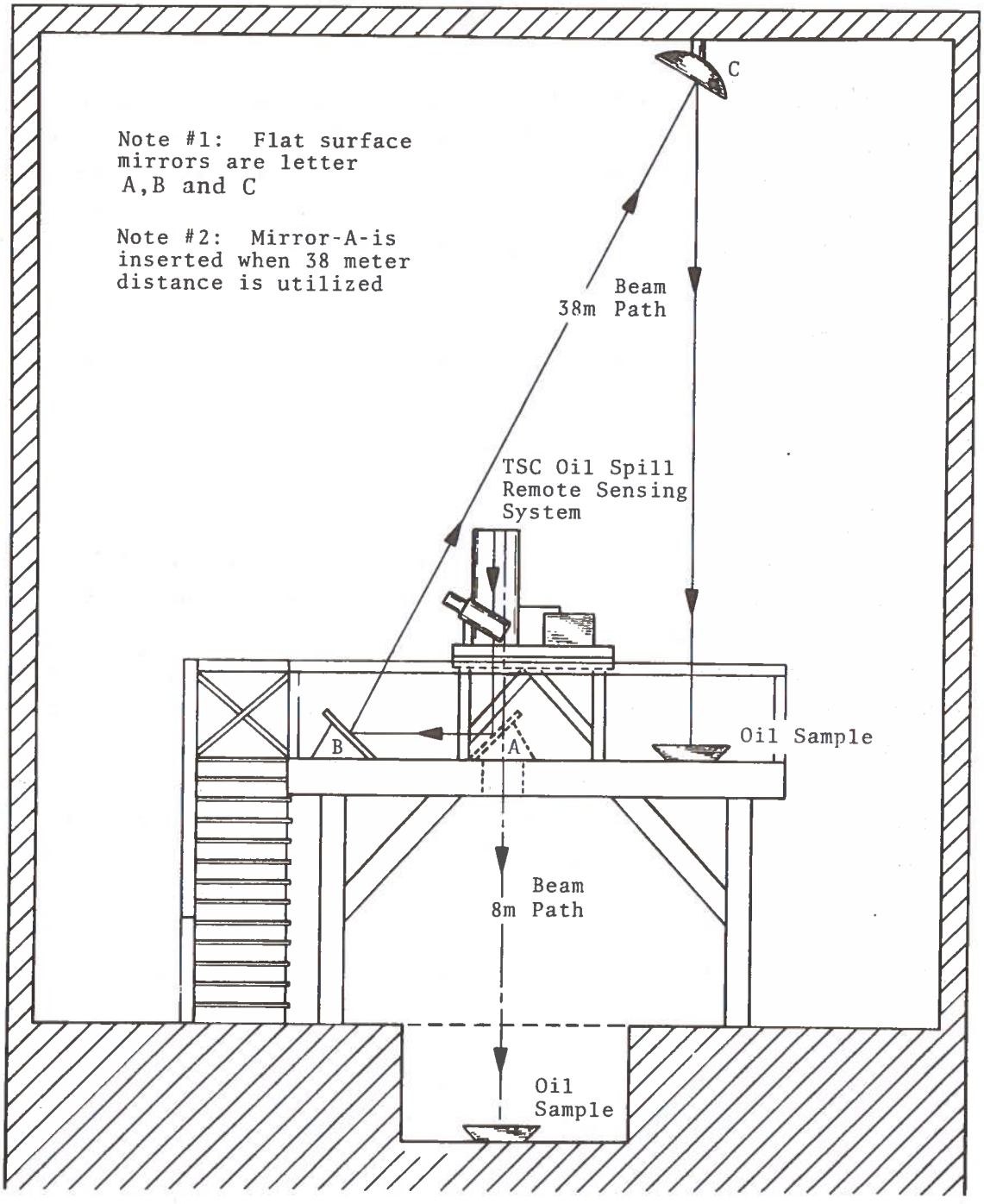

Figure 9. Schematic of the TSC Experimental Remote Oil Detection and Classification System (ERODAC), In-House Test Setup Used in the VOTF

3.2 TEST RESULTS

Fluorescence spectra* of twenty five of the twenty nine oil samples were measured by the system in the VOTF. The spectra of three of these oils were measured at two equivalent distances (8 and 38m). Figure 10 shows the normalized fluorescence spectra of heavy residuum (TSC classification A_3), °API - 1.7 obtained with the spectrophotofluorometer, with the ERODAC from an 8-meter and 38-meter distance. The spectra obtained with the spectrophotofluorometer is above those obtained with the ERODAC due to the usage of a 128 response in the spectrophotofluorometer photomultiplier tube and an S-20 response in the ERODAC.

Figures 11 and 12 show similar normalized fluorescence spectra for a heavy crude (TSC Classification B_5) °API: 25.0 and for a light crude (TSC Classification C_3), °API: 39.0.

The significance of these spectra is their close agreement with those obtained in the laboratory with the spectrophotofluorometer and the ERODAC. This proved the feasibility of obtaining the same fidelity in the spectral signatures with the ERODAC and with a laboratory type spectrophotofluorometer.

Also as part of the in-house system tests, measurements were conducted under both daytime (simulated) and nighttime conditions with no appreciable difference in the background noise level.

*Spectra obtained with the ERODAC did not preserve wavelength calibration to the same accuracy of the spectrophotofluorometer due to the usage of the waveform eductor. Therefore, to intercompare spectral signatures of the same oils obtained at different times by the ERODAC, the spectra has been shifted to make the maximums coincide.

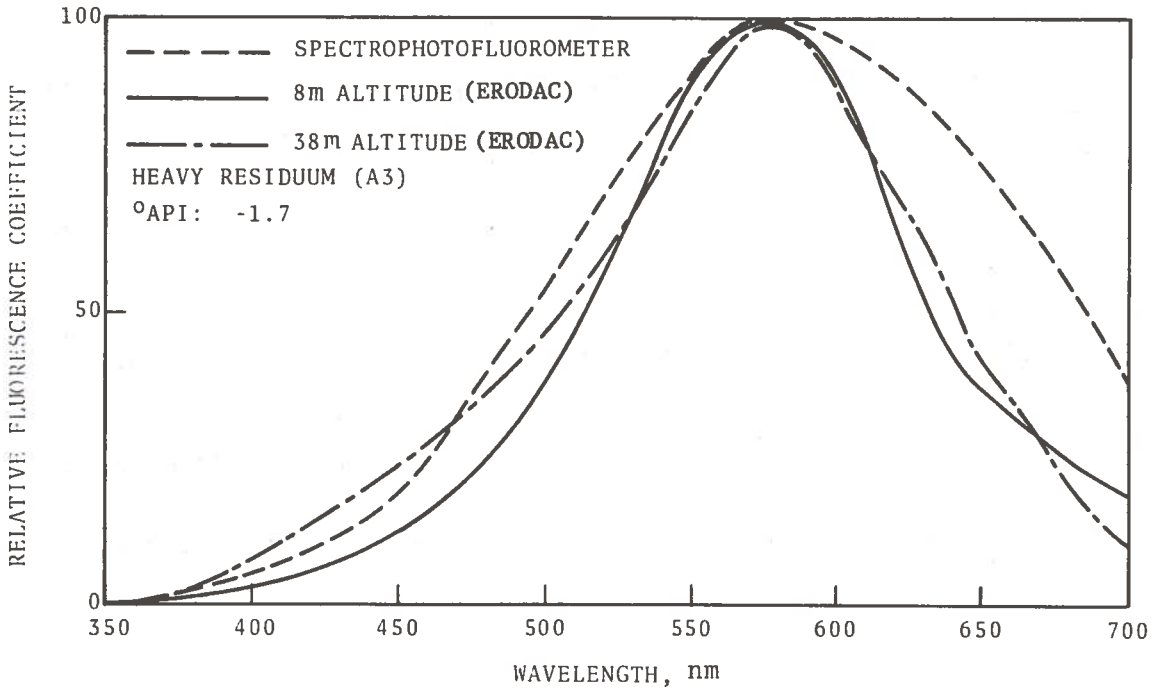

Figure 10. Normalized Fluorescence Spectra of Heavy Residuum (TSC Classification A_3)

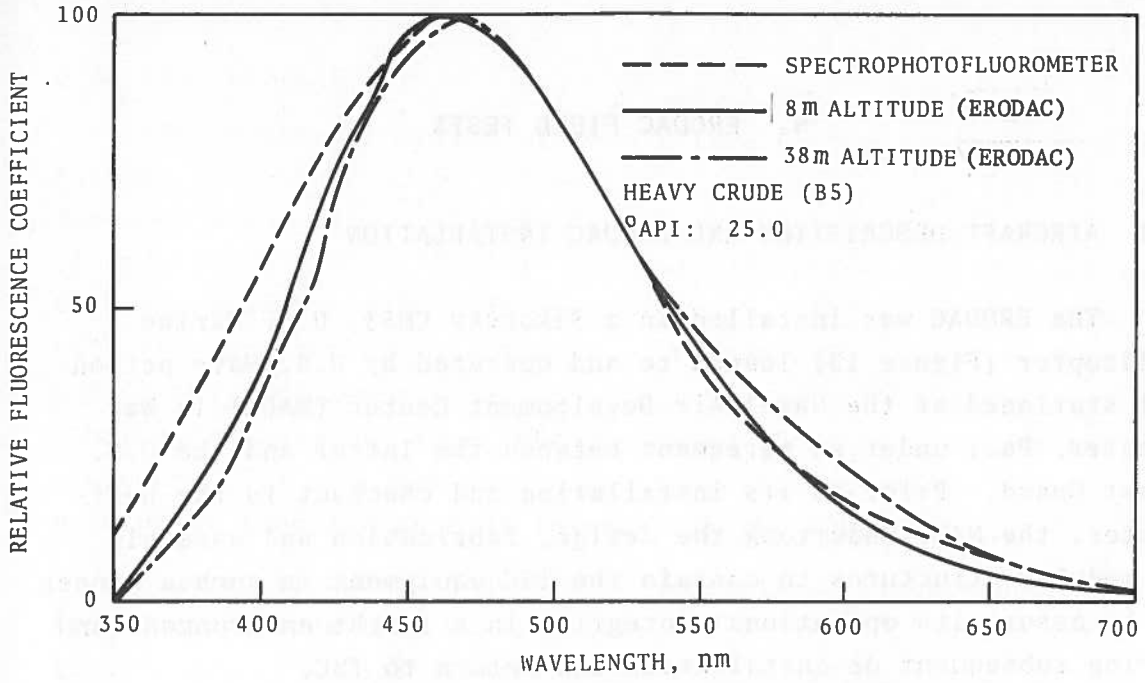

Figure 11. Normalized Fluorescence Spectra of Heavy Crude (TSC Classification B_5)

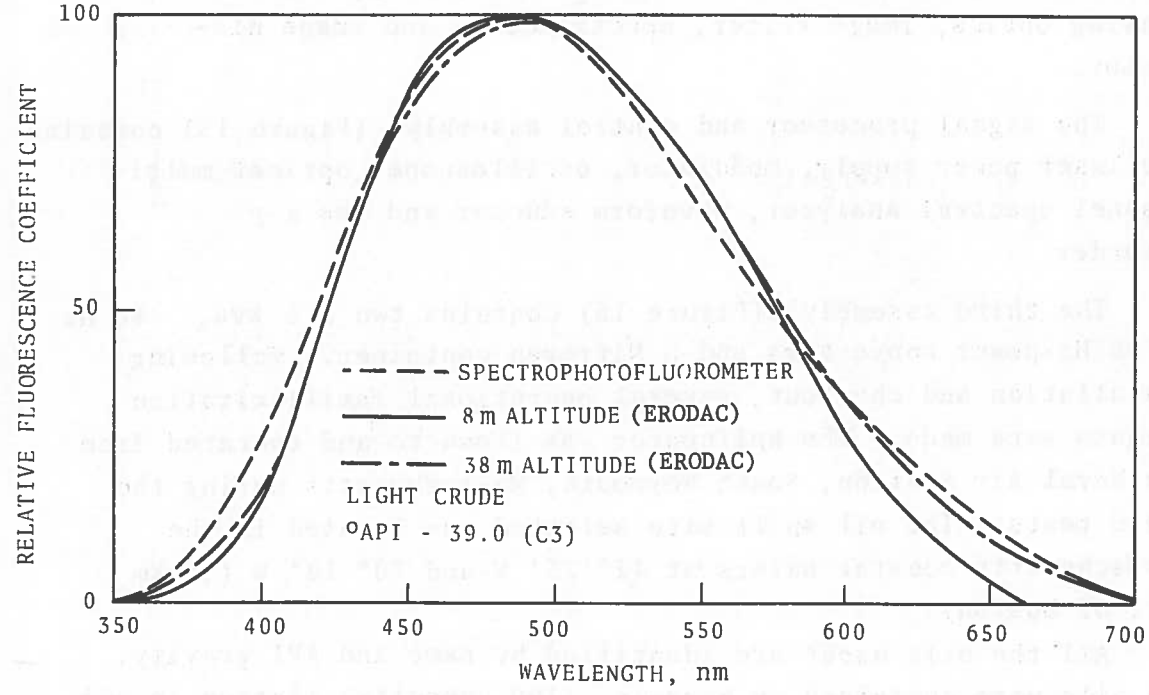

Figure 12. Normalized Fluorescence Spectra of Light Crude (TSC Classification C_3)

4. ERODAC FIELD TESTS

4.1 AIRCRAFT DESCRIPTION AND ERODAC INSTALLATION

The ERODAC was installed in a Sikorsky CH53, U.S. Marine helicopter (Figure 13) loaned to and operated by U.S. Navy personnel stationed at the Naval Air Development Center (NADC) in Warminster, Pa., under an agreement between the latter and the U.S. Coast Guard. Prior to its installation and checkout in the helicopter, the NADC undertook the design, fabrication and assembly of modular structures to contain the TSC equipment in such a manner as to assure its operational integrity in a flight environment and during subsequent de-installation and return to TSC.

The system was packaged in three major palletized assemblies, depicted in Figures 14, 15, and 16, and was powered through converters from the helicopter. The optical transmitter/receiver assembly (Figure 14) contains the N_2 laser, projection and receiving optics, image slicer, spectrometer, and image dissector.

The signal processor and control assembly, (Figure 15) contains the laser power supply, modulator, oscilloscope, optical multichannel spectral analyzer, waveform eductor and the x-y recorder.

The third assembly, (Figure 16) contains two 3.5 kva, 400 Hz to 60 Hz power converters and a Nitrogen container. Following installation and checkout, several operational familiarization flights were made. The helicopter was flown to and operated from the Naval Air Station, South Weymouth, Massachusetts during the field tests. The oil spill site selected was located in the Massachusetts coastal waters at 42° 25' N and 70° 10' W (84 km east of Boston).

All the oils used* are identified by name and API gravity. The oils were contained in barrels, (190 capacity) sixteen in all,

* All the oils used in these field tests were donated by the Exxon Corporation.

Figure 13. U.S. Marine Corps Helicopter, CH-53 Type, Used to Field Test the TSC Experimental Airborne Laser Oil Spill Remote Sensing System. This Helicopter is from the Naval Air Development Center (NADC), Warminster PA

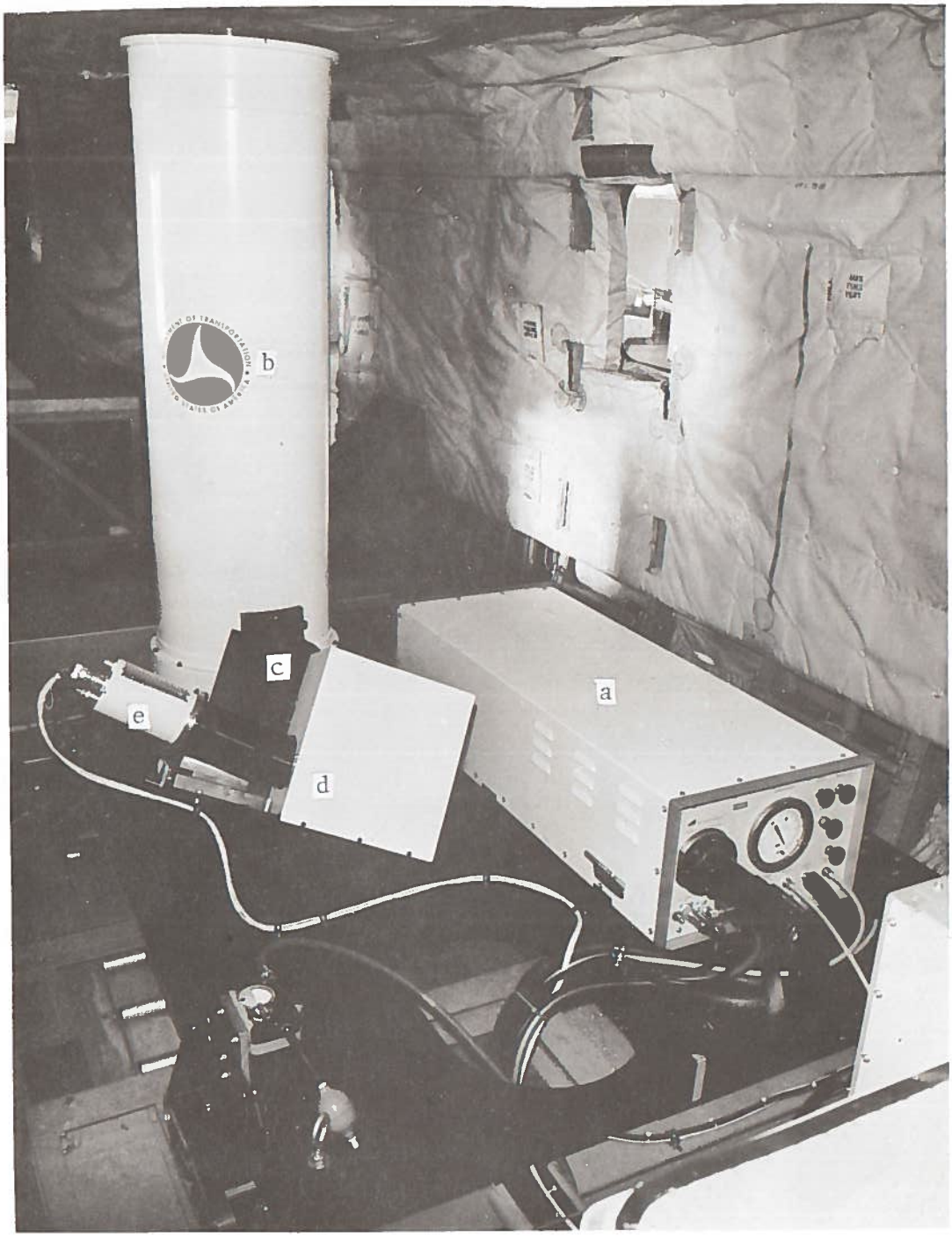

Figure 14. TSC Laser Remote Sensing System Mounted in Helicopter, Showing (a) Laser (b) Telescope (c) Image Slicer (d) Spectrometer and (e) Image Dissector

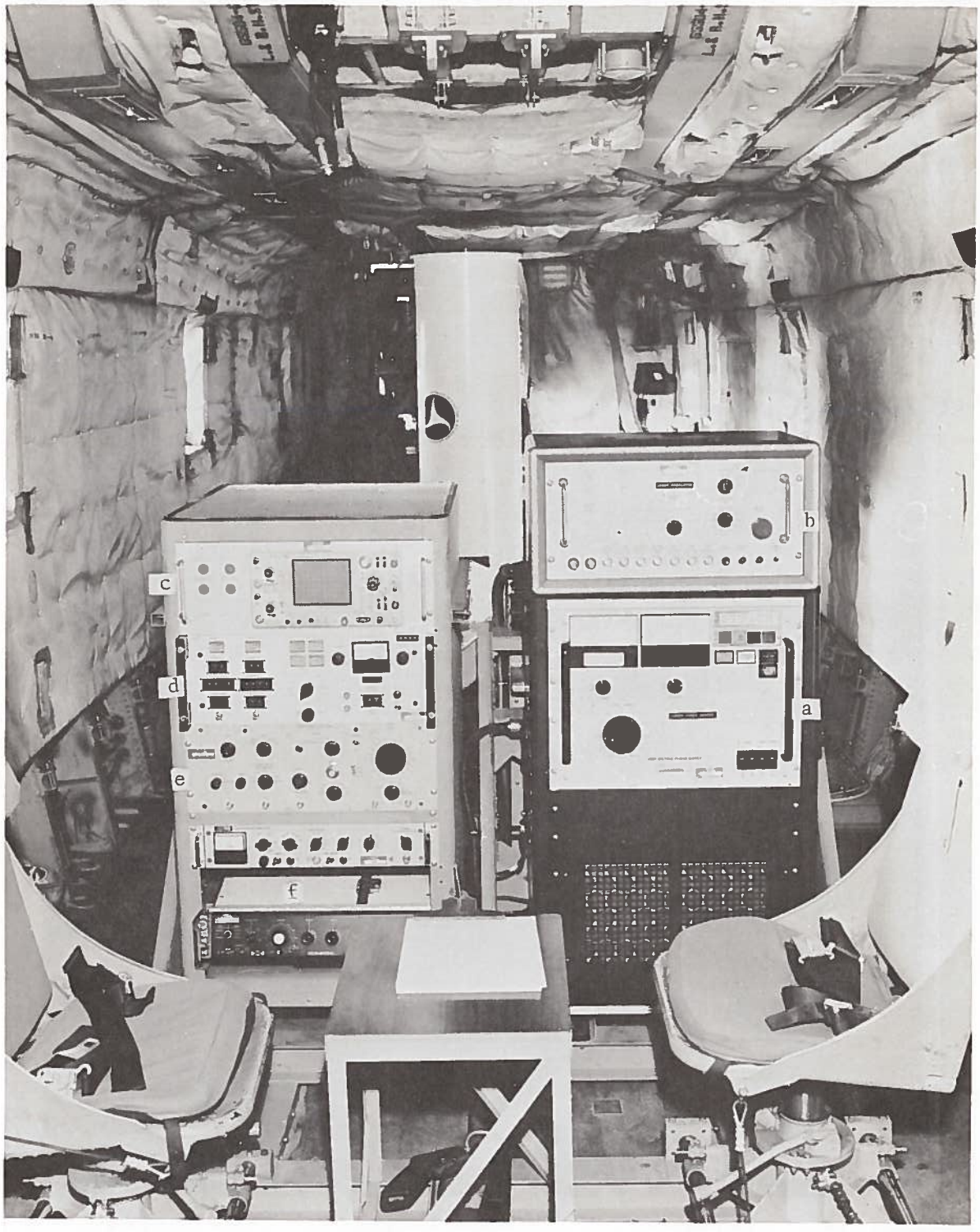

Figure 15. Power, Control and Processing Electronics of the TSC Airborne Laser Oil Spill Remote Sensing System. Systems Shown Include (a) Laser Power Supply (b) Modulator (c) Oscilloscope (d) Optical Multichannel Spectral Analyzer (e) Waveform Eductor and (f) X-Y Recorder. Eductor Output is Displayed on the Oscilloscope (c) and on the X-Y Recorder (f)

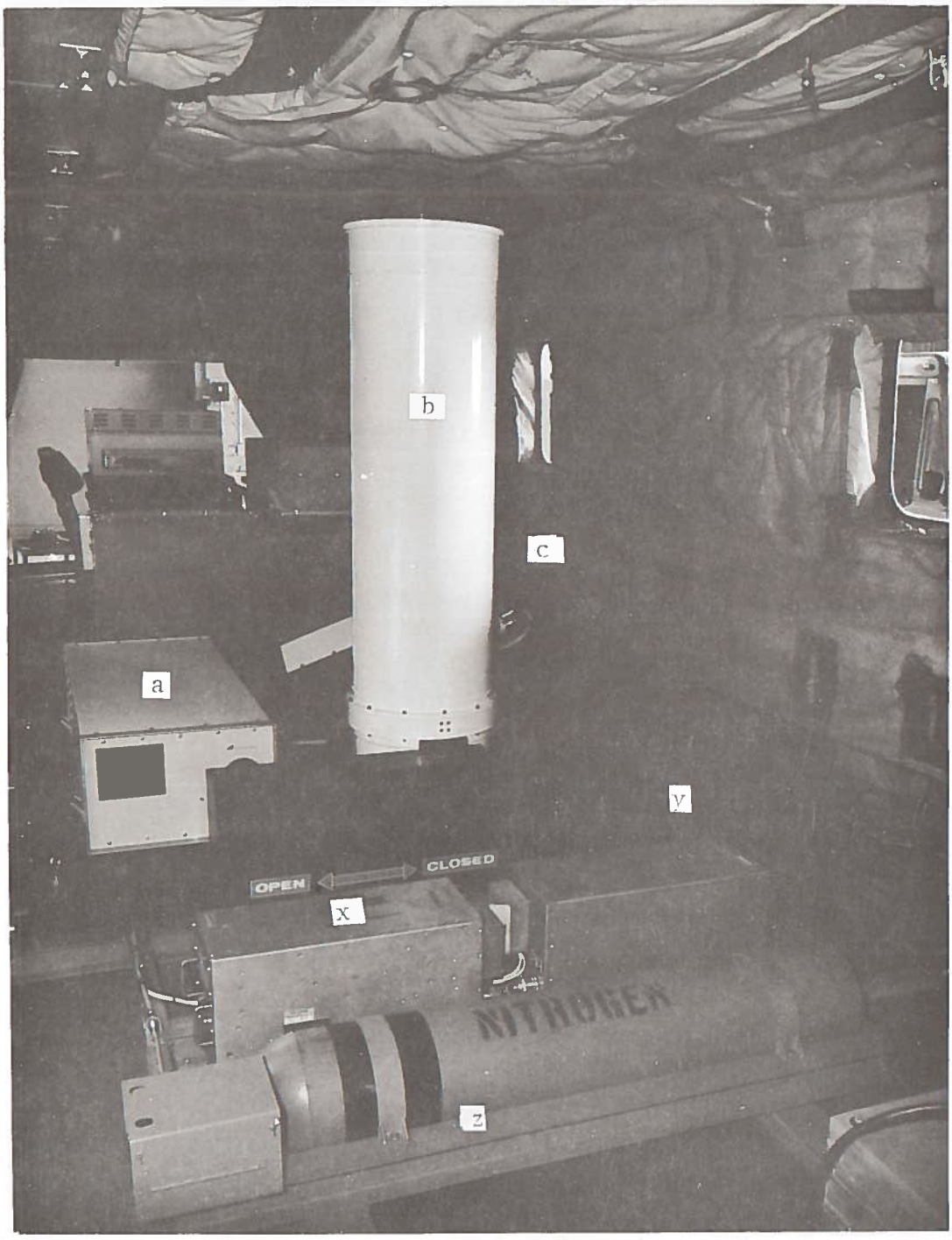

Figure 16. TSC Laser Remote Sensing System Mounted in the Helicopter Showing (a) Laser (b) Telescope (c) Image Dissector (x-y) Power Converters and (z) Nitrogen Container

four of each type. The barrels to be used for a given day were loaded onboard a US Coast Guard cutter of the type shown in Figure 17 and conveyed to the oil spill site. Once at the site the cutter acted as a radio beacon to guide the helicopter to the spill site and also recorded the sea truth data. Enroute to the spill site the system was calibrated over clean water (i.e., without oil spill). Once at the site the helicopter would direct the cutter to spill each oil at a designated time and place, one at a time. After each spill the helicopter flew a path directly over the spill, either at a constant altitude, or , if the spill had formed a small puddle a few meters or less in diameter, in a hovering position over the puddle, until a fluorescence spectrum was obtained.

4.2 TEST RESULTS

The first series of field tests of the ERODAC was conducted on October 24th (daytime) and November 5th (nighttime) 1973, totaling 5 hours of flight and 3 hours of remote sensing. On October 24th skies were clear with patches of sea fog, 13°C air temperature, 6 km h^{-1} wind from the East and wave heights from .3 to .6m. All measurements were made between 11:30 AM and 12:30 PM at an aircraft altitude of 31 to 46 m and at a forward speed of 64 to 80 km h^{-1}. On November 5, 1973 the space flight occured during twilight/night conditions. The air temperature was 8°C, with occassional clouds, a three quarter moon, winds NW at 24 km h^{-1} and a sea state defined by 1.2 to 1.5 m waves with white caps. All measurements were made between 4:00 PM and 5:30 PM at an altitude of 31m in either a hover or forward speed condition at 161 km h^{-1}. Figure 18 shows the normalized fluorescence spectra of No. 2 Diesel Oil, °API 37.0 obtained with the ERODAC during the October 24th (daytime) and November 5th (nighttime) flights. During the October 24th flight the No. 2 Diesel Oil, when viewed by the pilot, covered an area 1.6 km long by 0.4 km wide. The quantity spilled was 190 liters, creating an approximately 0.3 microns oil film.

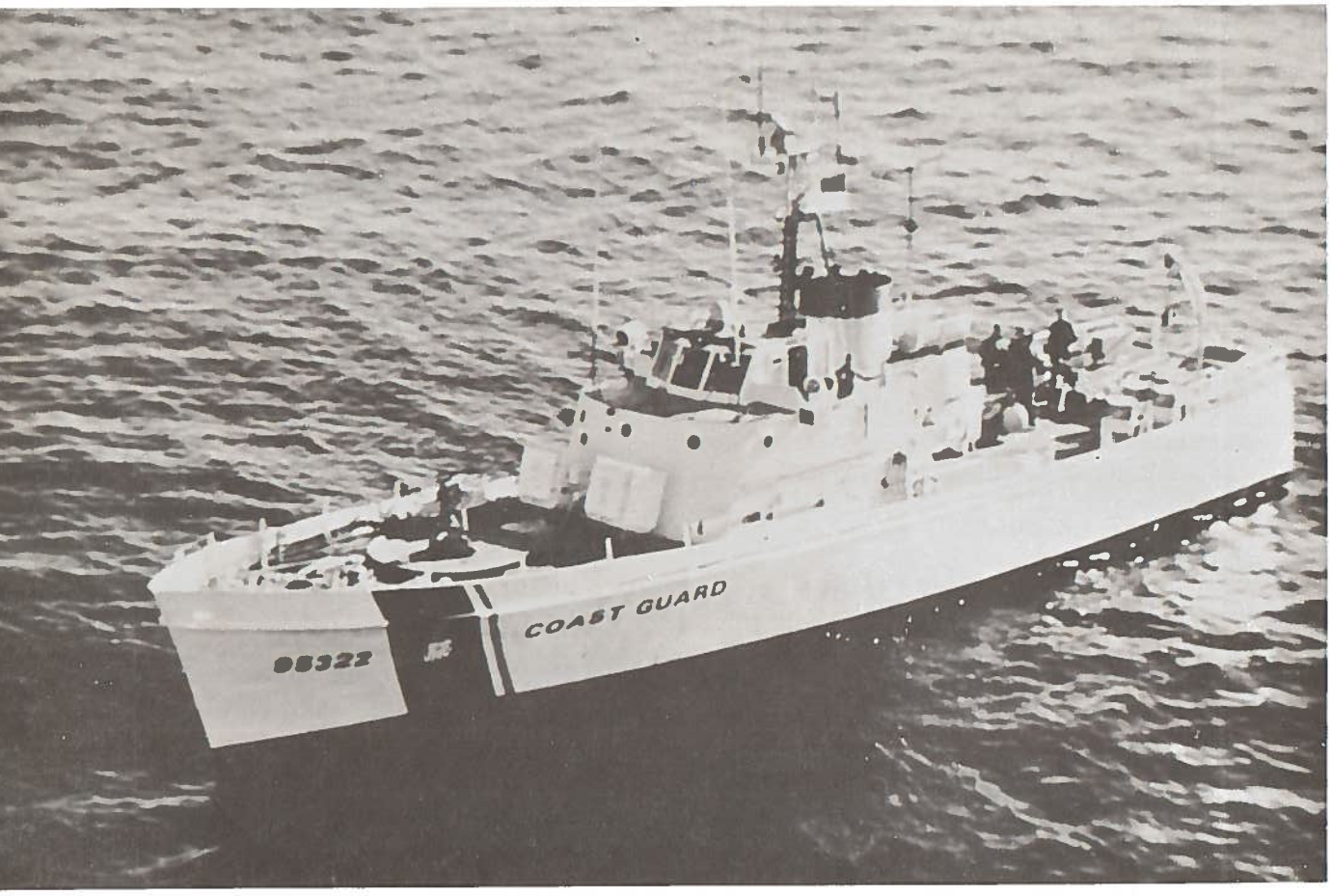

Figure 17. U.S. Coast Guard Cutter Cape Horn (WPB-95322), Used During the Field Tests of the TSC Experiment Airborne Oil Spill Remote Sensing System

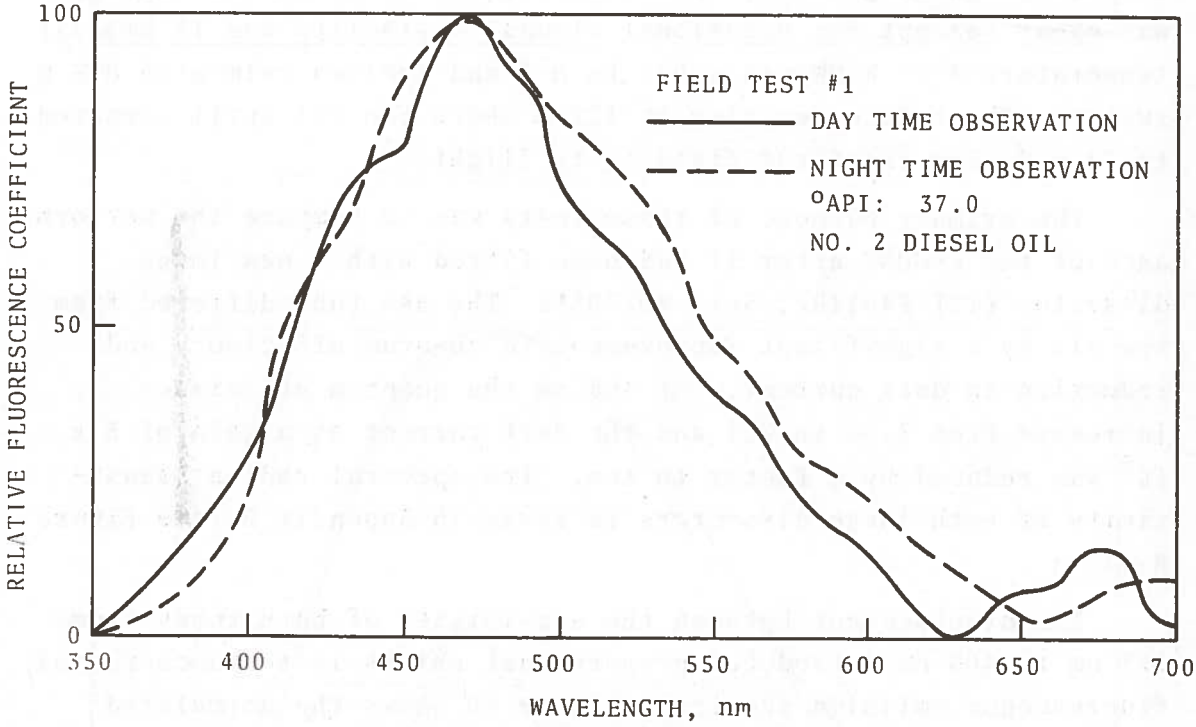

Figure 18. Normalized Fluorescence Spectra of No. 2 Diesel Oil, °API 37.0, Obtained with the ERODAC During the October 24th (Daytime) and November 5th (Nighttime) Flights

Figure 19 shows the normalized fluorescence spectra of a Nigerian medium crude, °API 26.6, obtained with the ERODAC during October 24th (daytime) and November 5th (nighttime) flights. The quantity spilled was 190 liters. Unlike the first oil this one formed small puddles and ropes inside a larger thin film. When viewed by the pilot the slick was 90 m long and oval shaped.

With the successful completion of the first series of field tests, a second series was performed. The helicopter and the oil spill site were the same as the first test series. Due to severe weather conditions the tests were limited to one day only, December 13th (day- and nighttime) 1973. During the observations the sky was clear (except for occasional clouds) visibility was 13 km, air temperature 4°C, W-NW winds 9.3 km h^{-1} and the sea calm with 0.3 m swells. The helicopter flew at 122 m above the oil spill compared to 31 m during the first field tests flights.

The primary purpose of these tests was to compare the performance of the ERODAC after it had been fitted with a new image dissector (ITT F4011RP, Ser. #07703). The new tube differed from the old by a significant improvement in quantum efficiency and reduction in dark current. At 408 nm the quantum efficiency increased from 7.5% to 22% and the dark current at a gain of 5 x 10^5 was reduced by a factor to two. The spectral radiant sensitivity of both image dissectors is given in Appendix B (see Figure B-8).

The displacement between the sensitivity of both tubes from 513 nm to 408 nm introduced proportional shifts in the uncorrected fluorescence emission spectra. Figure 20 shows the normalized fluorescence spectra of No. 2 Diesel Oil, °API 37.0, obtained with the ERODAC during November 13th (day- and nighttime) flights. Figures 21 and 22 show the spectra of a Nigerian medium crude °API 26.6 and a high residual DAV, °API 24.5, respectively, both obtained in the spectra given in Figure 19.

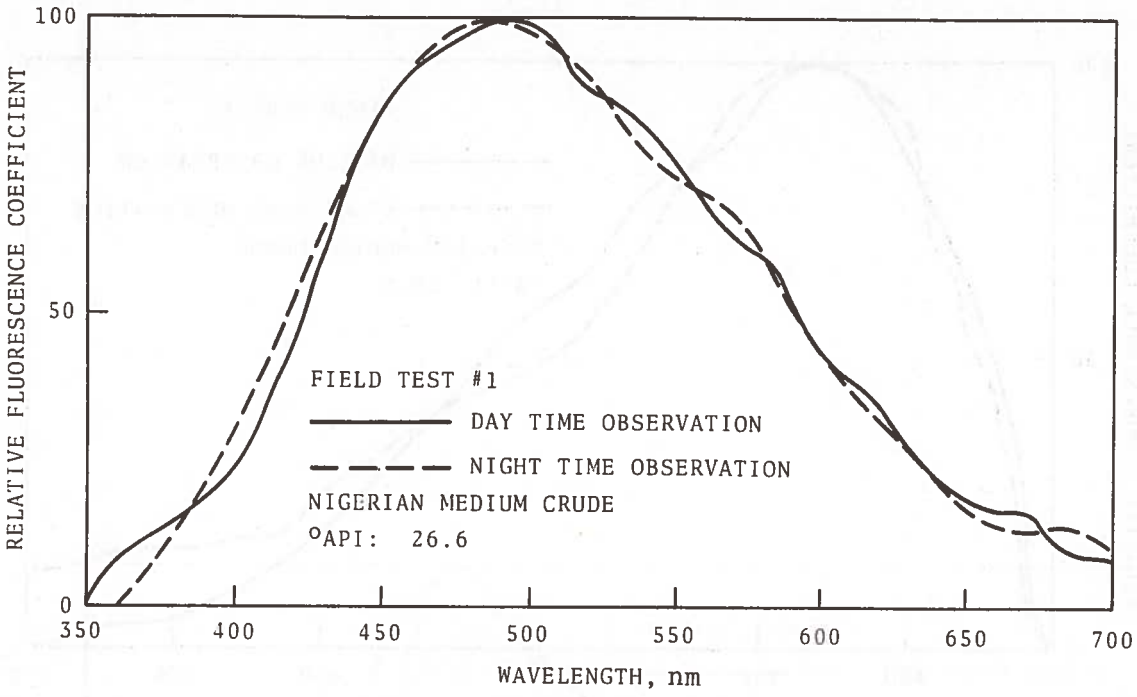

Figure 19. Normalized Fluorescence Spectra of a Nigerian Medium Crude, API 26.6, Obtained with the ERODAC During the October 24th (Daytime) and November 5th (Nighttime) Flights

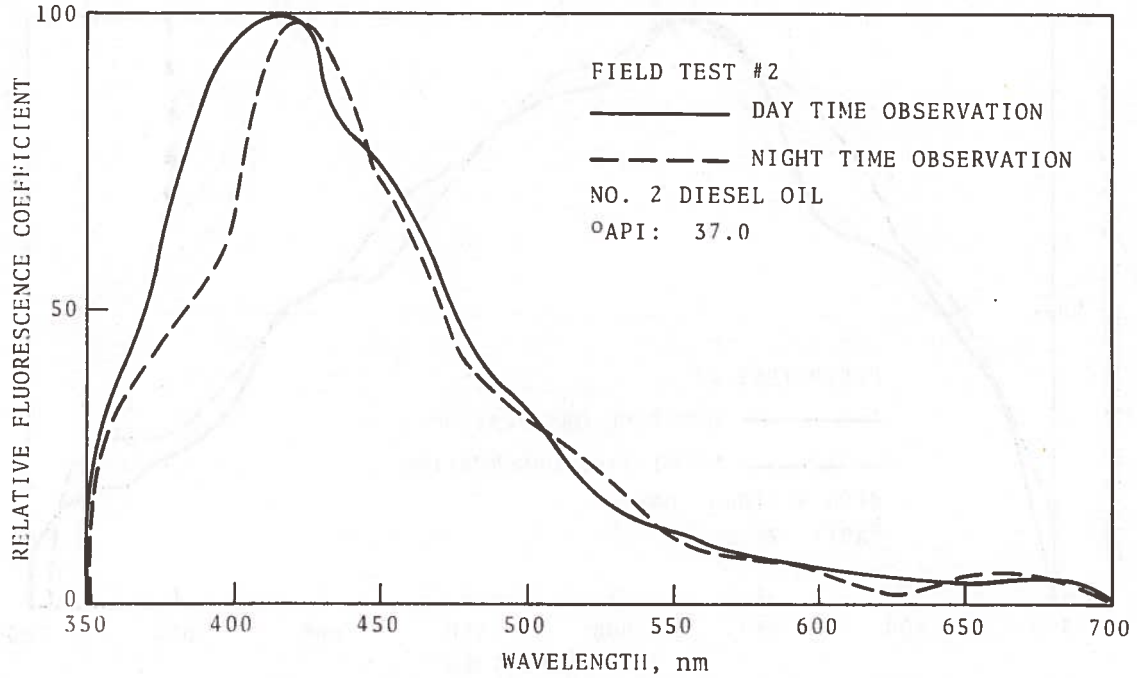

Figure 20. Normalized Fluorescence Spectra of No. 2 Diesel Oil, API 37.0, Obtained with the ERODAC During the November 13th (Day- and Nighttime) Flights

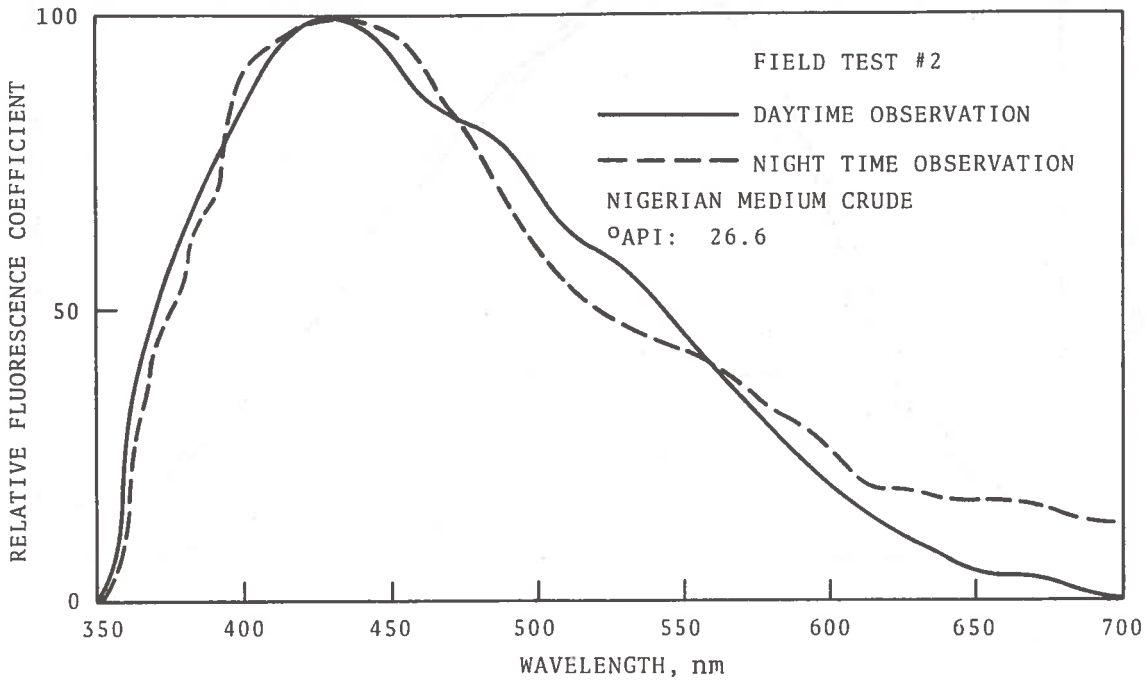

Figure 21. Normalized Fluorescence Spectra of a Nigerian Medium Crude, API 26.6 Obtained with the ERODAC During the November 13th (Day- and Nighttime) Flights

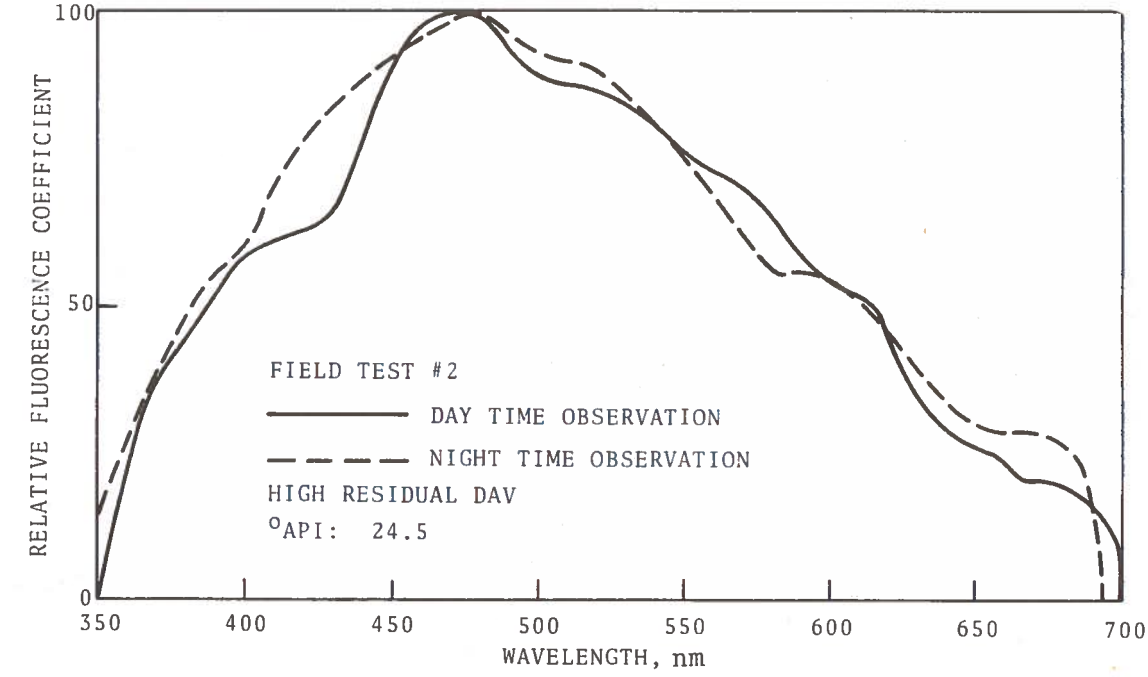

Figure 22. Normalized Fluorescence Spectra of a High Residual DAV, API 24.5, Obtained with the ERODAC During the November 13th (Day- and Nighttime) Flights

5. CONCLUSIONS

An experimental remote oil detection and classification (ERODAC) and classification in spills has been developed at TSC. Operating from a U.S. Marine helicopter, several controlled oil spills were remotely sensed by the system. Based on the laboratory and field data we concluded the following:

1. Detection of oil spills based on laser-excited oil fluorescence is feasible in the marine environment.
2. Broad classification of oils in real time or quasi-real time is feasible in the marine environment using a system based on the principles of the ERODAC.
3. An oil spill can be accurately surveyed by means of the ERODAC.
4. The background rejection scheme used in the ERODAC allows daytime operation without any noticeable performance degradation over the nighttime operation.
5. The TSC airborne laser oil spill remote sensing system operated reliably in the helicopter environment.
6. Future systems based on oil fluorometry should incorporate automatic correction of the oil fluorescence spectra for the spectral response of the photoelectric detector (in this case, the image dissector). Lack of this feature will reduce the capability to classify oils and allow intercomparison only between data gathered by a particular instrument.

BIBLIOGRAPHY

Aukland, J.C., J.D. Sohn and I.F. Rasmussen, "Multi-Sensor Detection and Tracking of Controlled Oil Spills," Spectran, Inc., Microwave Sensing Systems Division, 941 North Highland Ave., Hollywood, California: Final Report Contract No. DOT-CG-11997-A, May 1971.

Davis, A., H. Gross, J. Kruus, and R. O'Neil, "Remote Sensing of Water Quality Using Laser Induced Fluorescence." Inland Waters Directorate, Environment Canada, 562 Booth Street, Ottawa, Ontario, K1AQE7. February 1973.

Edgerton, A.T. and LCDR. G. Woolever, "Airborne Oil Pollution Surveillance System," Proceedings of the Ninth International Symposium on Remote Sensing of Environment, Environmental Research Institute of Michigan, Ann Arbor, Michigan, April 1974.

Fantasia, J.F., T.M. Hard, and H.C. Ingrao, "An Investigation of Oil Fluorescence as a Technique for the Remote Sensing of Oil Spills," Final Report DOT-TSC-USCG-71-7 (also NTIS No. PB 204 792), 1971.

Fantasia, J.F. and H.C. Ingrao, "Development of an Experimental Airborne Laser Remote Sensing System for the Detection and Classification of Oil Spills," Proceedings of the Ninth Inter-National Symposium on Remote Sensing of Environment, Environmental Research Institute of Michigan, Ann Arbor, Michigan, April 1974.

Gross, H.G., "Luminescence Signatures Induced by Lasers with Enhanced Specificity for Remote Active Sensing," Proceedings of the Conference on "Earth Resources Observation and Information Analysis System," The University of Tennessee Space Institute, Tullahoma, Tennessee, March 1972.

BIBLIOGRAPHY (CONTINUED)

Gross, H. Gerald and Howard A. Hyatt. "Luminescence Induced by UV and Visible Lasers for the Remote Active Sensing of Materials from Ground, Air, and Space," Proceedings of the Seventh International Symposium on Remote Sensing of Environment, Ann Arbor, Michigan, May 1971.

Gross, H.G. and Michiya Muramoto, "Crude and Refined Petroleum Oil Structured Luminescence Signatures Induced by UV Laser or Lamp and Their Remote Sensing Applications," Proceedings of the Ninth International Symposium on Remote Sensing of Environment, Ann Arbor, Michigan, 1974.

Gross, H.G. and Michiya Muramoto, "Laser Induced Luminescence Signatures of Refined and Virgin Petroleum, Their Composition and Remote Sensing Implications," Proceedings Remote Sensing of Earth Resources, Vol. III, University of Tennessee Space Institute, Tullahoma, Tennessee, 1974.

Guinard, N.W., C.G. Purves, "The Remote Sensing of Oil Slicks by RADAR," Chedabucto Bay Case Study, USCG Office of Research and Development Project, June 1970.

Horvath, R., W.L. Morgan, and S.R. Stewart, "Optical Remote Sensing of Oil Slicks: Signature Analysis and Systems Evaluation," Final Report, Project No. 724104.2/1, Willow Run Laboratories, The University of Michigan, October 1971.

Ketchel, Cdr. R.J., "Development of U.S. Coast Guard Prototype Airborne Oil Surveillance System," U.S. Coast Guard, Washington, D.C. and A.T. Edgerton, Aerojet Electro Systems Company, Azusa, California, Proceedings of Joint Conference on Prevention and Control of Oil Spills, March 1973.

Kim, H.H., "An Airborne Laser Fluoresensor for the Detection of Oil on Water," NASA, Wallops Station, Wallops Island, Virginia, and G.D. Hickman, Sparcom Inc., Alexandria, Virginia, 1973.

BIBLIOGRAPHY (CONTINUED)

Meeks, D.C., D.P. Williams, R.M. Wilcox, and A.T. Edgerton, "Microwave Radiometric Detection of Oil Slicks," Final Report No. 1335-2 Microwave Division, Aerojet-General Corporation, El Monte, California, March 1971.

Millard, J.P. and J.C. Arvesen, "Airborne Detection of Oil on Water," NASA Ames Research Center, Applied Optics, 11,102 (1972).

Mumola, P.B., Olin Jarrett, Jr. and C.A. Brown, Jr., "Multi-wavelength Laser Induced Fluorescence of Algae in-vivo: A New Remote Sensing Technique," Proceedings of the Second Joint Conference on the Sensing of Environmental Pollutants, Washington, DC, December 1973.

Horstein, Bernard, "The Visibility of Oil-Water Discharges," U.S. Environmental Protection Agency, Proceedings of Joint Conference on Prevention and Control of Oil Spills, March 1973.

Plascyk, J.A., "Oil Spill Surveillance System," Perkin-Elmer, Optical Group, Norwalk, Conn, Final Report No. 11633, July 1973.

Preston, K. Jr., "A Comparison of Analog and Digital Techniques for Pattern Recognition," Proceedings of the IEEE, Vol. 60, No. 10, October 1972.

Sprague, D.H., "Optical Multichannel Spectral Analyzer," Charles Stark Draper Laboratory, Cambridge, MA, Final Technical Report No. R-756, March 1973.

Stoertz, G.F. and W.R. Hemphill, "Airborne Fluorometer Applicable to Marine and Estuarine Studies," U.S. Geological Survey, Washington, D.C. and D.A. Markle, the Perkin-Elmer Corporation, Norwalk, Connecticut, Marine Technology Society Journal, Nov/Dec, 1969, Vol. 3, No. 6.

APPENDIX A

ERODAC TRANSMITTER AND RECEIVER

This appendix is based on material in Engineering Report No. 11633, July 1973, Oil Spill Surveillance System, Final Report, prepared by the Optical Group at Perkin-Elmer of Norwalk, Connecticut under U.S. Government Contract DOT-TSC-373 for the U.S. Department of Transportation, Transportation Systems Center, Optical Devices Group.

TABLE OF CONTENTS

A.1 INTRODUCTION

This report presents the design of the Oil Spill Surveillance System and results of the tests performed in this System. This system consists of the following subsystems:

1. Main Frame
2. Laser Transmitter Beam-Forming Module
3. Fluorescence Radiation Optical Receiver
4. Spectrometer and Auxiliary Optics
5. Combination Camera/Viewfinder Optical Module

A photograph of the unit is presented in Figure A-1.

The main frame is an aluminum honeycomb pallet structure of sufficient size to accommodate all the optical subsystems. Appropriate cut-outs, hard mounting points and reinforcements are provided to accommodate the individual components and provide a stable rigid base to furnish the necessary optical registration during operation on board an HU-16 Coast Guard amphibian aircraft. Stand-offs to mount vibration isolators and position the elastic center of these mounts at the center of gravity of the assembled unit are provided at four locations around the periphery of the pallet.

The laser transmitter beam forming module is a unit mounted at the rear end of the UV laser channel, replacing a reflecting flat originally supplied with the laser. The module consists of an aspheric lens color corrected at 3371Å, a quartz field stop in an adjustable mount, and a retro-mirror. This module provides the desired divergence angle of less than 4 mrad. The entire unit is mounted in an aluminum module which has angular adjustment about 2 axes. The field stop is adjustable via a micrometer screw. The module, in turn, is mounted to a pressure chamber attached to the rear of the laser tube which is purged with dry N_2 to eliminate

Figure 4.1 Oil Spill Surveillance System

condensation on the rear window of the laser and the beam forming lens of the module. The module is sealed into a recess in this chamber with an O-ring.

The fluorescence Radiation Optical Receiver is a Newtonian type telescope with an f/4.7 spherical primary mirror. The clear aperture of the primary mirror is 13.07 inches diameter, with an aluminum reflective coating and a Spinel protective overcoat. The material for the mounting tube of this telescope is aluminum, with internal baffles positioned along the length of the tube to suppress stray light. A double fold mirror is positioned on a spider structure at the base of the telescope tube. One mirror is coated with aluminum and a Spinel protective coating to fold the received fluorescent energy into a spectrometer, and the other mirror is coated with a dielectric coating (to peak the reflection efficiency at 3371Å) which folds the laser energy coaxially with the receiver axis to the target below. Two machined bulkheads are mounted at the radial exit ports of the telescope to provide registration surfaces for the spectrometer and the laser relative to the telescope. The entire telescope structure is registered and secured to the main frame via an accurately machined ring mounted integrally with the honeycomb structure of the pallet.

The spectrometer and auxiliary optics consist of an Ebert-Fastie grating spectrometer with a 3-mirror Bowen image slicer mounted forward of the entrance slit of the spectrometer. The energy from the telescope is sliced by the mirrors. Each slice is reoriented to fall on the entrance slit of the spectrometer, providing an elongated entrance aperture having 3 times the length of the single slit arrangement, and theoretically 3 times the energy input that could be obtained with the single slit. The width of the slit is maintained at a dimension providing the required spectral resolution of 100Å over the region from 3500Å to 7000Å. The entrance slit is also curved about the centerline of the spectrometer mirror to minimize the curvature of the exit image. Two spherical mirrors direct the energy to a diffraction grating fixed to position the proper spectral format on the face of an image dissector having a 1-inch diameter photocathode. The

image dissector is an ITT F4011 tube mounted in ruggedized housing designed and built by Perkin-Elmer for the Charles Stark Draper Laboratories of Cambridge, Mass., who provided the electronics to the Transportation Systems Center for processing the signal from the OMSA. The image dissector scans the spectra at the focal plane of the spectrometer. The detector is mounted on a precision slide to provide focus adjustment.

The entire spectrometer assembly is tilted relative to the exit beam of the telescope to provide alignment with the image slicer-entrance slit assembly. This tilt is accomplished by two bases of appropriate angles, one mounted atop the other to achieve the necessary compound angle relative to the telescope axis and the pallet mounting surface. The entire assembly is pinned in place to maintain registration. A baffle is provided from the exit port of the telescope to the entrance of the spectrometer to minimize the effect of stray light.

The combination camera/viewfinder consists of a commercially available ruggedized 35mm camera with a solenoid actuated shutter and a motorized film transport made by Robot, Inc. A standard 50mm wide angle lens and a 300mm telephoto lens are provided and are manually interchangeable. Remote actuation of the shutter and film transport is accomplished by a push-button control. The camera also incorporates a data block consisting of the time and date simultaneously recorded on a corner of film frame. This information is recorded via an auxiliary optical system which views a clock and data strip, which is an erasable material for recording the data. The unit operates from a 24 volt D.C. source. The entire assembly is mounted on a sturdy aluminum pedestal which has been aligned to the main frame. The camera optical axis is aligned parallel to the optical receiver axis.

The viewfinder consists of two units mounted on the same pedestal as the camera. One viewfinder is a standard Robot device for the 50mm lens and the other is a modified Bausch & Lomb rifle scope of 2.5x magnification which has the same FOV as the 300mm telephoto lens. A reticle framing the 35mm format was added to the

scope to allow the unit to serve as a viewfinder for the 300mm telephoto lens.

The test procedures and test results for this system are presented in Section A.8.

A.2 MAIN FRAME

A photograph of the main frame is shown in Figure A-2. The main frame is made of a rigid aluminum honeycomb structure. The aluminum core is 3 in thick and is bonded to .080-in aluminum skins with an epoxy cement (EPON 828, Shell Oil Co.). The overall dimensions of this structure are 54 in x 63-1/2 in x 3-3/16 in. The material used is 6061-T6 for the skin and reinforcing structure. The sides of the honeycomb structure are sealed with a 1/4 in aluminum frame welded at the corners for rigidity and bonded between the top and bottom aluminum skins.

A machined aluminum ring to mount the telescope and provide accurate registration is bonded between the aluminum skins to provide additional strength. The telescope is secured to this ring via tapped holes in the ring. All other components are mounted to the structure via Shur-Lok threaded fasteners straddling the top and bottom skins and epoxied to the skins and the cells of the honeycomb. Aluminum dowels are positioned between the skins at various locations to provide at least two pinning positions for each optical component.

Reinforcing plates 1/2-in thick are provided along the side frame for the vibration isolator stand-offs. These plates are secured to the side frame and further bonded to the skins. The isolator stand-offs are welded aluminum structures with sufficient reinforcement to react the loads from vibration and shock on the structure. They positioned the vibration isolators at the proper height to provide that the elastic center of the mounts are reasonably coincident with the center of gravity of the system, so that the rocking modes, which would tend to excite the long telescope, are suppressed.

The vibration isolators selected to support the system are Barry US-2060-ST mounts. These mounts contain a black elastomer material with a large amount of internal damping. The geometrical configuration is such that approximately equal spring rates are obtained in all three principal directions. These mounts meet the

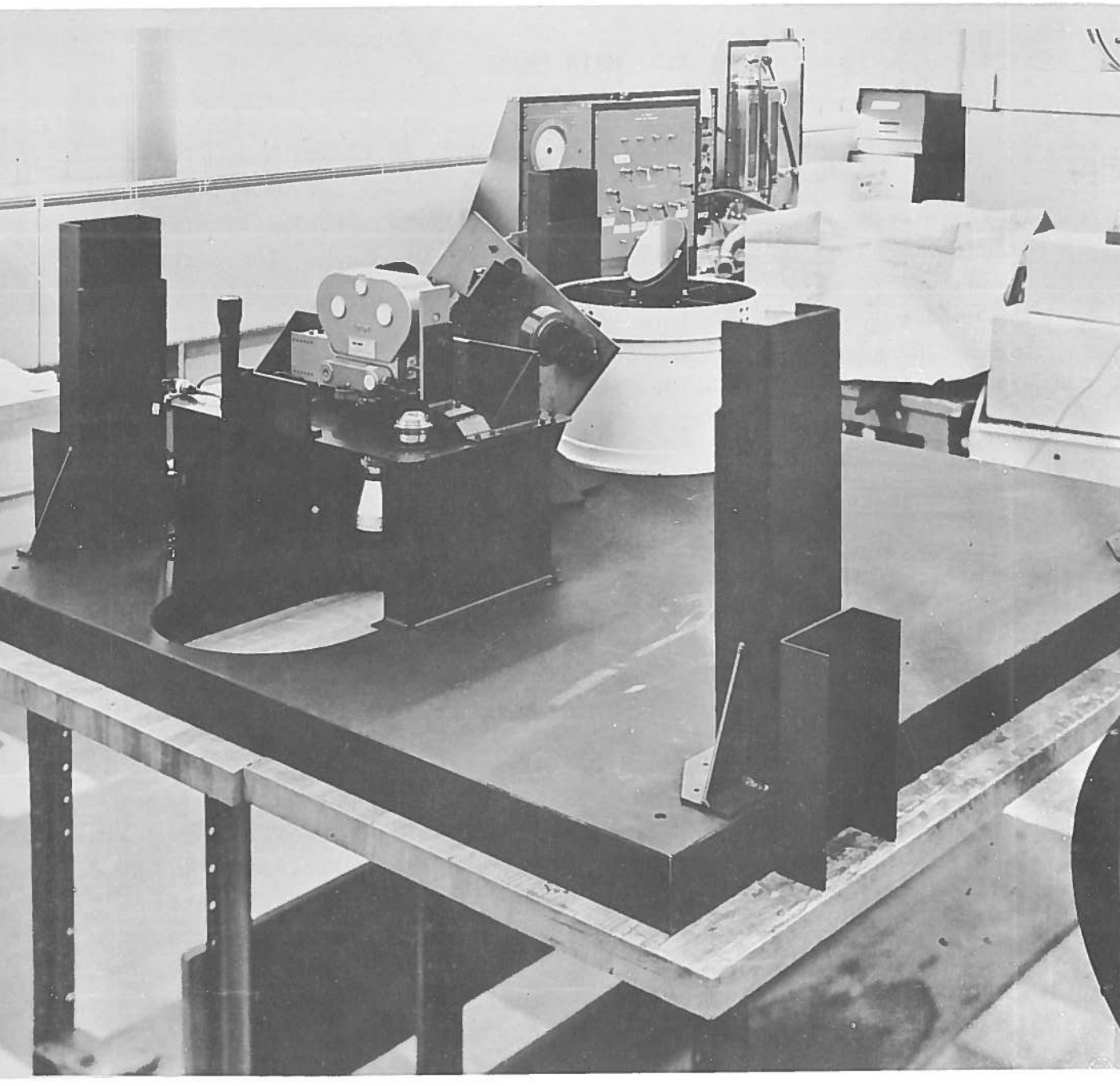

Figure A-2. Main Frame with Lower Section of Fluorescent Radiation Receiver, Spectrometer and Camera Viewfinder Mounted

requirements of MIL-T-17113 and MIL-S-901. The frequency requirement is such on this system that two units are mounted together in series to give 1/2 the spring rate and 0.707 of the frequency of a single mount.

The aircraft in which this unit was originally planned to fly was an Albatross Amphibian, designated as an HU-16. This aircraft is powered by 2 reciprocating engines which when cruising have a rotational speed of 2000 rpm, corresponding to a forcing frequency of 33-1/3 Hz. The engines drive a 3-bladed propeller, which give propeller frequencies of 33-1/3, 66-2/3, and 100 Hz. The selected vibration isolators will be loaded to about 130 lb each, which results in a resonant frequency of 22 Hz (from Barry data). The transmissibility at resonance will be about 4 at standard temperatures, and the fundamental excitation frequency will be about 1; therefore, the system should experience no magnification of the applied loads.

The loading to which the system is designed is based on MIL STD. 810B, "Environmental Test Methods." Figure 514-2, Curve H for equipment mounted in the rear half of the fuselage is used. For the resonant frequency of the isolators, the applied vibratory g load specified by this curve is 1 g. Since the transmissibility of these mounts is about 4, the magnification will give 4 g's. In addition, there is a half sine pulse specified to simulate maneuver loads of 15 g's for 11 msec and a steady state of 9 g's down. The shock load has an equivalent frequency of

$$f = 1/(2\Delta T) = \frac{1}{2(.011)} = 45.5 \text{ Hz}$$

At this frequency the transmissibility of the isolators is down to 0.4 so that the system will feel only 6 g's due to the shock. Using a very conservative approach that all loads add, the maximum expected downward load (weakest direction for the main frame) is

$$a/g = 4 + 6 + 9 = 19 \text{ g's.}$$

The design load used for this system will be based on a safety factor of 1.5, which gives

a/g design = 1.5 (19) = 28.5 g's.

Therefore the pallet, with a static load of 530 lb, must resist a dynamic load of

$$F_v = 530\ (28.5) = 15{,}105\ \text{lb}.$$

The pallet will react this load with a margin of safety of over 1000%.

The minimum natural frequency of the pallet alone is estimated to be about 35 Hz. The standoffs will react these loads with a margin of safety of about 50%. The natural frequency of the standoffs is 50 Hz, well above the resonant frequency of the isolators. All attachments to the pallet utilize passivated stainless steel hardware, and all screw threads are either steel (Shur-Lok fasteners) or helicoil steel inserts.

The vibration isolators essentially bottom out at a maximum load of about 1500 lb. This will react the maximum steady-state and vibration load. The probability of these loads occurring simultaneously is quite low. If they did occur simultaneously, the mounts would bottom out and transmit the loads directly. It is felt that with the 50% M.S. designed into the system there will be no danger of failure.

A.3 LASER TRANSMITTER BEAM FORMING OPTICAL MODULE

The design of this unit was suggested by Dr. Eisenberger of the Bell Laboratories in Murray Hill, New Jersey. The optical schematic of the unit built by Perkin-Elmer is presented in Figure A-3, and a photograph of the unit is shown in Figure A-4. The critical element in this module is a single element aspheric fused silica lens designed by Perkin-Elmer to give a well corrected image at 3371Å, the laser emission line. This lens also has an anti-reflection coating to minimize reflection at 3371Å, as does the fused silica field stop.

The field stop is made of fused silica to allow the impinging focused laser energy to be transmitted through the stop and refracted away from the FOV of the retro-mirror and absorbed by the blackened sides of the mounting tube. This mounting has sufficient mass to tolerate the high intensities without significant heating. The field-of-view of the laser is reduced from 60 mrad to less than 4 mrad by this stop.

The field stop has polished surfaces and anti-reflection coatings to minimize the back reflected energy. The stop has an end one-half inch wide with a 45° bevel, forming a sharp edge to provide the desired sharp cut-off and refracted angle. The stop is expoxied to a blackened stainless steel block, which in turn is secured to a four bar flexure. This flexure is mounted so that the field stop cuts across the focused laser beam in a direction prependicular to the beam axis. The stop was aligned on an optical bench with the violet line of a mercury lamp collimated and focused by the aspheric lens. The difference between the focal position of the Hg violet line and 3371Å was calculated and the stop offset by this amount. The field angle passed by this stop is adjustable with a micrometer which actuates the flexure to which the stop is mounted. The stop is set to a position which blocks half the field in the long direction of the laser exit aperture (60 mrad), and the other half of the field is blocked on the return pass from the retro-mirror by the rear of the same stop. This eliminates

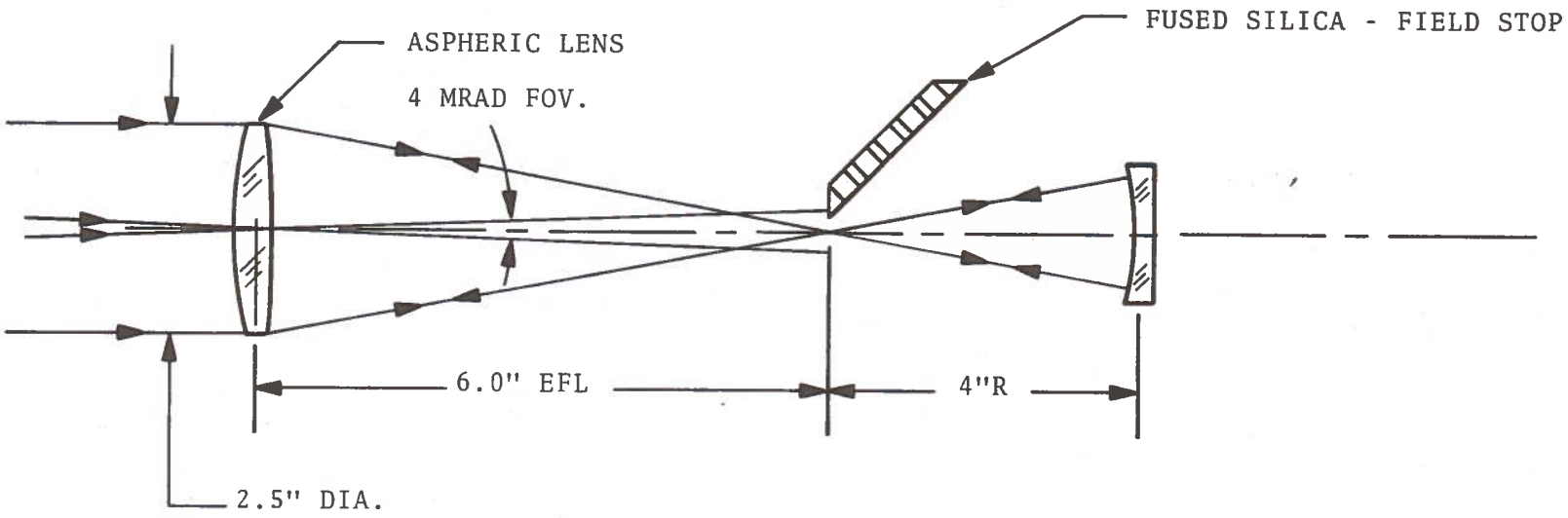

Figure A-3. Laser Transmitter Beam Forming Optical Schematic

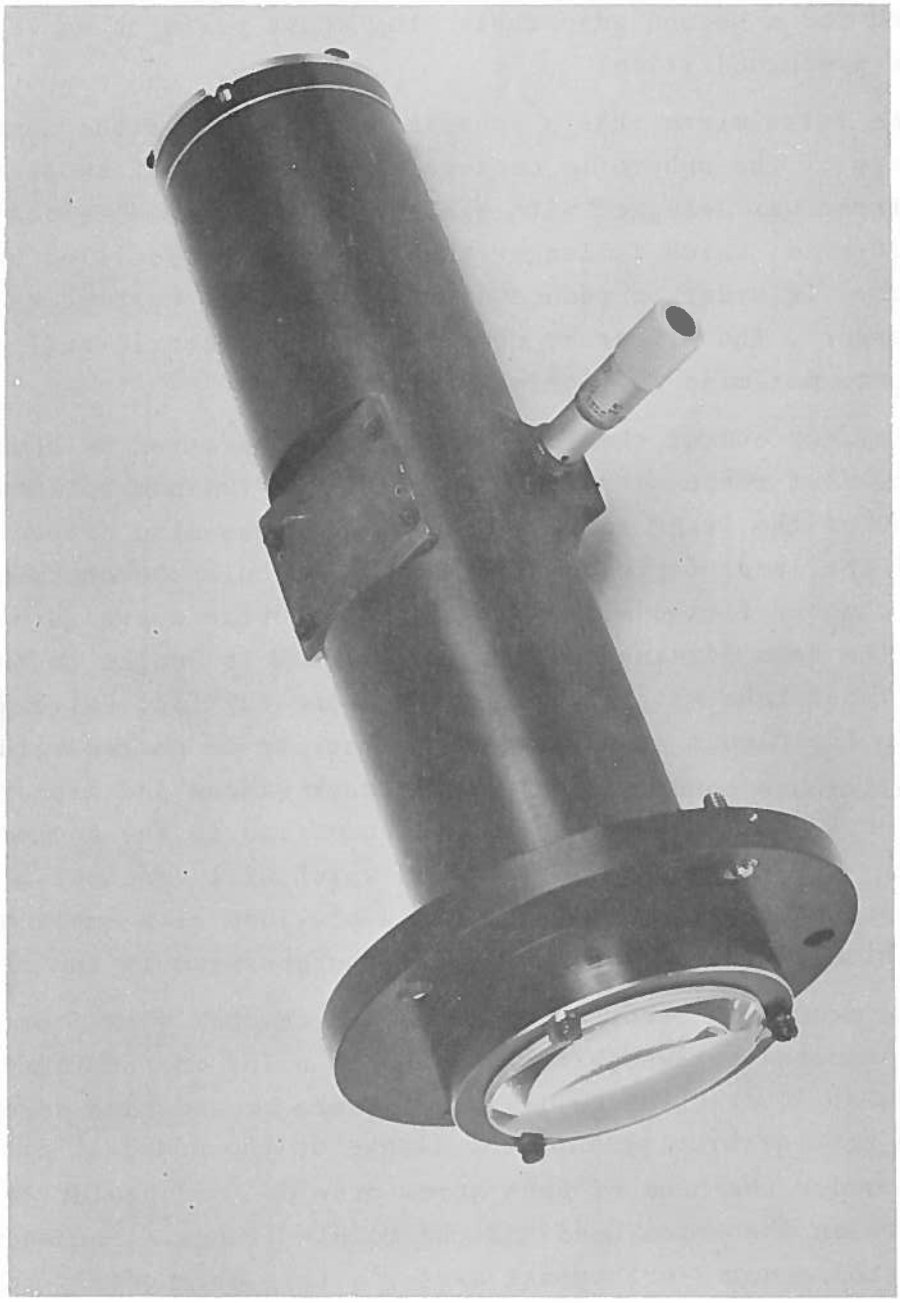

Figure A-4. Laser Transmitter Beam Forming Optical Module

the need for a second adjustable stop whose position would require precise synchronization.

The retro-mirror has a spherical surface, and the center of curvature of the sphere is centered at the focus of the lens. This mirror was designed with a clear aperture to accept a FOV of about 20 mrad, which is larger than the 4 mrad specified by the contract. In order to reduce size and minimize cost it was not made larger. The mirror is coated with a dielectric reflecting coating to maximize reflection at 3371Å.

The rear end of the laser channel was refitted by removing the existing flat retro-mirror and mounting an aluminum bulkhead to the rear end of the laser tube. This bulkhead was also bolted to the base of the laser for added rigidity. The bulkhead contains a plenum chamber fitted with an O-ring to provide a pressure seal around the beam forming module. The plenum is sealed to the end of the laser tube with RTV sealant. A one-way fill valve is provided in the plenum permiting the chamber to be purged with dry N_2 to eliminate condensation on the laser window and aspheric lens. This window and lens are cooled by conduction to the cooled laser channel. A safety valve is provided which will crack at a pressure difference of about 3 lb in^{-2}. Also provided is a small manual valve which can be opened to relieve the pressure in the chamber.

The module is secured to the plenum chamber with four orthogonally mounted screws through clearance holes in the flange of the module. A stack of belleville washers around each screw provides a return force against the flange of the module. Spherical washers under the head of each screw provide for angular misalignment between the screw head and the module flange. The module can be adjusted about 2 orthogonal axes via this arrangement to align the entire optical unit with the laser output.

The laser module was tested extensively to verify its performance. For testing,a silicon pin diode with a fused silica window was selected, with a 1-mm diameter pinhole aperture to obtain the desired resolution. Neutral density filters were used to attenuate sufficiently the laser beam so that the

detector was not saturated at the peak intensity. These neutral density filters were specified flat down to 2500Å. To verify their attenuation a Coherent Radiation Power Model 201 was used. A Corning #7-54 bandpass filter was inserted in front of the detector to eliminate energy in the visible portion of the spectrum.

The detector laterally and vertically scanned the laser. A Tektronix 547 oscilloscope was used to detect the signal. The output is the summation of the energy reflected from the beam forming module and the energy directly emitted from the front of the laser without being reflected from the beam forming module. The intensity distribution in the direction of the laser apertures (2 in) is plotted in Figure A-5. The beam divergence is 2.5 mrad. The average power output is 0.18 W (at 500 pps). Another distribution is plotted in Figure A-6 for an average power output of 0.26 W and a beam divergence of 9.3 mrad. Figure A-7 is the intensity distribution obtained in the y direction. The beam divergence in the y direction using the 10% power point as the equivalent width was 2.3 mrad. Since the field stop is effective in the x direction only, the divergence in the y direction is not affected by the beam forming module.

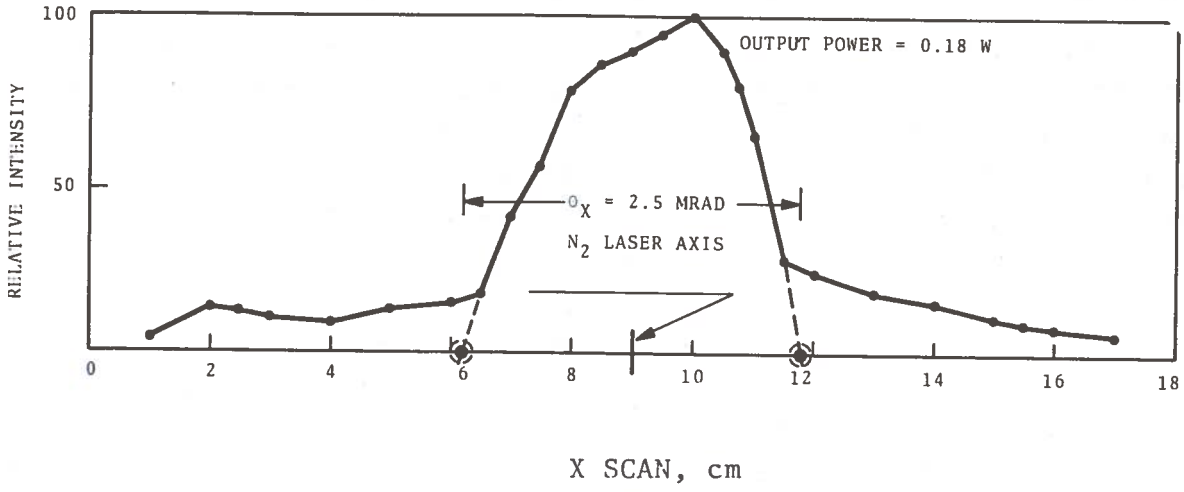

Figure A-5. N_2 Laser Intensity Distribution, X Direction (Output Power = 0.18 W)

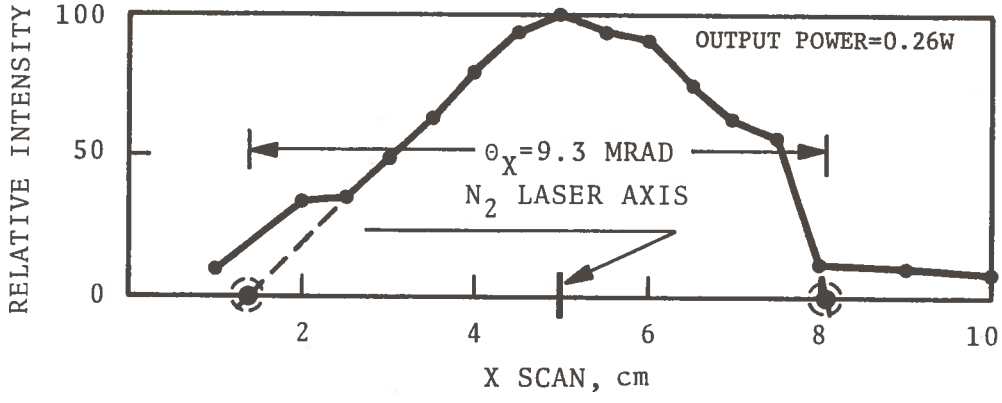

Figure A-6. N_2 Laser Intensity Distribution, X Direction (Output Power = 0.26 W)

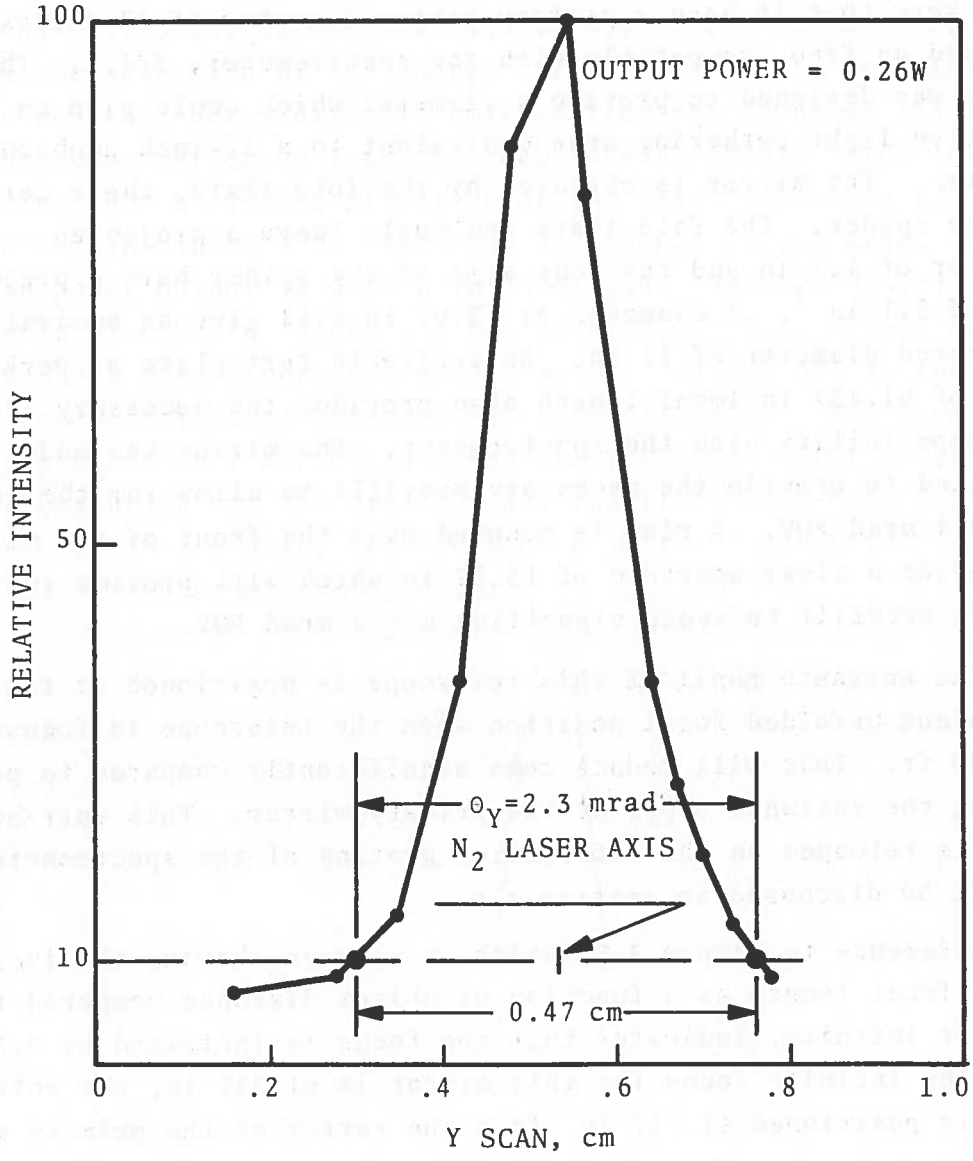

Figure A-7. N_2 Laser Intensity Distribution, Y Direction (Output Power = 0.26 W)

A.4 FLUORESCENCE RADIATION OPTICAL RECEIVER

The optical receiver is a Newtonian type telescope with an f/4.7 spherical primary mirror. The specifications for this telescope were that it have a primary mirror diameter of 12-inches minimum and an f/no. compatible with the spectrometer, f/4.7. The system was designed to provide a diameter which would give an effective light gathering area equivalent to a 12-inch unobscured diameter. The mirror is obscured by the fold flats, their cell and the spider. The fold flats and cells leave a projected diameter of 4.9 in and the four arms of the spider have a projected area of 2.1 in ^{2}. A diameter of 13.07 in will give an equivalent unobscured diameter of 12 in. An available test plate at Perkin-Elmer of 61.437 in focal length also provides the necessary f/4.7 for compatibility with the spectrometer. The mirror was made oversized to provide the necessary overfill to allow for the required 4 mrad FOV. A ring is mounted over the front of the mirror to provide a clear aperture of 13.32 in which will provide sufficient overfill to avoid vignetting a $\pm$ 2 mrad FOV.

The entrance pupil of this telescope is positioned at the equivalent unfolded focal position when the telescope is focussed at 1000 ft. This will reduce coma significantly compared to positioning the entrance pupil at the primary mirror. This entrance pupil is reimaged on the diffraction grating of the spectrometer, as will be discussed in section A.5.

Reference to Figure A-8, which is a curve showing the increase in the focal length as a function of object distance compared to the focus at infinity, indicates that the focus is increased by 0.32 in. Since the infinity focus for this mirror is 61.437 in, the entrance pupil is positioned 61.757 in. from the vertex of the primary mirror.

The main aberrations in this telescope are spherical and tangential coma (which is 3 times larger than the sagital coma). Astigmatism is negligible. If the entrance pupil was positioned

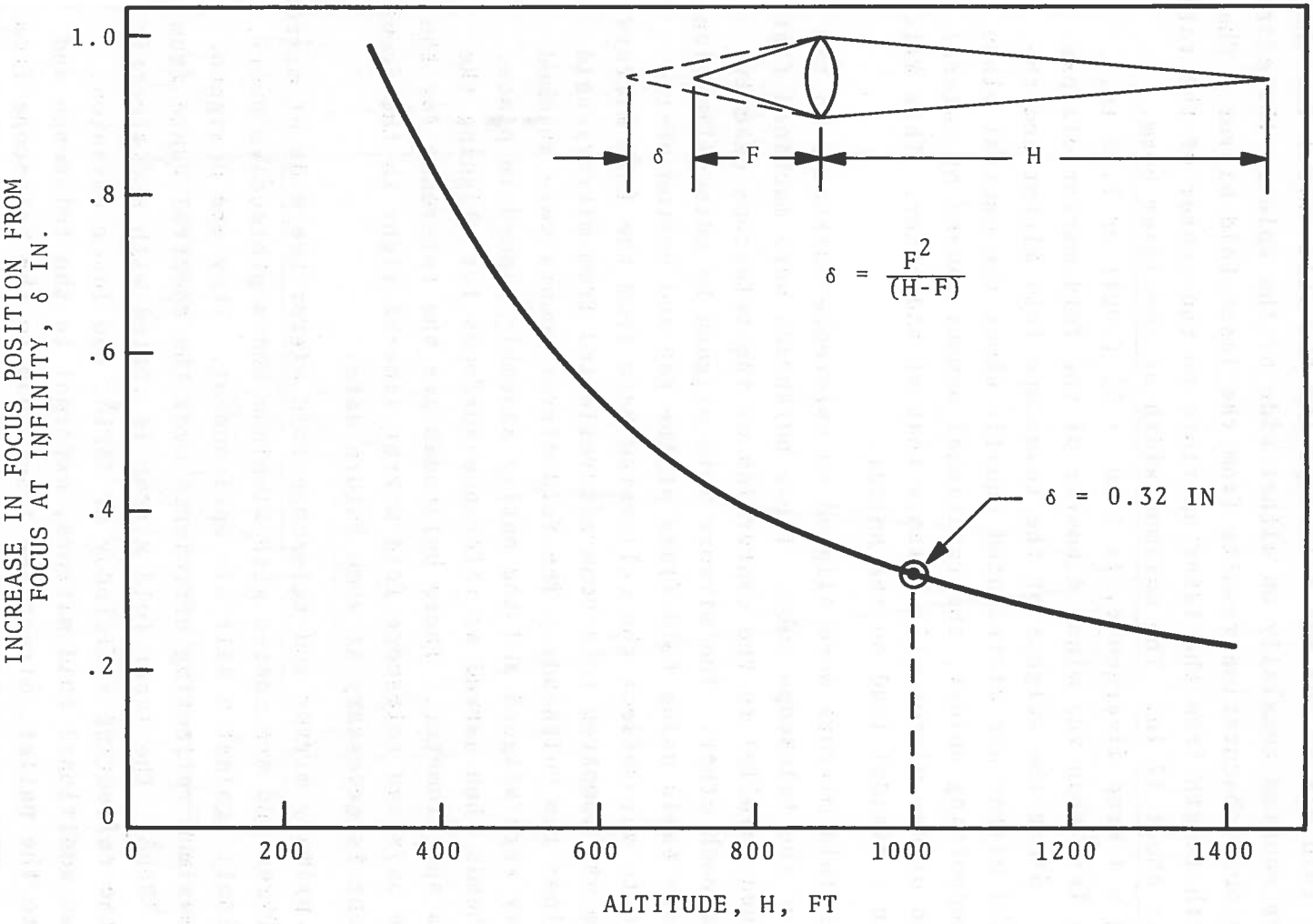

Figure A-8. Focal Position Shift

at the mirror, the coma would have been twice as large. A summary of the aberrations in this system is presented in Table A-1.

The fold mirror for the telescope and the fold mirror for the laser are mounted coaxially on either side of the spider; therefore no additional obscuration results from the laser fold mirror. The total path length from the laser aperture to the center of the fold mirror is about 32 in. The maximum width of the laser beam, assuming a 4 mrad divergence, is 2 in + 32 (.004) or 2.13 in, which is less than the minor diameter of the fold mirror ellipse of 4 in. Since the weights of the telescope fold mirror and the laser fold mirror are distributed equally about the central plane of the supporting spider, the rotational moment caused by lateral vibration of one mirror will balance that of the other. This will result in a minimal load on the spider.

Both fold mirrors were aligned to reference bulkheads on the outside of the telescope tube. These bulkheads were machined flat and aligned parallel to the centerline of the telescope exactly 180° from each other. The mirrors were aligned by autocollimation on a rotary table using fold flats at the top and bottom of the telescope to autoreflect the collimated beam from the fold mirrors. This beam was compared to a beam autoreflected from mirrors held flat against the bulkheads. The fold mirror mounts were shimmed until they were aligned and the entire assembly pinned in place. The bulkheads then served as reference surfaces for aligning the laser and spectrometer. These bulkheads are the reference for the telescope axis and telescope fold mirror line-of-sight in the event realignment is necessary at some future date.

The primary mirror and telescope fold mirror are made of mirror quality Pyrex and are coated with aluminum and a protective overcoat (Spinal) against a salt air environment. They are designed to give maximum reflecting efficiency over the spectral range from 3500Å to 7000Å. The laser fold mirror is coated with a dielectric to peak the reflecting efficiency at 3371Å, the laser emission line. Two additional fold mirrors, external to the telescope and mounted to the pallet, direct the laser beam to the telescope from the laser. These are also coated with the same dielectric to peak the reflection efficiency of 3371Å.

TABLE A-1. SUMMARY OF TELESCOPE ABERRATIONS FOR A 2 MRAD HALF-FIELD-OF-VIEW

ABERRATION	BLUR ANGLE (mrad)
SPHERICAL	$= \frac{1}{128\ (f/No.)^3}$ $= .075$
TANGENTIAL COMA	$= 3\ \alpha/16\ (f/No.)^3$ $= .017$
ASTIGMATISM	$= \alpha^2/2\ (f/No.)$ $= .0004$
TOTAL	.0924

The fold mirrors discussed above each have one axis adjustment (the axis of one being orthogonal to the other) for trimming the laser alignment. Both mirrors are covered with a welded aluminum box sealed at either end to the laser and to the telescope with black felt cemented to the cover.

A baffle is also provided from the output side of the telescope to the laser/image slicer assembly. This baffle is cylindrical and is bolted to the laser bulkhead at one end. The other end has a sliding sleeve with black felt cemented around its edge. This sleeve is cut at an angle to match the spectrometer mount, and the sliding sleeve provides a means of increasing the pressure of the felt against the surface of the spectrometer base to assure a light tight seal.

The telescope tube is a weldment fabricated from .063" thick 6061-T6 aluminum. The tube was made in two sections joined by a sturdy intermediate ring. The upper section mounts the primary mirror, the intermediate ring mounts the fold mirror spider and the lower end interfaces with the main frame. This arrangement allowed the fold mirrors to be aligned independently of the primary mirror and facilitated the entire alignment procedure.

Flanges were welded to both ends of the upper and lower tube and were machined flat and concentric after welding. The inside of the tube was sprayed with a matte black paint and the outside was sprayed with a white enamel and baked. Circular baffles were positioned along the length of both tubes to suppress stray light, as shown in the photograph presented in Figure A-9. The entrance pupil stop is mounted in the circular cutout of the pallet. A cover is provided to cap off the bottom opening in the pallet for protection when the instrument is not is use.

This telescope was designed to react the same load as specified for the main frame. It was assumed that the system would be isolated in the plane of the center of gravity, and therefore no rotational forces would be acting on the unit. The natural frequency of this structure is 55 Hz in a lateral direction.

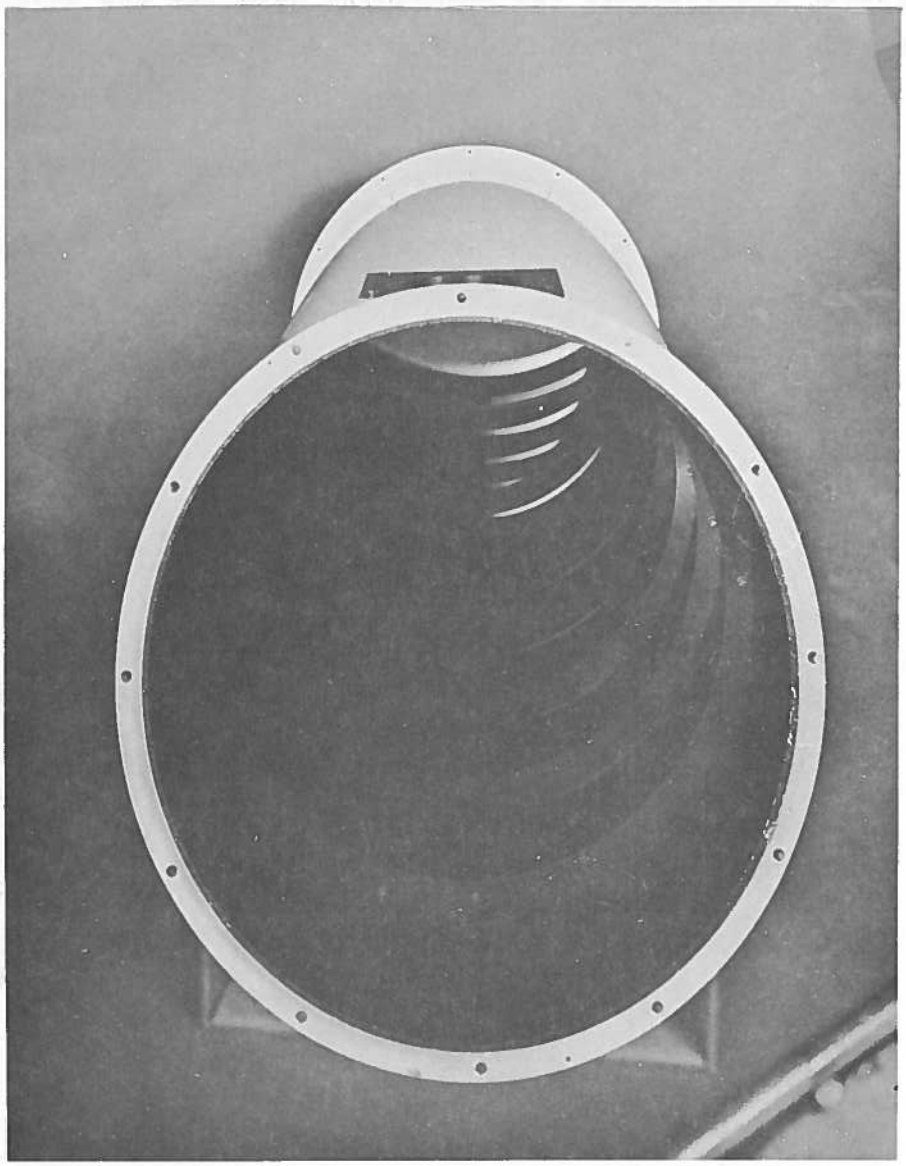

Figure A-9. Upper Section Fluorescence Radiation Optical Receiver - View of Primary Mirror and Baffling

Section A-8 presents the procedures used for the acceptance test and the results obtained during these tests.

A.5 SPECTROMETER AND AUXILIARY OPTICS

The spectrometer design selected for this system is an Ebert-Fastie type with an image slicer in front of the enterance slit to increase the energy throughput. The individual mirrors of the image slicer are positioned at a compound angle relative to the entrance slit. Photographs of this assembly are presented in Figures A-10 and A-11.

The specifications for this spectrometer are presented as follows:

1. Grating: reflective replica, flat grating, Jarell-Ash No. 980-28-40-22, 295 lines mm^{-1}, blaze angle = 4.2°
2. f/No. = 4.7
3. Spectral bandwidth: $\Delta\lambda$ avg. = 102.5Å
4. Linear dispersion: a) $\Delta\lambda/\Delta x$ = 180Å/mm
   b) from 4358Å (Hg V) to 5461Å (Hg G), $\Delta\lambda/\Delta x$ = 178.5A (avg.). The dispersion will vary somewhat across the image plane because of the dependence on the cosine of the diffracted angle.
5. Spectral range at focal plane to spectrometer (tilted 6.9° to align image plane with the tangential astigmatic focal plane): 3500Å to 7000Å.
6. Grating angle of incidence = 30.89°
7. Diffraction angle for 4500Å = 22.37°
8. Wavelength of peak spectral efficiency when used in Ebert type grating mount: 4436Å
9. Peak grating efficiency in Littrow mode: 5500Å

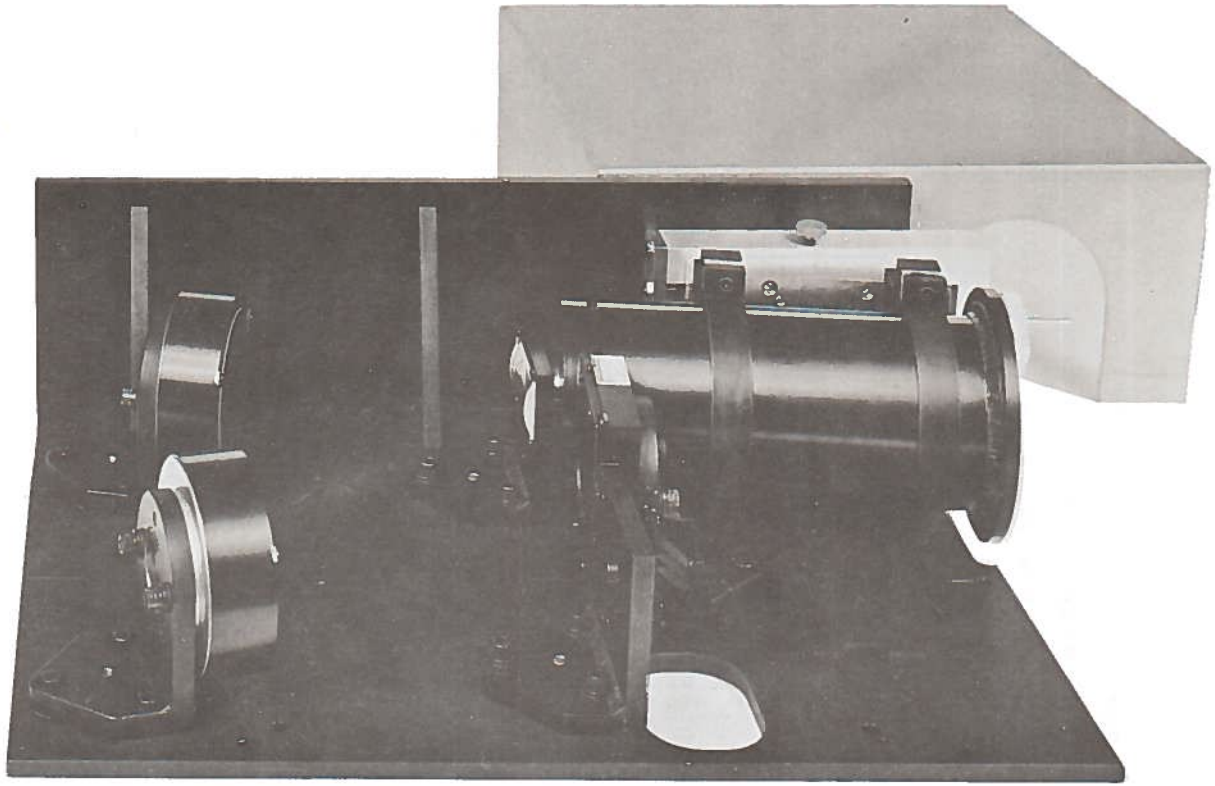

Figure A-10. Spectrometer and Image Slicer Assembly

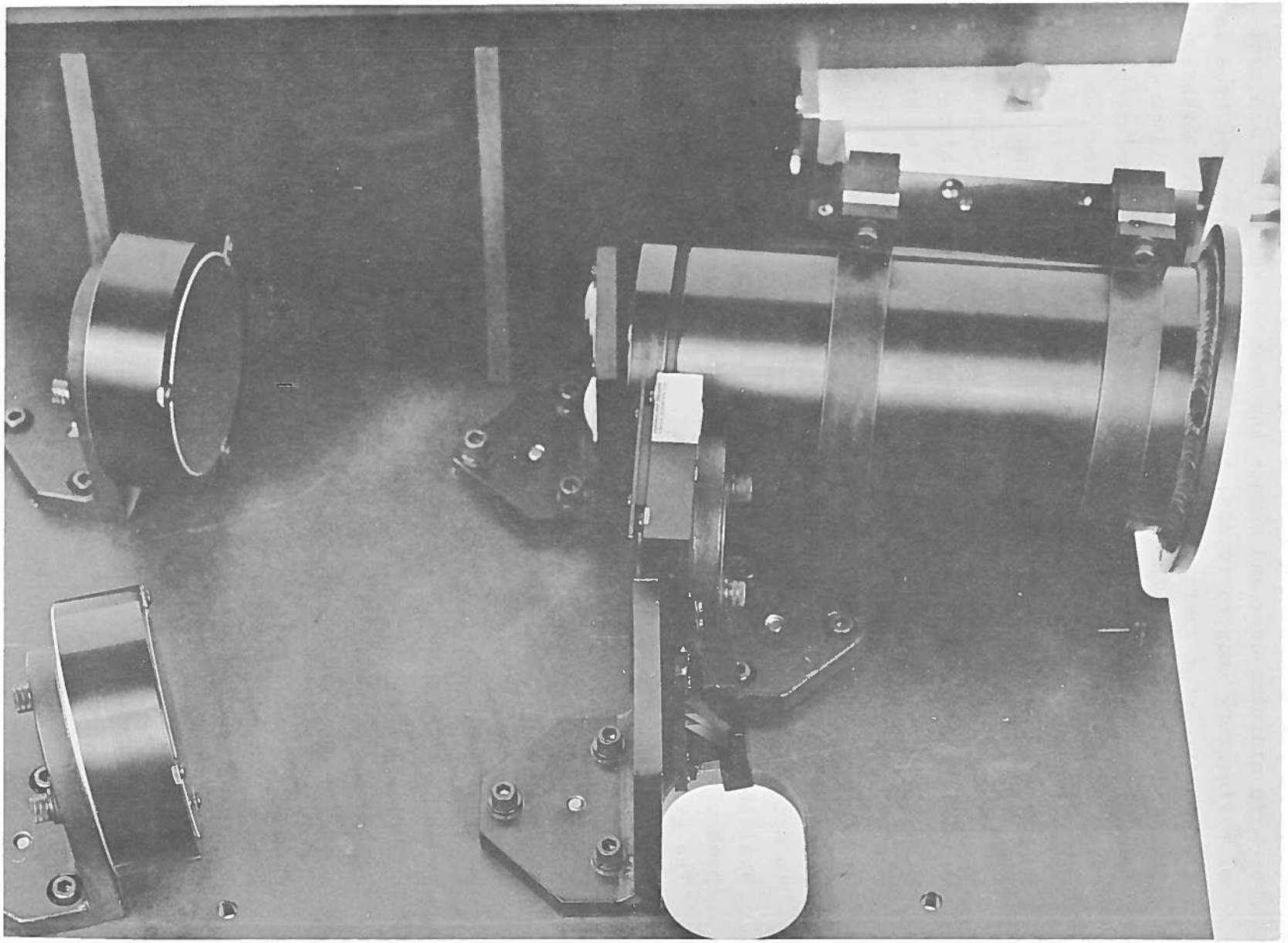

Figure A-11. Closeup of Image Slicer Assembly Mounted in Spectrometer

To minimize cost and reduce the mass of the mirror and minimize vibratory induced forces, two spherical mirrors were used in this spectrometer instead of one, as is often used on conventional Ebert spectrometers. The mirrors have a curvature of 360mm (180mm focal length) and are used in an f/4.7 cone from the telescope. They are coated with aluminum and an overcoat for protection against a salt air atmosphere. The mirrors are secure in a rugged aluminum mount and retained with beryllium copper spring clips.

The diffraction grating was purchased from Jarrel-Ash and is a 295 line mm^{-1} replicated grating made of Pyrex with a blaze angle of 4.2°. This grating was selected since it provided the proper nominal dispersion and a peak efficiency, when used in this system, at about 4500Å. Initially, a trade-off between a Littrow mount was made. One of the reasons for selecting the Ebert, in addition to mechanical packaging problems, was that there was no grating available which could give the desired dispersion as well as a peak efficiency at 4500Å with a reasonably sized optical system. The grating has an aluminum coating, and it was decided not to overcoat because of the resulting loss in efficiency.

A circular blackened mask is positioned over the front of the grating to match the size of the entrance pupil, which is imaged on the face of the grating. This was provided to minimize the effects of stray light which might be reflected from the unused portion of the grating. Imaging the entrance pupil on the grating results in a minimum size for the grating.

The entrance slit is curved in a direction away from the centerline of the instrument and is 0.57mm wide by 18.9mm long. A 4 mrad image of the oil slick will produce an image height 6.3mm (δ = 6.2 x .004 x 25.4 ≈ 6.3mm), but a total of three segments of the oil slick are viewed by the spectrometer via the 3 mirror image slicer mounted in front of the slit, resulting in a total image height of 18.9mm. The width of the slit will provide 100Å resolution at a nominal dispersion of 175Å mm^{-1} at 4500Å. The actual instrument design resulted in a somewhat larger dispersion of 178.5Å at 4500Å, and consequently the spectral resolution is

somewhat larger at about 102.5Å. The slit is also curved away from the centerline of the instrument. The curvature has a radius of 1116.30mm, resulting in a sag of 42 μm relative to the ends of the slit. This slit was chemically etched for precision and pinned in the proper oreientation on the image slicer assembly. The curvature of this slit results in essentially a straight image at the focal plane. Typically, an Ebert-Fastie spectrometer will have a curved image if the entrance slit is straight. Since the exit slit is integral with the image dissector, it must be straight due to electronic scanning requirements.

A two element cylindrical lens is positioned in front of the detector (BFL = 24.817mm on the centerline). The purpose of this lens is to demagnify the length of the slit from 18.3mm to 6.3mm, the length of the aperture on the image dissector. The 0.57mm dimension is unchanged to maintain the spectral resolution. This lens has anti-reflection coatings on all surfaces.

The dimensions for the image were selected to fit within the quality diameter of the photocathode, 0.825 in (the total effective diameter is 1.03 in). The spectral format on the tube is 20mm x 6.3mm.

This dimension will fit the spectral format within the quality diameter of the tube. During the detailed optical design phase for the spectrometer, it was realized that the bands at 3500Å and 7000Å, with a 100Å wide resolution element and a spectral dispersion of 175Åmm^{-1}, would cause some of the energy to spill over beyond the quality diameter of the tube. It was therefore decided to reduce the linear distance between 3500Å and 7000Å from 20mm to 19.49mm to avoid this spillover. This resulted in a slightly higher average dispersion, 180°mm^{-1}, from the nominal 175Åmm^{-1}.

The incidence angle selected was based on that angle which would give a peak efficiency at 4500Å. This occurs when the individual facets of the grating are used in specular reflection. The blaze angle for this grating is 4.2°.

The grating equation is

$$n\lambda = d\ (\sin i - \sin \theta),$$

where n is the diffraction order, λ the wavelength, d the groove width of the grating, i the angle of incidence of light on the grating and θ the diffraction angle. The equation can be solved for the proper incidence angle to position the wavelength of maximum efficiency.

Several trade-offs were made during this design, and an angle of i = 30.89° was selected. This angle results in a wavelength of peak efficiency λ_{max} for n=1 and d=33,900Å given by:

$$\lambda_{max} = \lambda_{max}\, n = 33{,}900\ (\sin 30.89° - \sin 30.89° \cos 8.4° + \cos 30.89° \sin 8.4°) = 4436Å.$$

The diffraction angle is calculated by rearranging the grating equation:

$$\sin\theta = \sin i - \frac{n\lambda}{d}$$

$$= \sin 30.89° - \frac{\lambda}{33{,}900Å}\ .$$

This gives the following diffraction angles:

λ(Å)	3500	4500	7000
θ (deg.)	24.21°	22.37°	17.87°

The theoretical line spread function is shown in Figure A-12. For the center of the exit slit the line spread is only 70μ and at the top of the slit only 125μ. The distribution at the top of the slit is not symmetrical, and hence the bandwidth defined by 50% power points might not be meaningful for this distribution.

The detector was mounted in a ruggedized housing by Perkin-Elmer for the Charles Stark Draper Laboratories. The entire housing was mounted on an accurate slide, which can be adjusted manually to focus the detector. A wedge was fabricated to tilt the detector 6.5° so that it is aligned with the tangential astigmatic focal plane of the spectrometer. This will give the best imagery, since the minimum dimension of the tangential astigmatic blur is aligned with the resolution direction of the spectrometer.

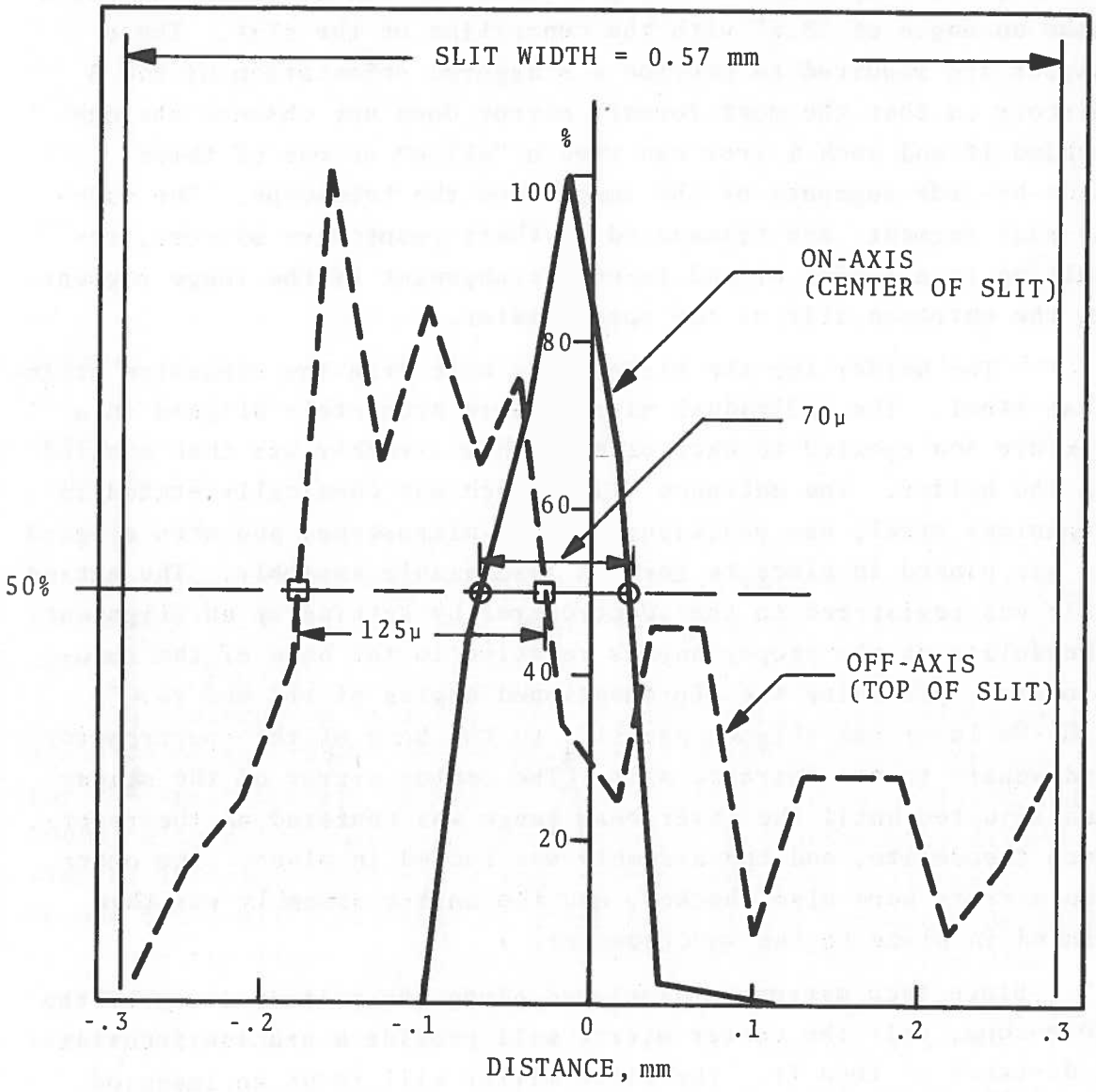

Figure A-12. Theoretical Line Spread Function of the Spectrometer

The principal ray from the telescope makes an angle of 11° with the plane of the entrance slit when viewing the slicer mirrors edge on. When the plane of the slit is viewed in a perpendicular direction, the projection of the principal ray out of this plane will make an angle of 23.6° with the centerline of the slit. These angles are required to provide a staggered orientation of the 3 mirrors so that the most forward mirror does not obscure the one behind it and each mirror can view a "slice" or one of three side-by-side segments of the image from the telescope. The side-by-side segments are transposed by their respective mirrors, resulting in a series or end-to-end arrangement of the image segments on the entrance slit of the spectrometer.

The holder for the mirrors was made from low expansion stainless steel. The individual mirrors were accurately aligned in a fixture and epoxied to each other. This assembly was then epoxied in the holder. The entrance slit, which was chemically etched in stainless steel, was positioned with a microscope, and when aligned it was pinned in place to form an inseparable assembly. The entire unit was registered to the spectrometer by setting up an alignment theodolite at the proper angles relative to the base of the spectrometer, providing the aforementioned angles of 11° and 23.6°. A He-Ne laser was aligned parallel to the base of the spectrometer and square to the entrance slit. The center mirror of the slicer was adjusted until the laser beam image was centered on the reference theodolite, and the assembly was locked in place. The other two mirrors were also checked, and the entire assembly was then pinned in place to the spectrometer.

Since each mirror is displaced along the principal ray of the telescope, only the center mirror will provide a precise focus at a distance of 1000 ft. The first mirror will focus an image on the slit at 3660 ft and the third mirror (furthest from the telescope) will provide a focus at 595 ft. Therefore, there will be a loss of some energy in these two mirrors when flying at 1000 ft due to the blur resulting from the out-of-focus positions.

The test procedure acceptance test results for the spectrometer and image slicer assembly are presented in Section A-8.

A.6 COMBINATION CAMERA/VIEWFINDER OPTICAL MODULE

The specification for this assembly required that visual monitoring be allowed in both a wide and narrow field-of-view, as well as permitting a photographic recording of the scene. A photograph of this optical module is presented in Figure A-13. A ruggedized 35mm camera, made by the Robot Photo and Electric Co. (West Germany) and distributed by Karl Heitz in the U.S., was selected. This camera has been widely used by the military and NASA for Airborne and Sounding rocket applications. The model selected was the Motor-Recorder Model 26BE, which incorporates a solenoid actuated shutter and motor driven film advance. The shutter in this camera is an extremely rugged all-metal rotary unit. This type of shutter, though, eliminated the possibility of a reflex system and required separate viewfinders for the lenses. The film format for this camera is 24 x 36mm and utilizes standard 35mm film.

In addition, a secondary optical system is incorporated into the camera, which superimposes an 8 x 8mm image in the corner of the negative. This second optical system views a clock and a data block with an erasable white surface to inscribe the date.

The camera is mounted into a Robot holder which supports the data block and clock in proper registration to the second optical system. This data block is automatically illuminated by two bulbs when the shutter of the camera is actuated. The intensity of the illumination is adjusted by a rheostat mounted on the holder.

A 100-foot magazine with a capacity of 800 frames is provided. This magazine was selected over a larger unit with twice the capacity because the larger unit was position sensitive and jammed quite easily, depending upon its orientation. The 100-foot roll is also a standard size, whereas the larger 200-foot roll would have required loading from a bulk roll in a dark room. The magazine can be removed from the camera in daylight, since the film chamber is automatically sealed when removed from the camera.

The unit requires a 24 volt D.C. power supply and draws about one-half amp. A pushbutton is provided for remote actuation. The

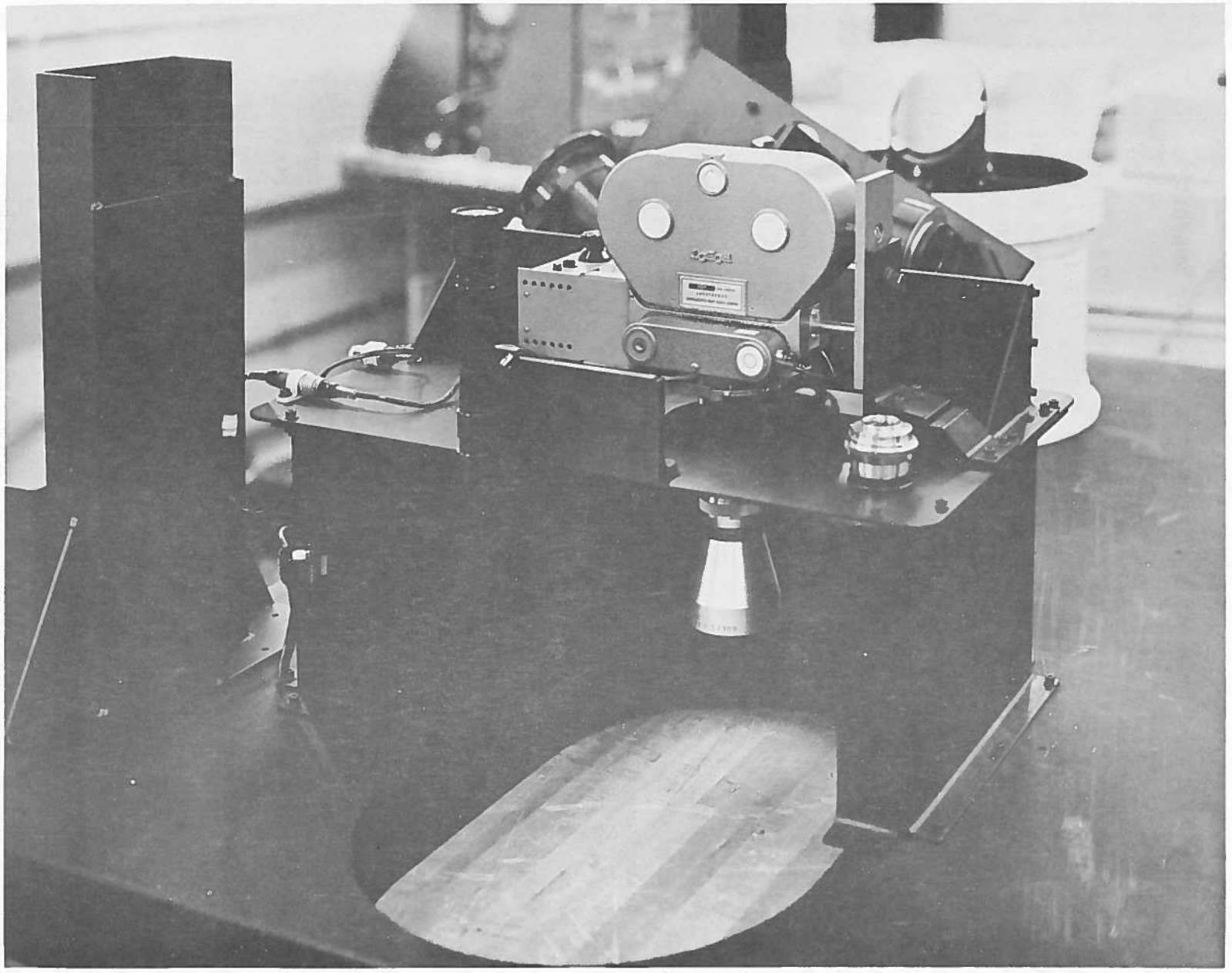

Figure A-13. Combination Camera/Viewfinder Mounted on Main Frame

pushbutton is stowed in a clip mounted on the module support structure.

Two lenses are provided, one a standard Xenon 50mm, f/1.9 lens, and the other a telephoto Tele-Xenar 300mm, f/5 lens. The 50mm lens has a FOV of 27.0° x 38.0°, and the 300mm lens has a FOV of 4.5° x 6.5°. These lenses are secured to the camera with a locking bayonet mount. Replacement of these lenses is accomplished quite easily by actuating a lever protruding above the camera body at the base of the lens. The lens is grasped in one hand as the lever is actuated and removed downward until it clears the mounting's structure. To avoid the danger of dropping the lens through the port in the main frame an aluminum cover has been provided which fits between the stand-offs of the support structure and covers the opening.

A standard Robot viewfinder was used for operation with the 50mm lens. This viewfinder does not magnify but simply frames the 24 x 36mm format. It clips into a standard camera accessory shoe mounted to a bracket on the front of the support structure. This unit also incorporates a thumbscrew which tilts the viewfinder relative to its base to correct for parallax. Since the target will be essentially at infinity, this unit was set parallel to the optical axis of the lens.

There was no commercially available viewfinder for the telephoto lens; therefore, a rifle telescope was purchased which had an adequate field angle of at least 7.9° to match the diagonal of the 4.5° x 6.5° FOV of the lens. A B&L Baltur A rifle telescope with a magnification of 2-1/2X met this requirement. A modification of this scope was made by inserting a special reticle to frame the 35mm format. This reticle, presented in Figure A-14, positions the eye at the exit pupil as well as provides a cushion during vibration. This telescope was mounted alongside the viewfinder for the 50mm lens. The camera and viewfinders were aligned parallel to the optical axis of the telescope.

Also supplied with the unit was a ground glass viewer permitting the viewing of the image at the focal plane of the camera. By

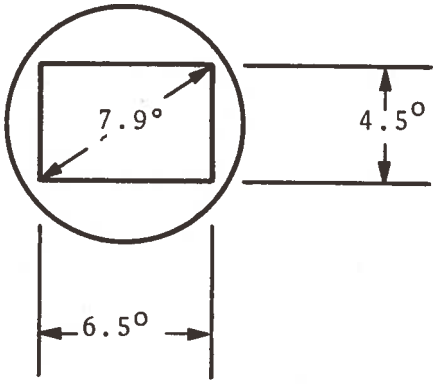

6.5° @ 100 YD = 34.1 FT
4.5° @ 100 YD = 23.6 FT
7.9° @ 100 YD = 41.6 FT

Figure A-14. Bausch & Lomb Baltur A (2-1/2X) Telescope Reticle Pattern Requirements

setting the shutter open the positioning of the camera and the FOV of the lens can be checked with this device.

A.7 SUGGESTED MODIFICATIONS

Since the laser beam forming module mounted at the rear end of the laser results in a greater power loss than anticipated, it is suggested that the laser collimation be accomplished at the front end of the laser. With the proper design, all the energy (neglecting coating efficiency) in the 60 mrad beam could be collected and reimaged at the proper distance, which, for this instrument, was selected as 1000 feet. In principle the 4 x 60 mrad output beam from the laser could be transformed into a beam illuminating a 4 x 4 foot region at a 1000 feet by use of a cylindrical lens of 500 in focal length and a 2 in x 30 in aperture. This large system would be completely unacceptable, but by slicing the output beam into several segments and by the use of fold mirrors, the optical system could be made small enough so that it could be packaged into a module which is compatible with the existing instrument. In fact, a nominal amount of focus could probably be achieved by providing a movable cylindrical lens. The focusing requirement has not been studied in any depth and would require consideration of the telescope's focus as well, since it images the spectrometer slit at a distance of 1000 feet as presently conceived. The following discussion presents a concept for the front end beam forming module which would adapt to the present instrument configuration.

A.7.1 FRONT END LASER TRANSMITTER BEAM FORMING OPTICAL MODULE

The optical system for transmitting the laser beam is illustrated in Figure A-15. The system is composed of a Bowen image slicer, mirrors, and cylindrical lens objective. A detailed sketch of the image slicer, with the fold mirrors deleted for clarity, is shown in Figure A-16. The image slicer is positioned at the laser aperture and will be mounted to the laser face as a sub-module. The mirrors of the slicer could be individually coated with a dielectric to peak the reflection efficiency at 3371Å to about 99%. The dimensions shown in this figure are compatible with the existing instrument.

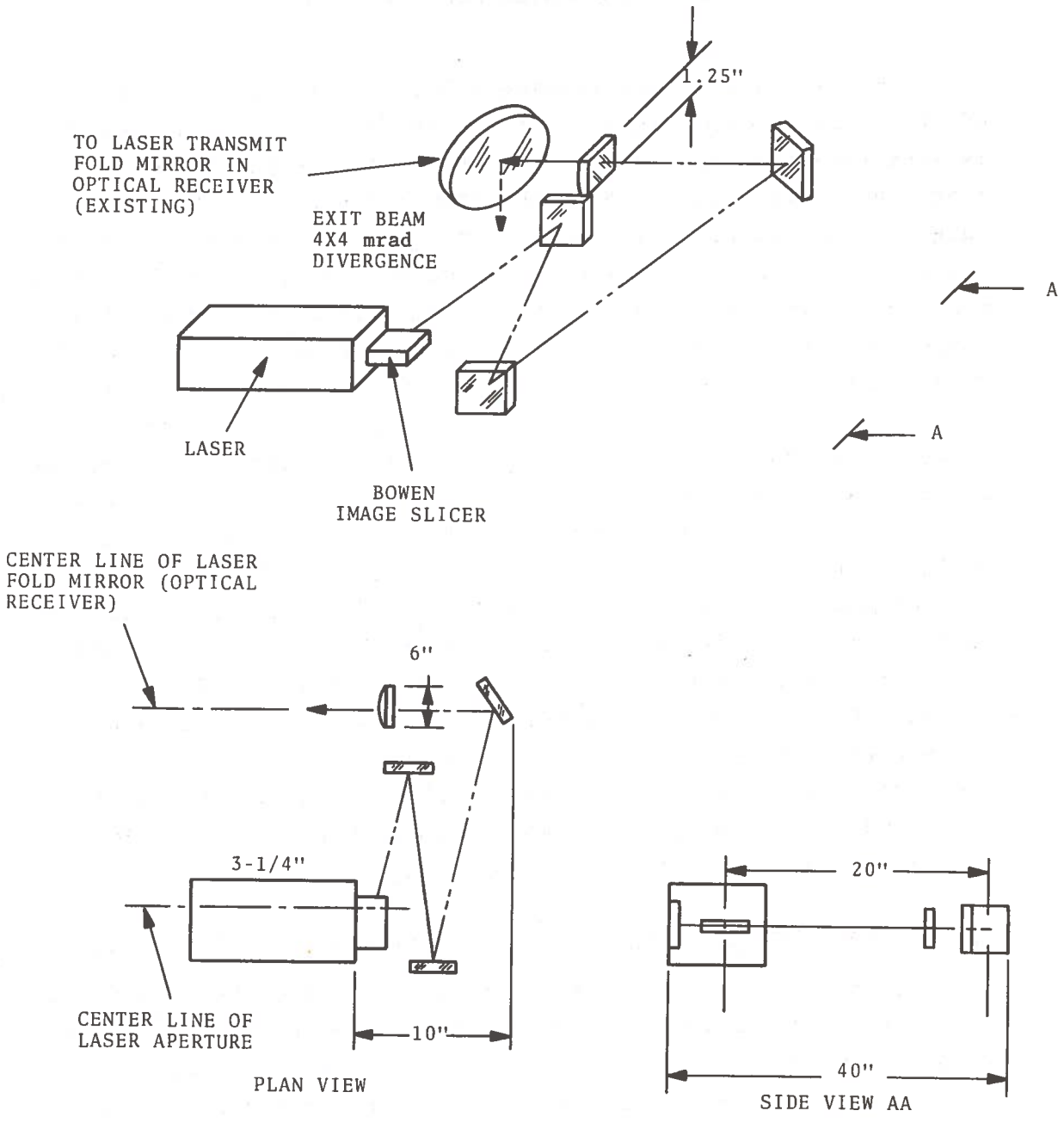

Figure A-15. Laser Transmitter Optics Image Slicer-Cylindrical Lens-Objective

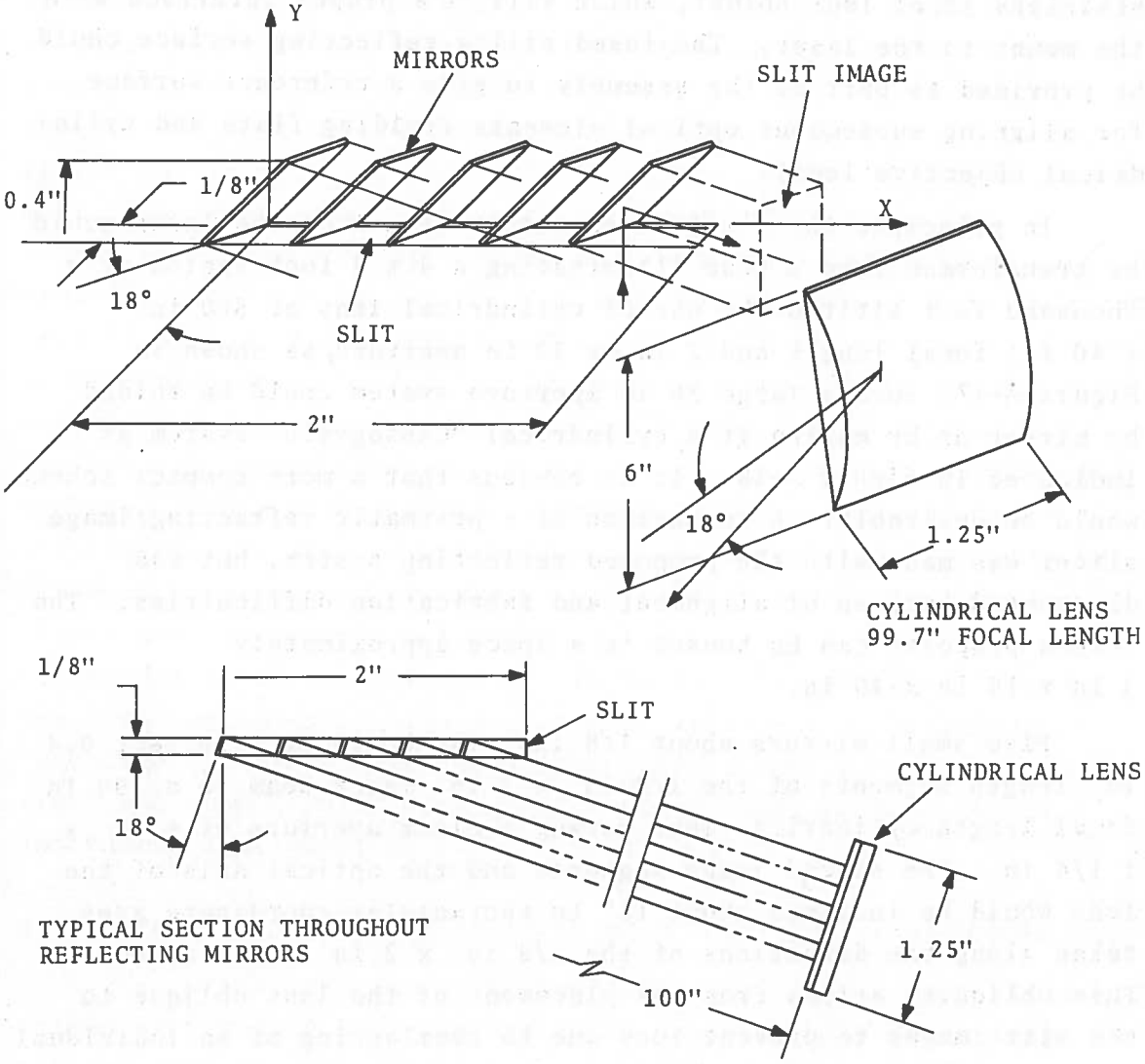

Figure A-16. Bowen Image Slicer Laser

Spacer blocks would be ground from fused silica to obtain the proper registration of one mirror relative to the other. The mirrors and spacer blocks would be aligned and then bonded together. The entire optical assembly will be mounted in a low expansion stainless steel lens holder, which will be a proper interface with the mount to the laser. The fused silica reflecting surface could be provided as part of the assembly to give a reference surface for aligning subsequent optical elements (folding flats and cylindrical objective lens).

In principle the 4 x 60 mrad output beam from the laser could be transformed into a beam illuminating a 4 x 4 foot region at a thousand feet altitude by use of cylindrical lens of 500 in (~40 ft) focal length and 2 in by 30 in aperture, as shown in Figure A-17. Such a large 30 in aperture system could be folded by mirror or by making it a cylindrical "Cassegrain" system as indicated in Figure A-18. It is obvious that a more compact scheme would be desirable. A comparison of a prismatic refracting image slicer was made with the proposed reflecting system, but was discounted because of alignment and fabrication difficulties. The system proposed can be housed in a space approximately 3 in x 10 in x 40 in.

Five small mirrors about 1/8 in wide would each reflect 0.4 in length segments of the 1/8 in x 2 in laser beam to a 100 in focal length cylindrical lens having a clear aperture of 6 in x 1 1/4 in. The sliced image segments and the optical axis of the lens would be inclined about 18° to rectangular coordinate axes taken along the directions of the 1/8 in x 2 in laser window. This obliquity arises from the placement of the lens oblique to the slit images to prevent loss due to overlapping of an individual mirror into the beam path from the image to its rear.

The fused silica lens would have a thickness of about five millimeters. Since fused silica transmits about 93% per centimeter thickness at wavelengths of 3371Å, losses in this lens would be slight. Careful attention to the geometry and fabrication of the individual slicer mirrors, which would be assembled in a solid cemented module, would ensure that vignetting losses due to their geometry with respect to the reflected beams would be

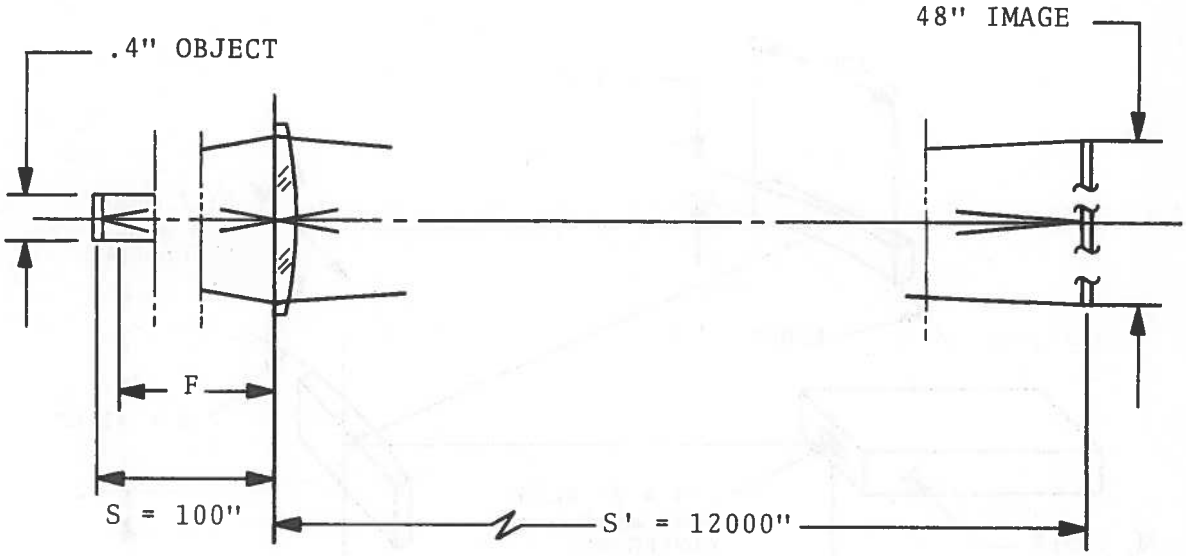

Figure A-17. Cylindrical Lens Ray to Transform Rectangular Laser Output Beam into a Square Beam

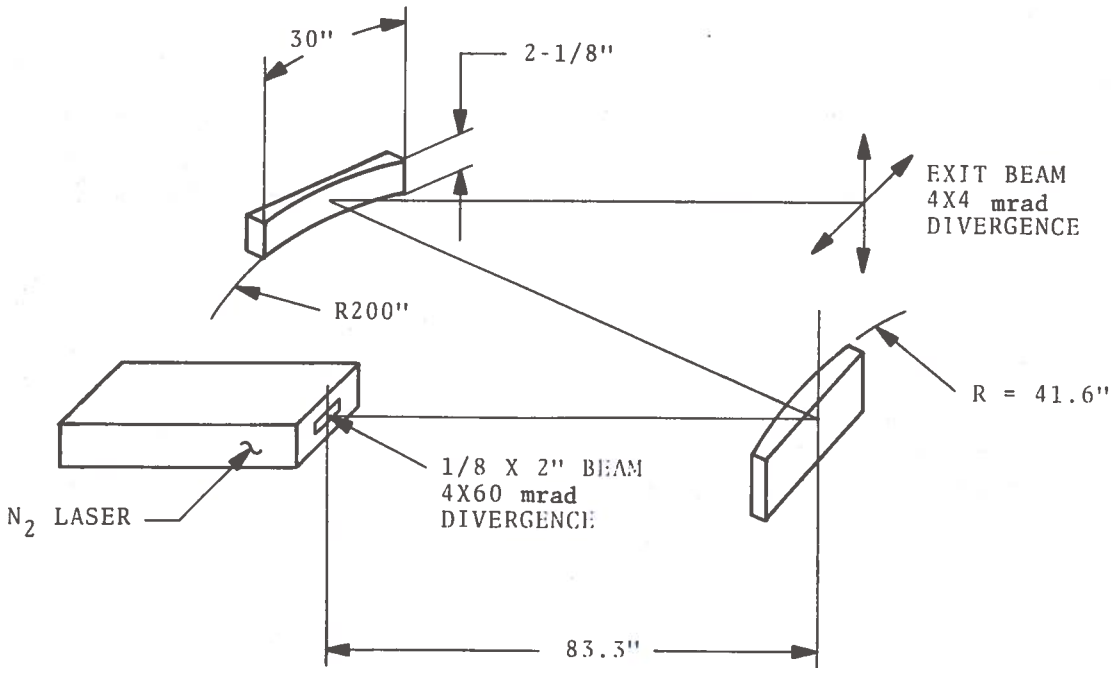

Figure A-18. Proposed Cylindrical "Cassegrain" System Laser Transmitter to Implement Laser Beam Forming Optics

minimal. The mirrors would have sharp proper bevels at the facet which crosses the laser window. The inclined side of the mirror adjacent to the light beam would also be properly beveled to avoid vignetting.

The required focal length of the cylindrical lens is determined by considering the required magnification and applying the standard lens formula as follows:

$$\text{Required magnification} = m = \frac{48 \text{ in}}{0.4 \text{ in}} = 120$$

$$m = \frac{S'}{S}$$

S = Object Distance

S' = image distance = 1000 (12 in) = 12,000 in

$$S = \frac{12{,}000 \text{ in}}{120} = 100 \text{ in}$$

$$\frac{1}{f} = \frac{1}{S} + \frac{1}{S'} \quad \frac{1}{100} + \frac{1}{12{,}000}$$

f = 99.17 in

One of the slices most remote from the central slice differs in distance from the lens compared to the central slice by 0.8 in and will consequently project with a differing divergence of 0.8% or 4 (0.008) = 0.032 mrad with the projection distance or focal length of about 100 inches. It can also be concluded, therefore, that small longitudinal changes in the projection geometry such as may be due to thermal or other causes are insignificant.

An obvious possible advantage of the image slicer technique that could be utilized if desired in this or a later configuration would be projecting each slice separately onto the identical area of the oil slick in such a fashion as to match precisely the slope and location of the entrance slit of the monochromator, as projected by the Newtonian telescope. This could result in a significant increase in signal strength by matching the shape of the illuminated area to the projected images of the monochromator slit, as viewed by the 3 image slicer mirrors. This would require a proper system study to match appropriate parameters of the several modules involved.

A.8 SYSTEM ACCEPTANCE TESTS

A.8.1 FOCUSING OF FLUORESCENCE RADIATION OPTICAL RECEIVER AT 1000 FEET

a. A telescope which has been previously focused at 1000 ft will be used as the reference for aligning the Optical Receiver. The reticle of this reference telescope will be viewed with an alignment telescope. This alignment telescope will be focused on the reticle of the reference telescope, as shown in Figure A-19.

b. A tungsten light source will be positioned in back of the pin hole set at the focus of the alignment telescope to illuminate the pin hole. The light projected from this telescope will be divergent, and these rays will illuminate the Optical Receiver. This will simulate a target at 1000 ft and the focus of these rays by the Optical Receiver will correspond to the focus of an object at 1000 ft, as shown in Figure A-20.

c. The alignment telescope will be positioned beneath the main frame and will view a fold flat placed directly below the entrance pupil of the Optical Receiver. The alignment telescope will be registered to the Optical Receiver, as shown in Figure A-21.

A.8.2 VERIFICATION OF ALIGNMENT OF SPECTROMETER AND AUXILIARY OPTICS WITH FOCUS OF OPTICAL RECEIVER

The fold mirror assembly and upper telescope tube will be replaced. (Note that all parts are pinned for registration.) A microscope will be positioned so that it is focused on the entrance slit of the spectrometer, and its reticle will be aligned to the center of the slit, which is illuminated by the middle mirror of the 3-mirror image slicer. In order to center the microscope reticle at the center of the entrance slit, a fine thread has been precisely positioned across the center of the slit. This operation

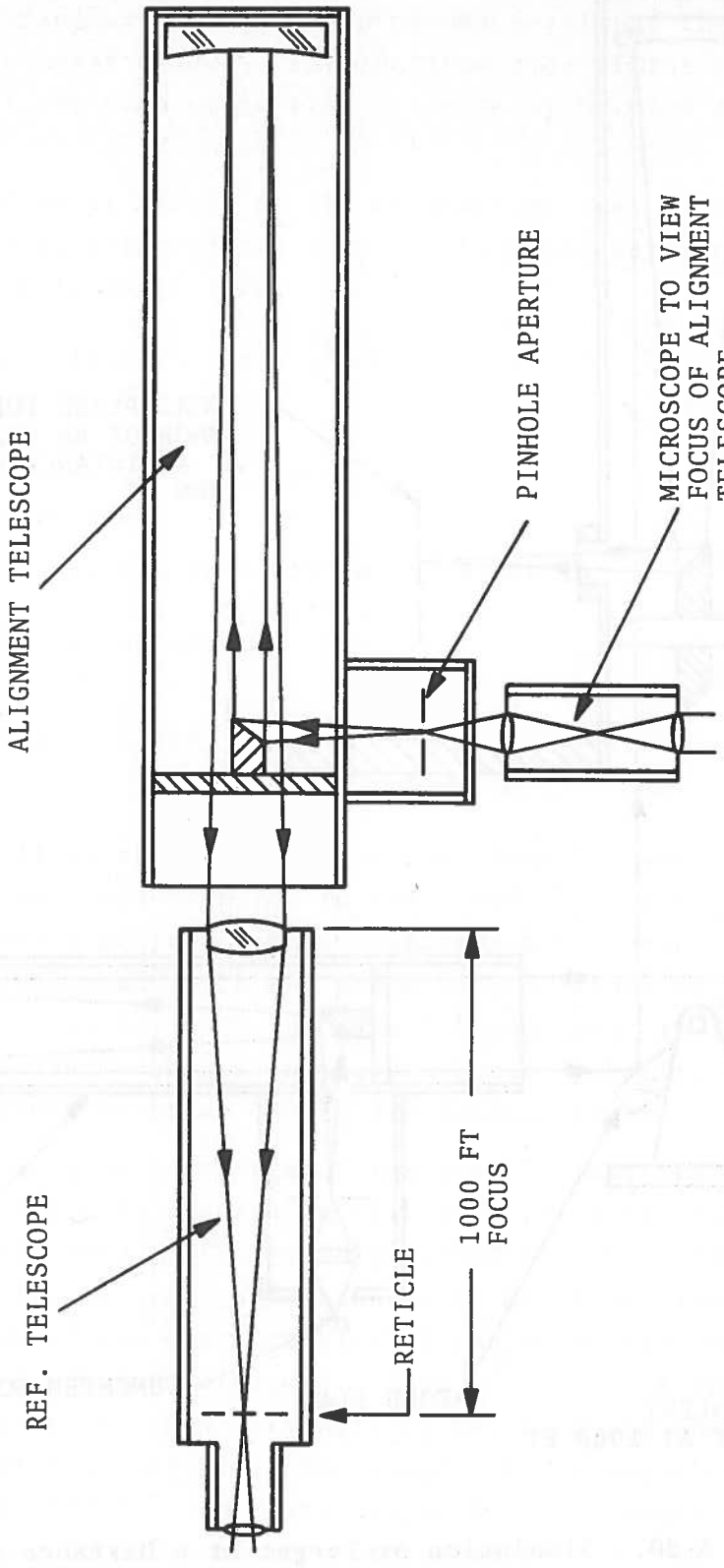

Figure A-19. Setting of Alignment Telescope

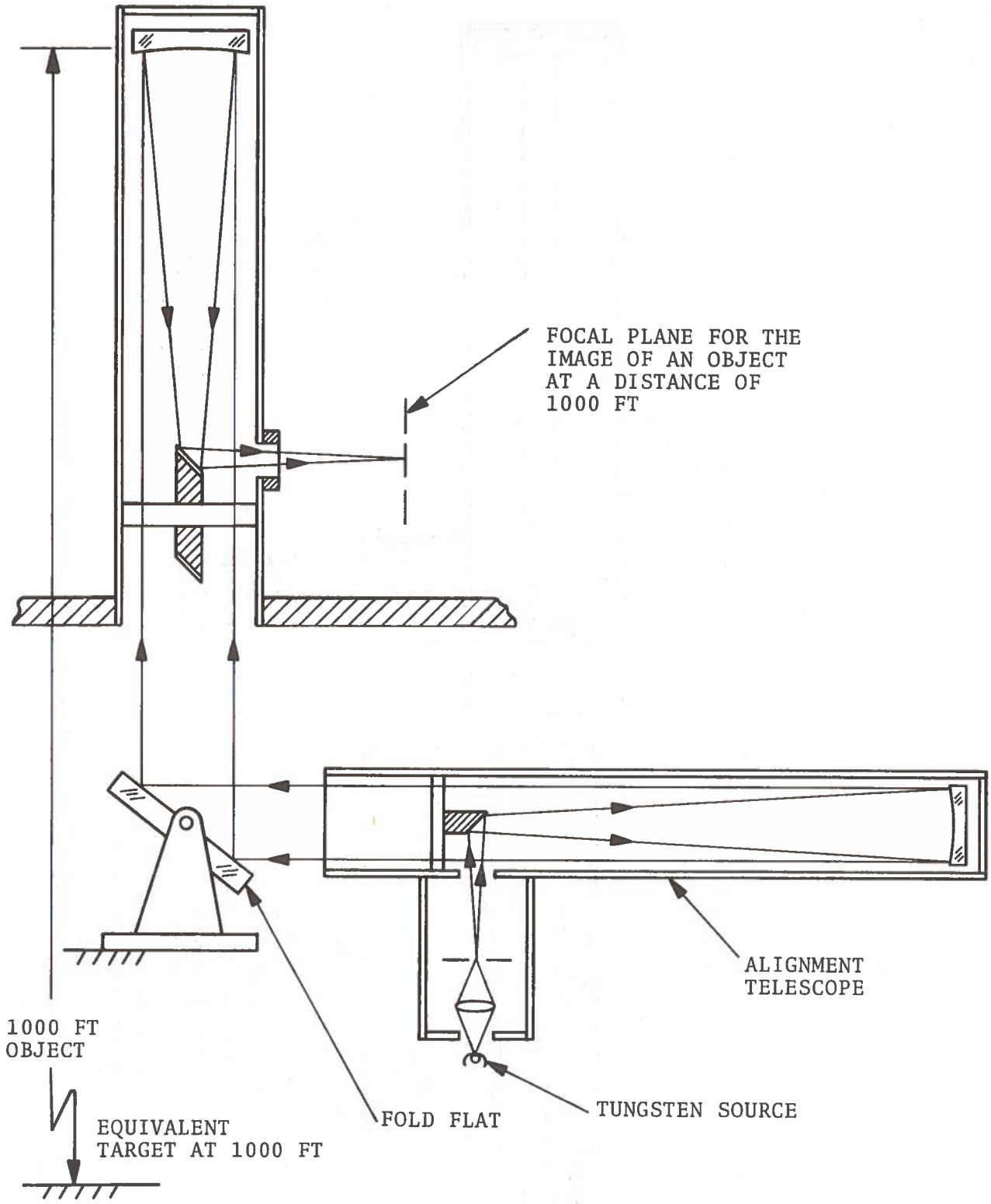

Figure A-20. Simulation of Target at a Distance of 1000 Ft

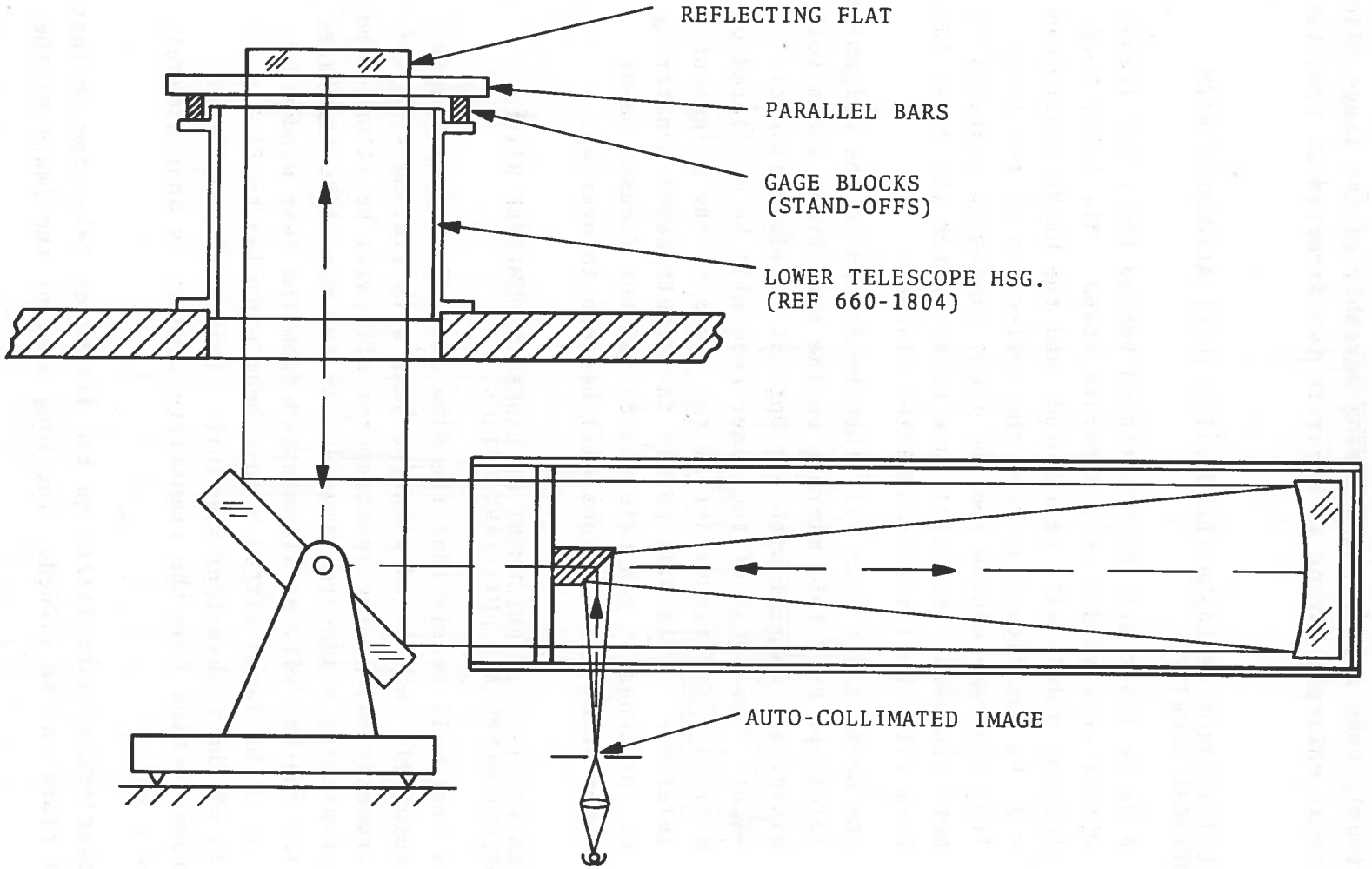

Figure A-21. Registration of Alignment Telescope with Optical Receiver

had previously been accomplished during assembly of the image slicer on an optical enlarger having an accurate two directional translation stage.

A.8.3 VERIFICATION OF LASER TRANSMITTER (GFE) ALIGNMENT WITH OPTICAL RECEIVER

a. A He-Ne laser will be positioned behind the Laser Transmitter rear window on a separate stand. The Laser Beam Forming Module will be removed, and the He-Ne Laser beam will be positioned so that the reflection of the laser from the rear window and the front window is centered on both windows. This will have bore-sighted the He-Ne laser beam with the laser transmitter channel.

b. The He-Ne laser beam will then be folded to the alignment telescope by 2 fold mirrors on the main frame and a fold mirror set coaxial with the Optical Receiver line-of-sight. The focus of the laser beam will be monitored on a translucent target set at the focus of the alignment telescope. This will permit the simultaneous monitoring of the tungsten pin hole source and the focused He-Ne laser beam. Both images will be seen to overlap.

A.8.4 VERIFICATION OF ALIGNMENT OF LASER TRANSMITTER WITH SPECTROMETER AND AUXILIARY OPTICS

This test will verify that the 51mm axis of the laser aperture is angularly registered with the long axis (18.9mm side) of the spectrometer slit. The spectrometer slit will be illuminated from the rear with a tungsten source. At the same time the laser transmitter channel will be illuminated from the rear window by means of an He-Ne laser fitted with a beam expander to fill a 1-inch width of the transmitter aperture. This will provide an output cross-section from the transmitter, which is approximately 1/8 in by 1 in.

An eyepiece will be fitted on the alignment telescope so that the focal plane can be viewed. The long axis of the image of the

laser beam and the long axis of the spectrometer entrance slit will be seen to be oriented in the same direction.

APPENDIX B

OPTICAL MULTICHANNEL SPECTRAL ANALYZER

This appendix is based on material from the OPTICAL MULTICHANNEL SPECTRAL ANALYZER, FINAL TECHNICAL REPORT R-756, March 1973, prepared by the Charles Stark Draper Laboratory, Massachusetts Institute of Technology, Cambridge, Massachusetts under U.S. Government Contract DOT-TSC-350 for the U.S. Department of Transportation, Transportation Systems Center, Optical Devices Group.

TABLE OF CONTENTS

B.1 INTRODUCTION

This Appendix describes the design features and operations of the image processor section of the system for Experimental Remote Oil Detection and Classification (ERODAC). The image processor, identified as the Optical Multichannel Spectral Analyzer (OMSA), was designed and fabricated at the C.S. Draper Laboratory under contract to the Transportation Systems Center of the Department of Transportation.

B.2 PRINCIPLES OF OPERATION

B.2.1 INTRODUCTION

The OMSA consists basically of an image dissector to scan the fluorescence spectral image produced by the spectrometer and a signal processing section with supporting electronics (see Figure B-1). The layout of the OMSA front panel is shown in Figure B-2.

The OMSA has been designed to provide a practical means to automate the detection of an oil spill and to process the spectral content of the laser excited oil fluorescence into a usable form for display and/or computer analysis. In this phase of design, the OMSA is not capable of classifying oil in spills; however, all of the required outputs are provided such that the OMSA can interface with a mini-computer to perform this operation.

A basic guideline in designing the OMSA was the provision of maximum flexibility in the areas of gain, range gate width, detection channels, detection thresholds, etc.

The OMSA operates in three modes: calibration (CAL.), detection (DETECT.), and classification (CLASS.). A brief description of these operational modes follows.

B.2.2 DESCRIPTION

The principles of operation of the OMSA can be better described refering to one cycle of operation. The operational flow diagram is given in Figure B-3 and the block diagram of the OMSA is given in Figure B-4.

The cycle starts with the selection of the Channel (1-35). Depending on the mode of operation, the timing logic will interrogate one of the following channel registers and load the contents of that register into the CHANNEL buffer:

CAL. mode: contents of BAND SELECT

DETECT. mode: contents of CHANNEL A BAND or CHANNEL B BAND, alternately

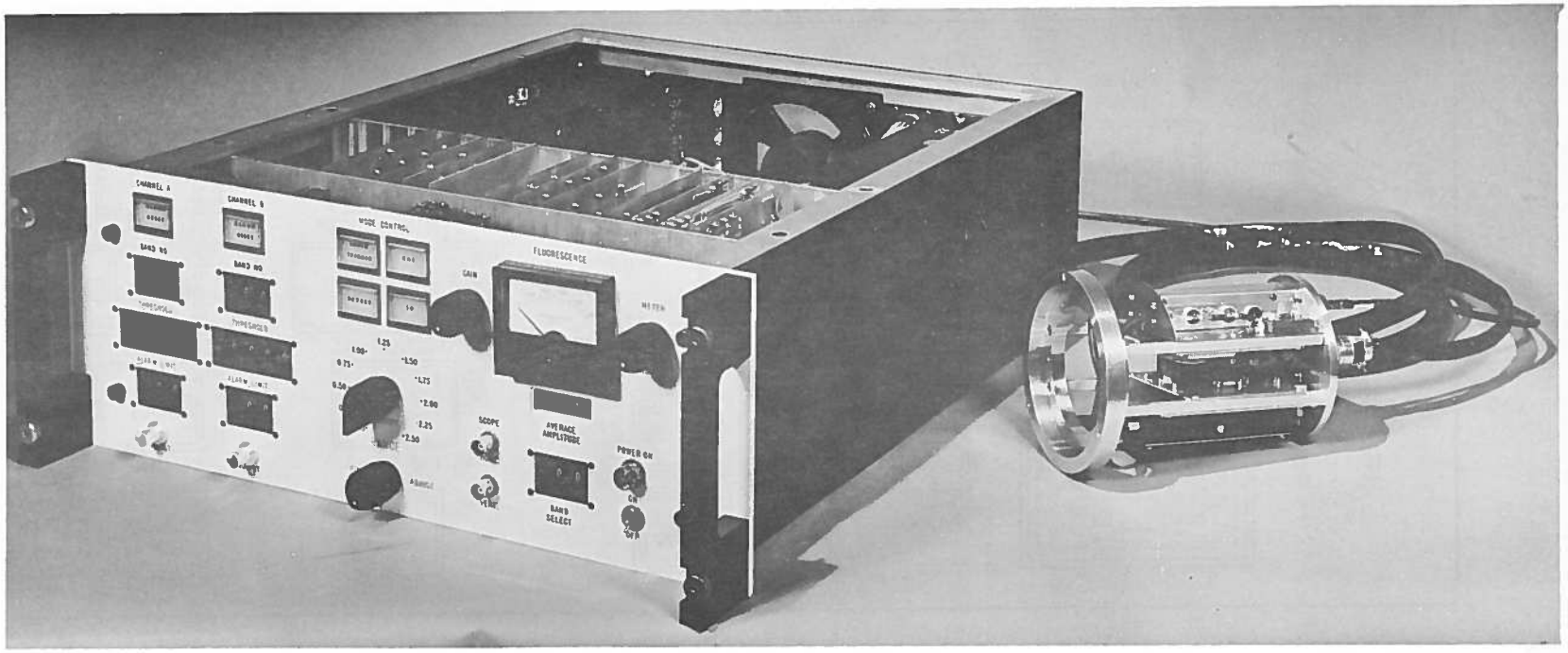

Figure B-1. Optical Multichannel Spectral Analyzer (OMSA)

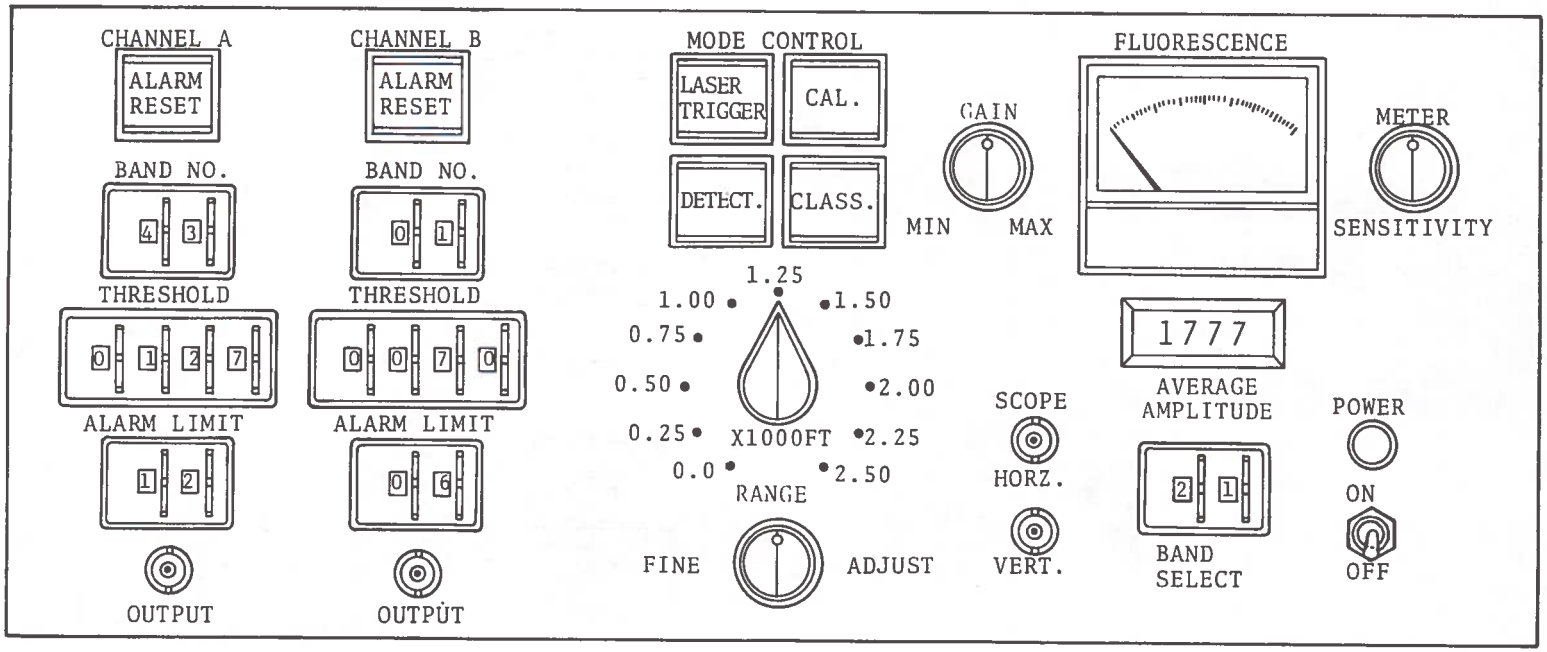

Figure B-2. Layout of the OMSA Front Panel

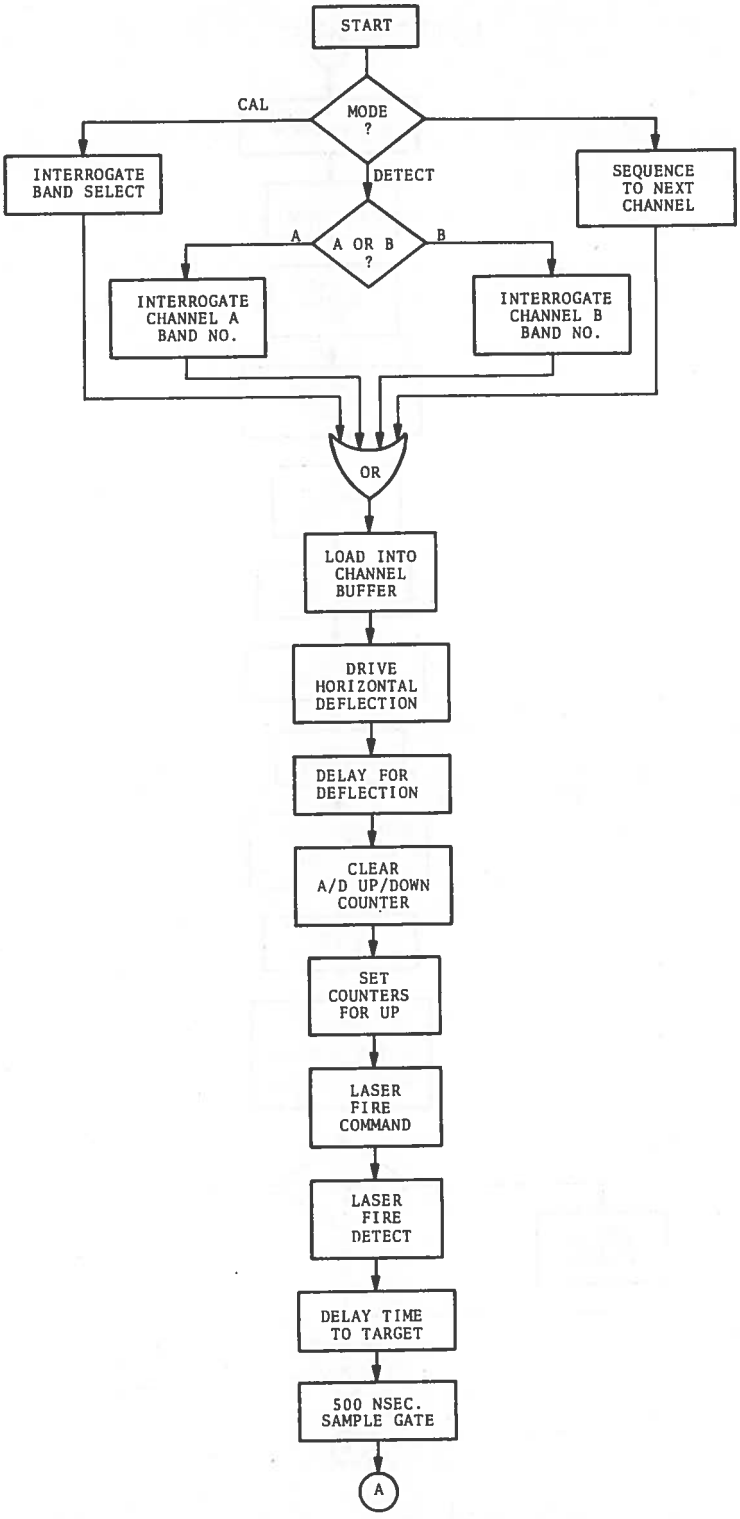

Figure B-3a. Operational Flow Diagram of the OMSA

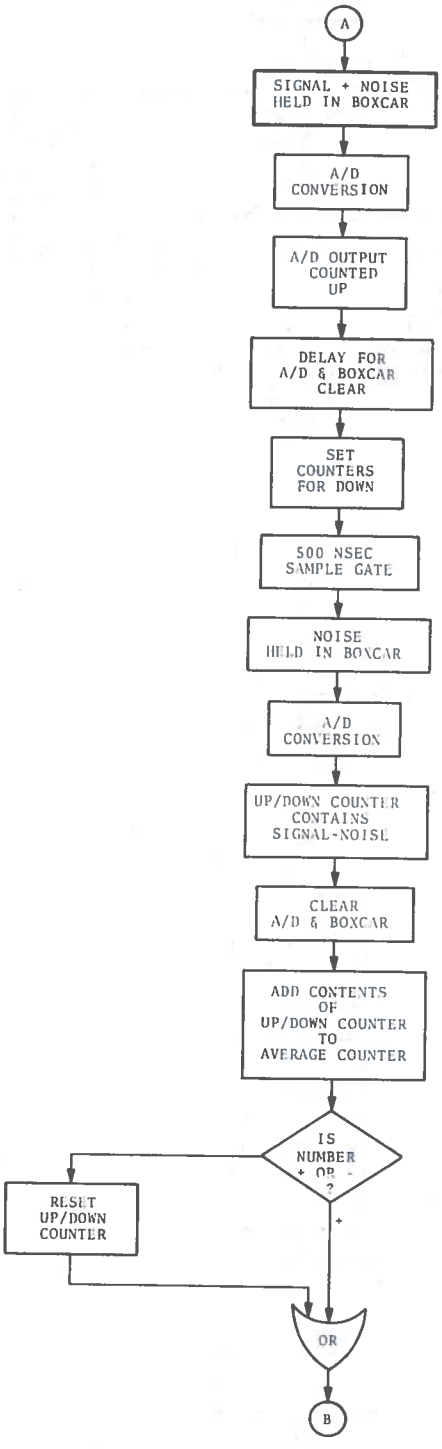

Figure B-3b. Operational Flow Diagram of the OMSA (Continued)

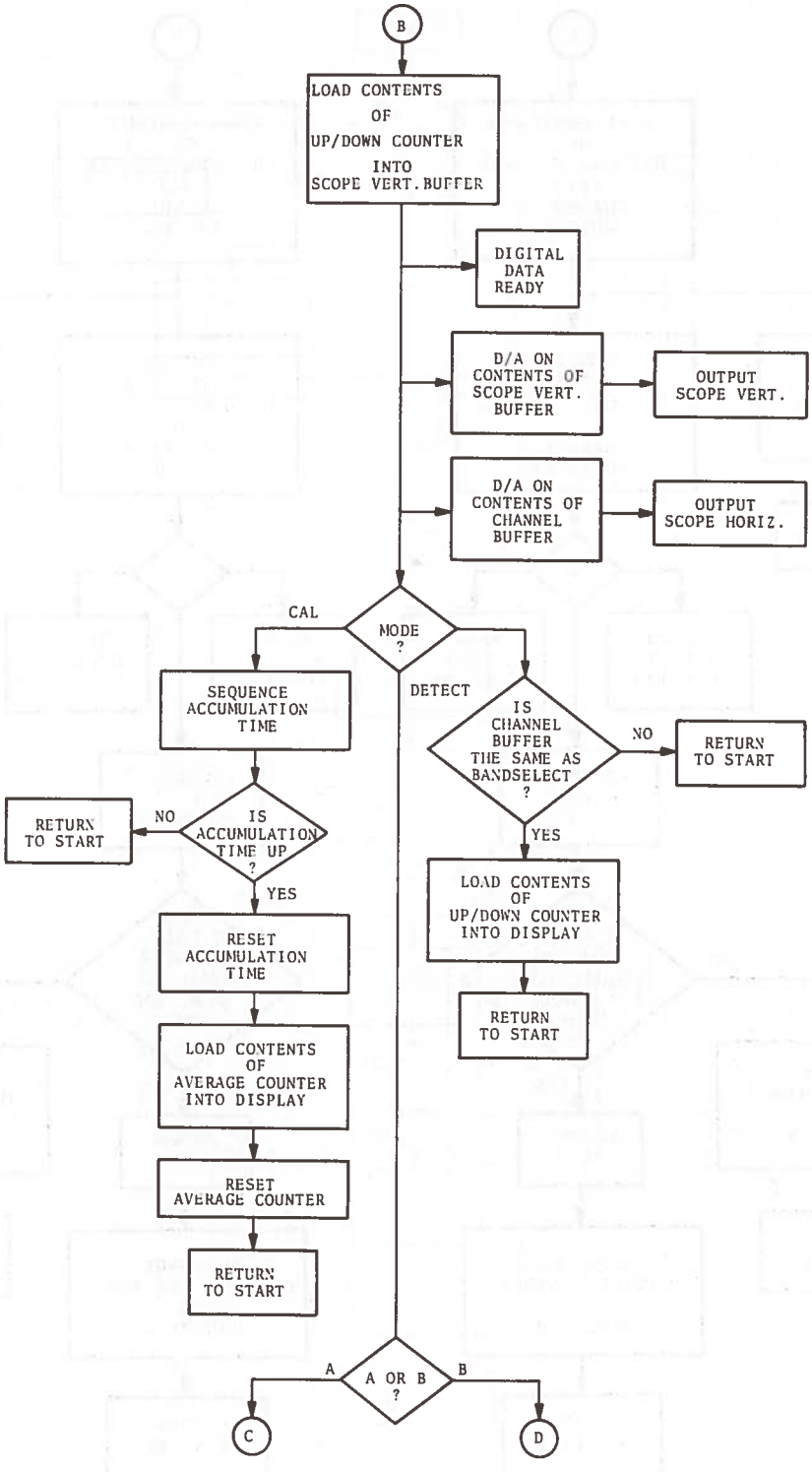

Figure B-3c. Operational Flow Diagram of the OMSA (Continued)

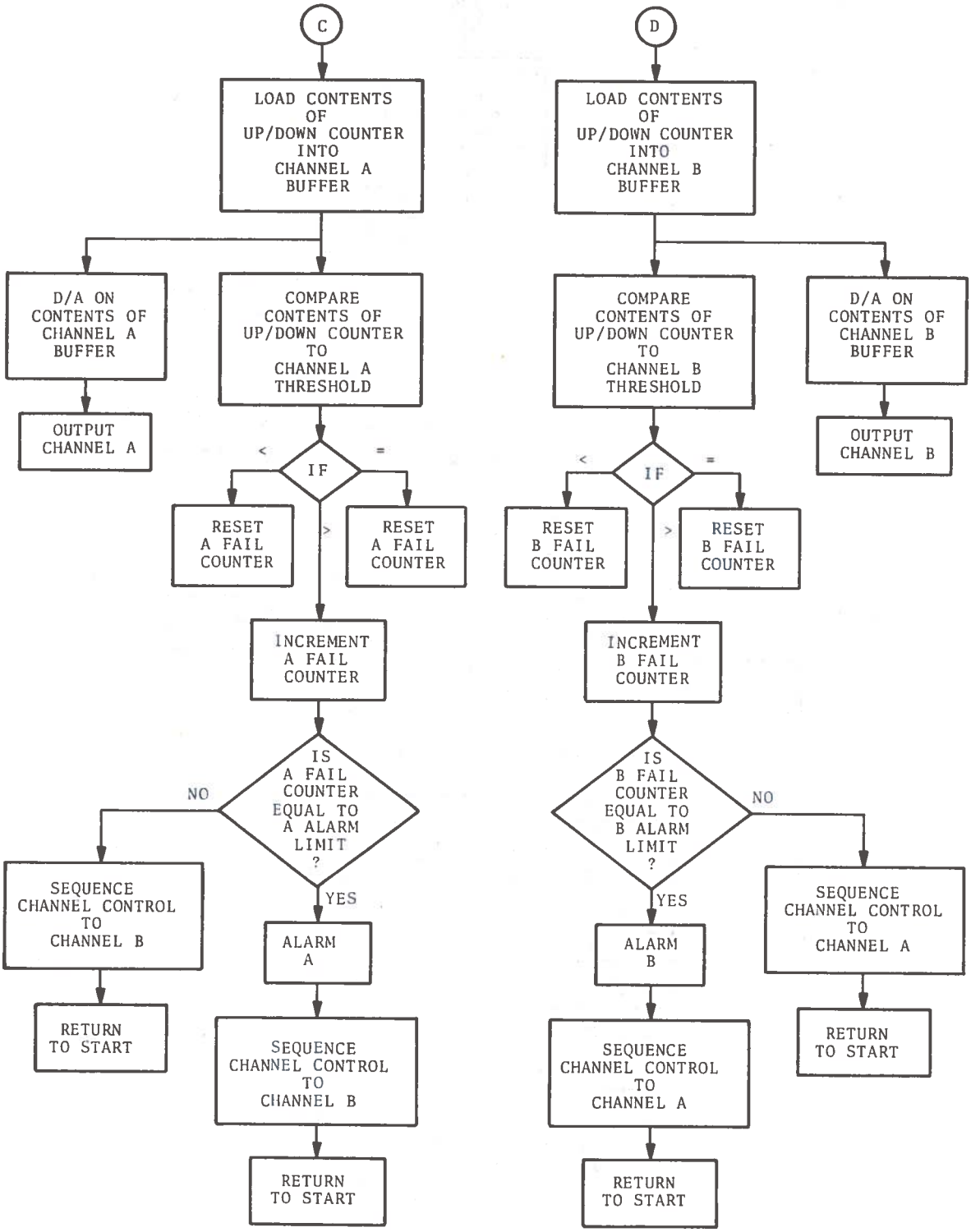

Figure B-3d. Operational Flow Diagram of the OMSA (Concluded)

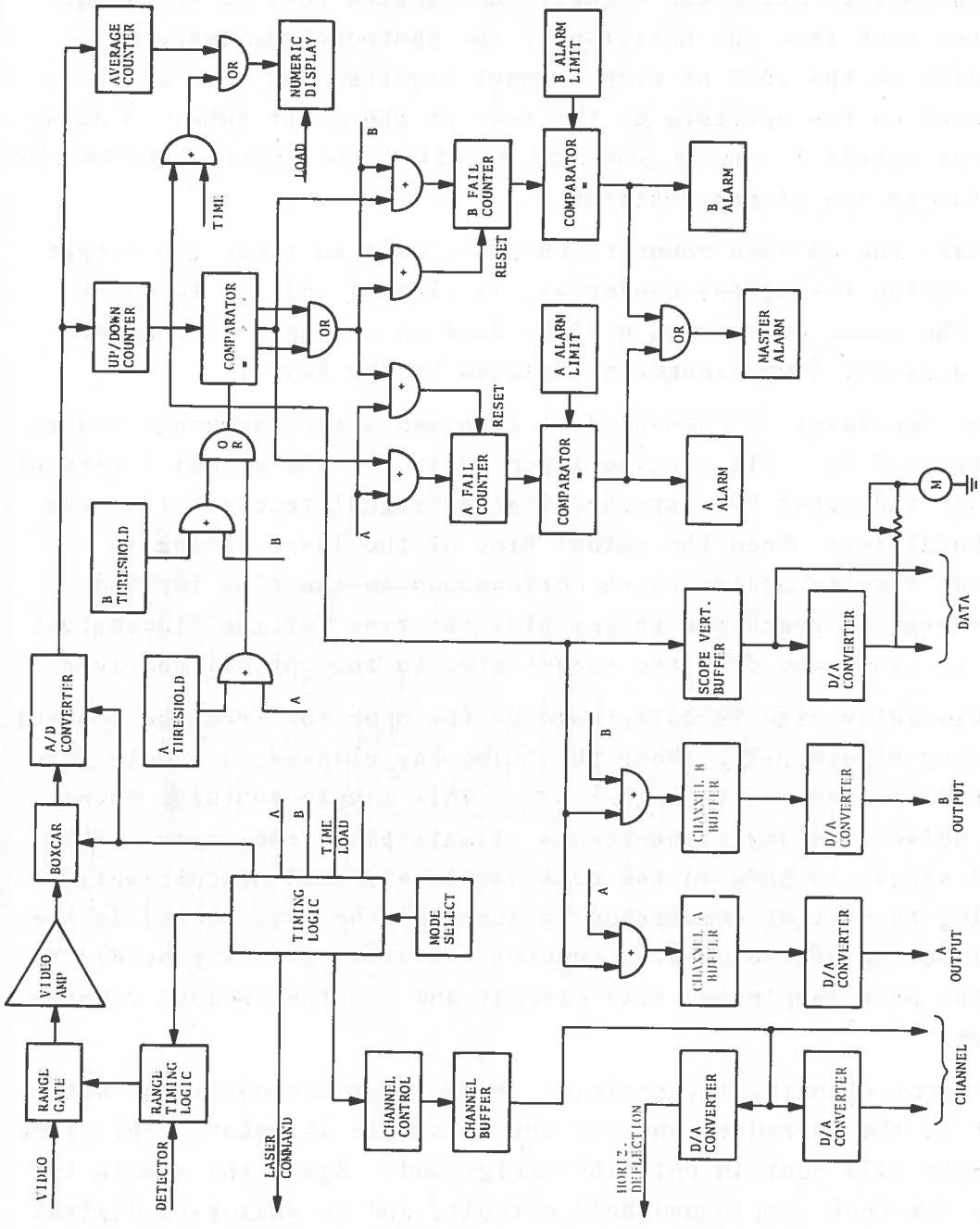

Figure B-4. Block Diagram of OMSA

CLASS. mode: state of automatic channel sequencer.

The contents of the CHANNEL buffer are converted into analog form and used to drive the magnetic deflection coil of the image dissector such that the position of the photocathode image corresponding to the 10.0 nm wide channel required for this cycle is positioned on the aperture at the rear of the drift tube. A delay of approximately 1.5 ms is provided to allow the magnetic deflection to settle to the proper position.

Next, the up-down counter, which is used to store the output of the analog-to-digital converter, is cleared and set to count "up". The first conversion will be done on a sample of the background plus any fluorescence stimulated by the laser.

Now the laser is commanded to fire and a time sequence starts (see Figure B-5). All ranging logic waits for the actual firing of the laser indicated by a synchronization signal received from the laser modulator. When the actual time of the laser firing is detected, a delay begins which corresponds to the time for the laser energy to reach the target plus the time for the fluorescent energy to propagate from the target area to the optical receiver.

This delay time is adjustable by the operator from the control panel (see Figure B-2). When this time has elapsed, a sample gate is opened for 500 ns (5×10^{-7} s). This sample contains background noise plus any fluorescence stimulated by the laser. The sampled signal is held in the peak sample and hold circuit while an analog-to-digital conversion is done and the data stored in the "up" direction of the up-down counter. A delay is now provided to clear the peak sample and hold circuit and set the up-down counter to "down."

Without changing the position of the photocathode image with respect to the aperture, another 500 ns sample is taken. This time the sample will contain only the background. Again the sample is held in the peak sample and hold circuit, and an analog-to-digital conversion is made. Thus, by counting this new data "down" a simple subtraction is performed, and the up-down counter contains just the digital equivalent of the amplitude of any oil fluorescence

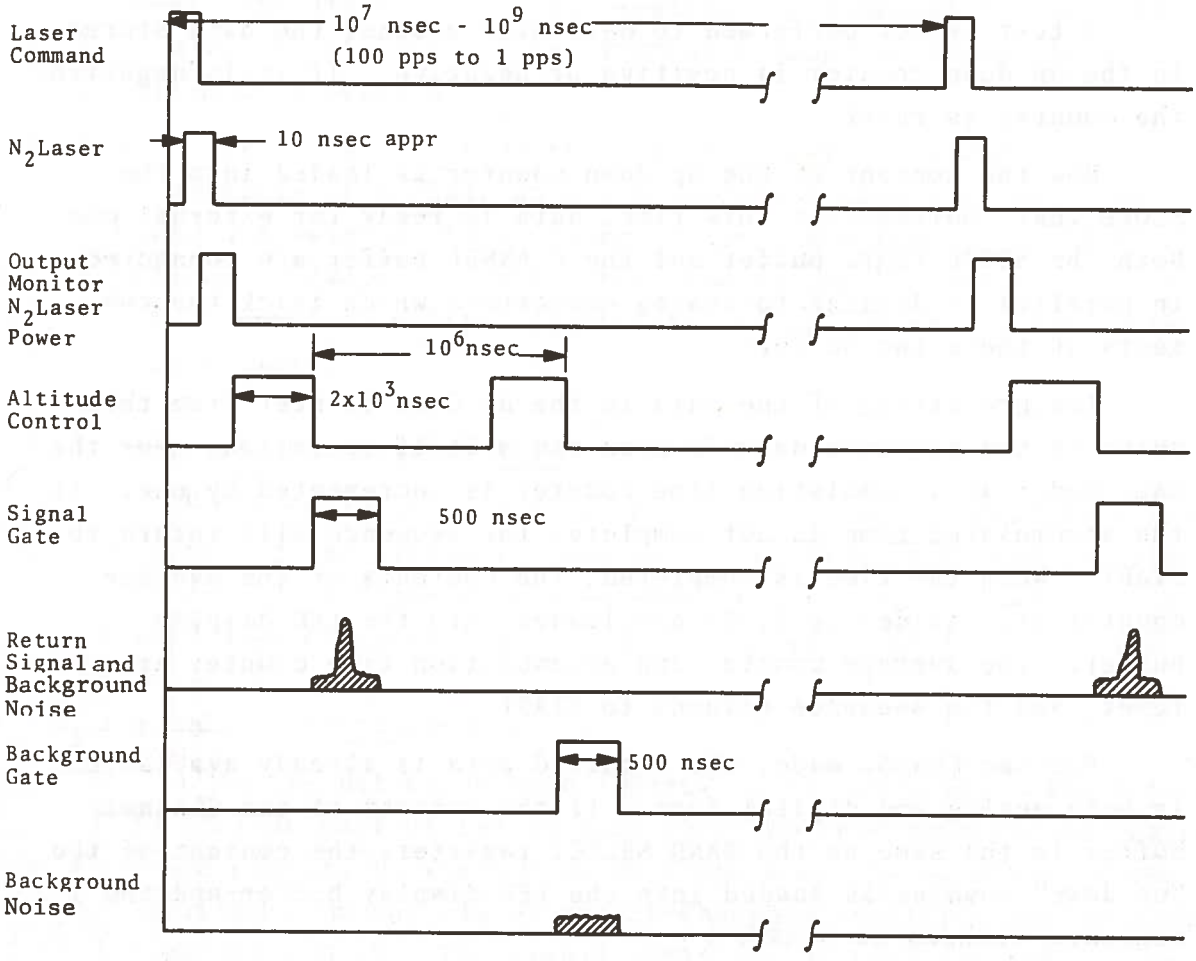

Figure B-5. ERODAC Time Sequence

steps is processed and is available in both analog and digital form for display and/or analysis.

TABLE B-1. OMSA CHANNEL WAVELENGTHS

Channel Number	Nanometers		Channel Number	Nanometers	
	From	To		From	To
1	350	360	18	520	530
2	360	370	19	530	540
3	370	380	20	540	550
4	380	390	21	550	560
5	390	400	22	560	570
6	400	410	23	570	580
7	410	420	24	580	590
8	420	430	25	590	600
9	430	440	26	600	610
10	440	450	27	610	620
11	450	460	28	620	630
12	460	470	29	630	640
13	470	480	30	640	650
14	480	490	31	650	660
15	490	500	32	660	670
16	500	510	33	670	680
17	510	520	34	680	690
			35	690	700

B.3 RECEIVER - IMAGE DISSECTOR

The heart of the OMSA receiver is an image dissector tube with an S-20 response (ITT Vidissector F4011 RP type) and a .248 in x .022 in aperture. This tube is housed in a ruggedized housing along with its magnetic shield, focusing coil, and deflection yoke (see Figure B-6). Attached to the rear of this housing in its own shielded compartment is the image dissector electronic module. This module contains all the necessary support hardware, such as high voltage power supply, focus coil regulator, deflection yoke driver, and signal preamplifier.

The receiver is remote from the OMSA signal processor and is mounted with the receiving optics in such a fashion that the output image of the spectrometer can be focused directly onto the photocathode of the image dissector tube of the receiver (see Figure B-7).

This image, 19.6mm x 6.3mm in size (350 nm - 700 nm), is magnetically focused on the aperture plate in the rear of the drift section of the dissector tube. The electron image is magnetically deflected to a position with respect to the output aperture upon command of the OMSA signal processor. The energy passing through the aperture is amplified by a ten dynode electron multiplier in the image dissector tube. The amplified signal appears as a small current through the anode load resistor, and the voltage thus produced is amplified in a wide band preamplifier.

The spectral radiant responsivity of ITT Vidissector F4011 RP serial numbers 077303 and 107201 are given in Figure B-8.

The test data of the ITT Vidissector F4011 RP (serial #107201), including gain, anode signal and dark current are given in Table B-2. Measurements of Vidissector photocathode responsivity profile are given as equal responsivity contour lines in Figure B-9. Results of the tests to determine the existence of photocathode blemishes are shown in Figure B-10.

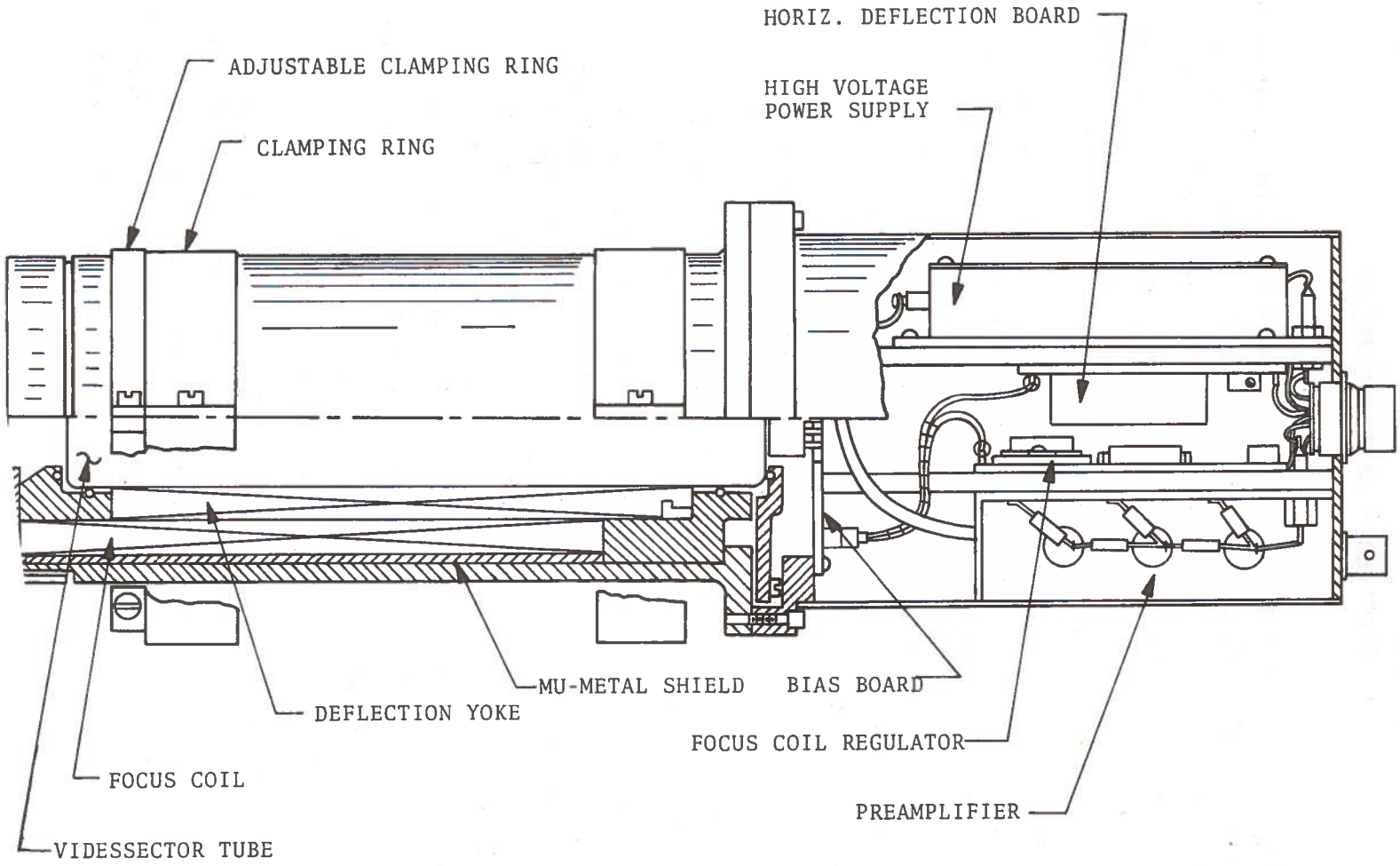

Figure B-6. Schematic of the Image Dissector and Associated Circuitry

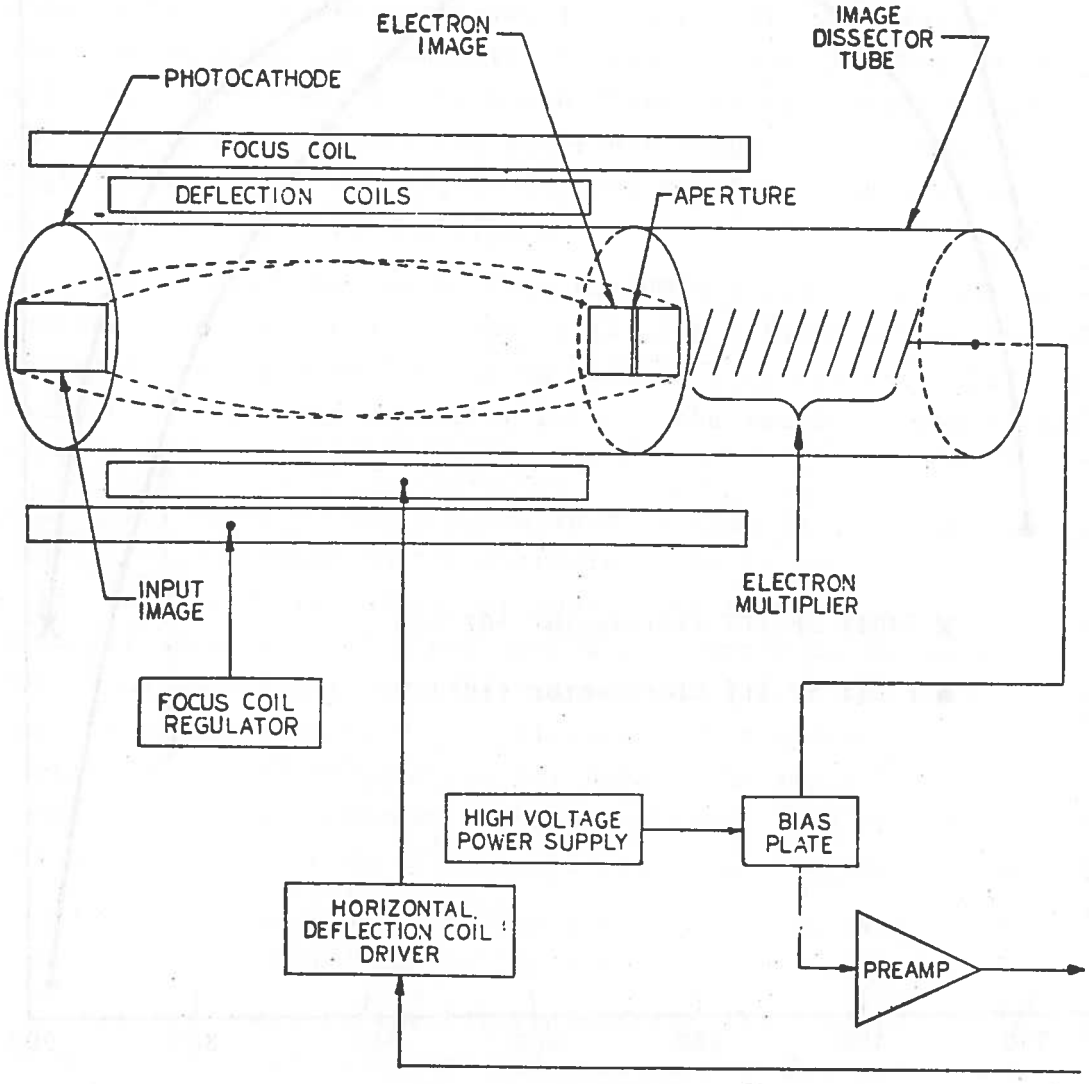

Figure B-7. Block Diagram of the Image Dissector and Associated Electronics

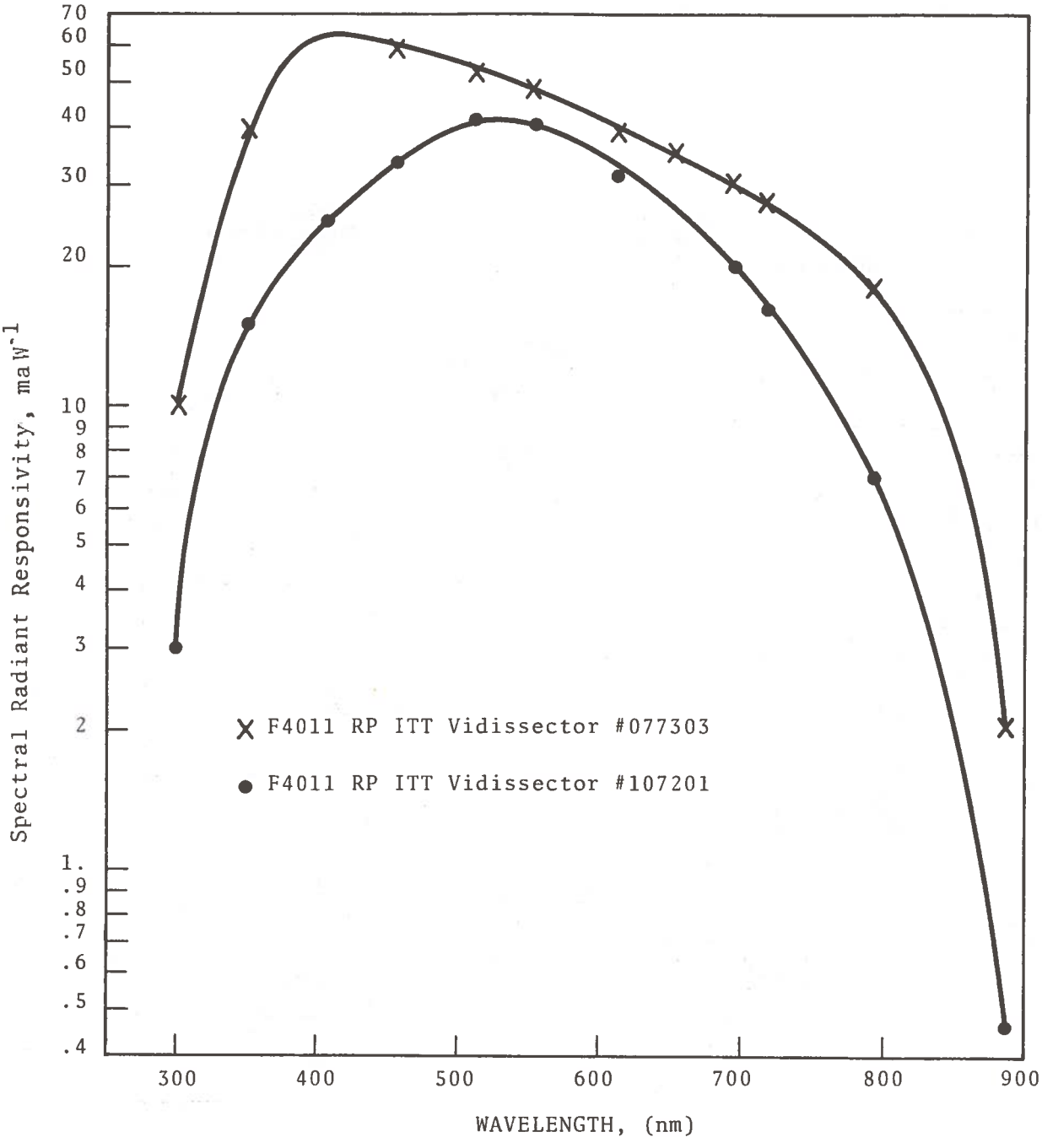

Figure B-8. Spectral Radiant Responsivity of the ITT Vidissector (Image Dissector) F4011RP Serial Numbers 077303 and 107201

TABLE B-2. ITT VIDISSECTOR F4011 RP (SERIAL #107201) TEST DATA*

$A_{aper.}$ in ^{2}**	$A_{illum.}$ in ^{2}	I_{pc} amp	$I_{aper.}$ amp	Gain	I_{anode} amp	$E_{mult.}$ volts	I_{dark} amp
5.456×10^{-3}	.95	1.9×10^{-8}	7.1×10^{-11}	1×10^{5}	7.1×10^{-6}	1395	7×10^{-11}
				2×10^{5}	14.2×10^{-6}	1600	1×10^{-10}
				5×10^{5}	35.5×10^{-6}	1910	3×10^{-10}
				1×10^{6}	71×10^{-6}	2260	6×10^{-10}

*Operating voltages at 5×10^{5} gain measured with respect to the drift tube: photocathode, -600V Dynode #1, 0V Dynode #2, 200V; Dynode #3 = #4 = #5 = #6 = #7 = #8 = #9, 190V; Anode, 1910V.

**Aperture size is .248 in x .022 in.

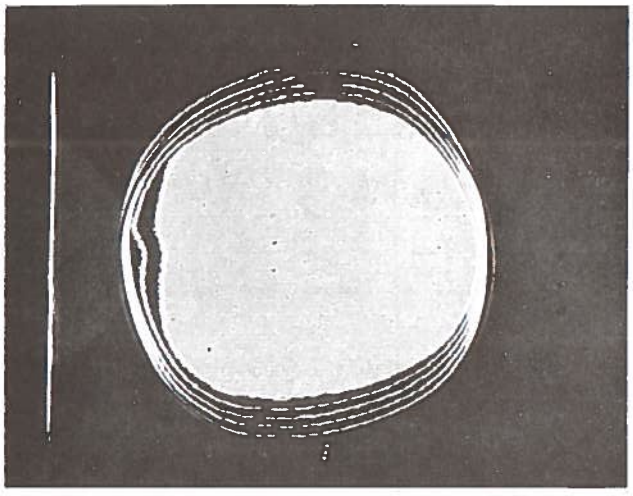

Figure B-9. Equal Responsivity Contour Lines of the Vidissector F40011RP (Serial# 107201). Photograph Shows 100% of the Photocathode. Contour levels of 50%, 60%, 70%, 80% and 90% are Shown. Gray Area Is within 90% of Maximum Responsivity. Videssector Operating Voltages As Recommened by the Manufacturer

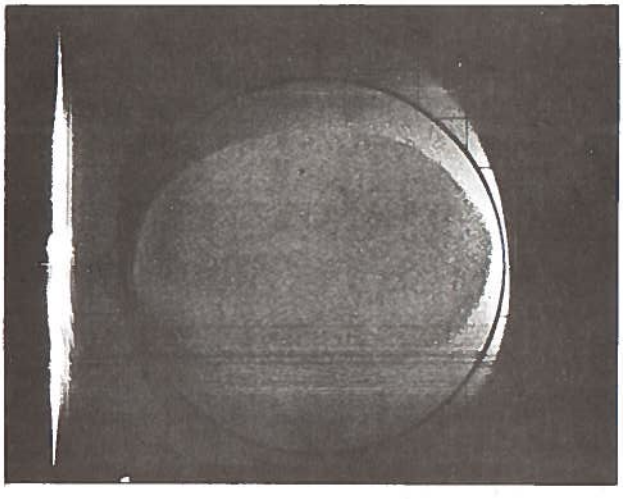

Figure B-10. Test of the Videssector F40011RP (Serial # 107201) Showing That the Photocathode Is Not Affected by Blemishes

B.4 SIGNAL PROCESSOR

B.4.1 INTRODUCTION

The signal processor section of the OMSA controls the operation of the image dissector and processes the signal seen by the dissector according to a selected operational mode. All the electronics, both analog and digital, needed to accomplish these operations are contained in this one unit along with needed power supplies.

The signal received from the image dissector is first converted from analog into digital form for ease of handling. All the manipulations of the signal — i.e., noise substraction, comparison, averaging, etc. — are done in digital form. After the signal processing is completed, the digital signal is reconverted into analog form and provided as an output to whatever equipment might be used to further process or display the data. Digital outputs are also provided.

All the electronics, with the exception of the Range Gate, are located in card file just behind the front control panel.

B.4.2 BASIC FUNCTIONS

1. Range Gate (Variable distance to target)
2. Video Amplifier (Gain variable)
3. Boxcar (Peak sample and hold)
4. Analog-to-Digital Converter (10 bits)
5. Digital Processor
   a. Variable Threshold Limits (1_8 to 1777_8)
   b. Variable Consecutive Fail Limits (1_8 to 77_8)
6. Alarm Indicators
7. Output Data Processor
   a. Digital-to-Analog Converter (0-10 volts)
   b. BIN Data Output (10 bits)

8. Mode Switching

   a. CAL.

   b. DETECT.

   c. CLASS.

9. 5 MHZ Clock Oscillator (A/D converter)

10. Laser Sync Pulses (15 V, 2 usec)

11. Range Timing (0-2500 ft)

12. Digital-to-Analog Converter (10 bits)

13. BIN Channel Output (6 bits)

B.4.3 POWER REQUIREMENTS

The power requirements of the OMSA are:

115 VAC $\pm$ 15%, 50 to 400 Hz, 40 VA.

B.5 ACCEPTANCE TEST

B.5.1 INTRODUCTION

This test procedure has been prepared to demonstrate that the OMSA fulfills the requirements set out by Contract DOT-TSC-350.

Laboratory testing of the OMSA requires simulation of the spectrometer output image. In this test procedure, the following technique will be used to accomplish this simulation.

The light source to be used is a light emitting diode (LED). A channel slit mask (see Figure B-11a) is placed between the light source and the photocathode of the image dissector. The light passing through the transparent bars of the mask will simulate the spectrometer image. This mask will pass light in odd channels and inhibit light in even channels. The transparent bars are of various heights. The light energy passing through each bar is proportional to its height, making channel identification possible.

The LED is triggered from a HP 214A pulse generator which is itself triggered by the OMSA LASER TRIGGER Output. The pulse delay function is used to demonstrate the distance to target adjustment of the OMSA.

B.5.2 CALIBRATION AND CLASSIFICATION MODE

1. Turn on OMSA power.
2. Reset Alarms.
3. Depress LASER TRIGGER (lamp on).
4. Depress CAL. (lamp on).
5. With pulse generator (HP 214A) set at no delay make the following adjustment on the OMSA:
   a. Set BAND SELECTOR to channel 17 (21 octal).
   b. Adjust RANGE FINE ADJUST for maximum deflection on FLUORESCENCE meter.
   c. Note number of AVERAGE AMPLITUDE display.

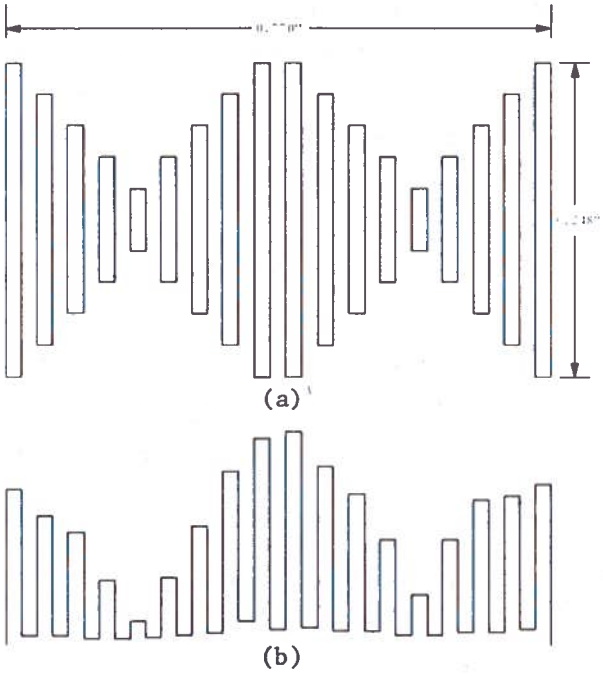

Figure B-11. (a) Pattern of the Channel Slit Mask to Test the OMSA (b) Scope Display Resulting from the Use of the Channel Split Mask

d. Set BAND SELECTOR to channel 19 (23 octal).

e. Again note number in AVERAGE AMPLITUDE display. This number should be within ±5% of the number recorded in step c. above.

6. With Step 5 successfully completed each of the 35 channels can be manually stepped through by switching the BAND SELECTOR to the desired channel number in octal form. Note that even numbered channels will read near zero on AVERAGE AMPLITUDE display.

7. Connect the horizontal and vertical oscilloscope inputs to SCOPE HORZ. and SCOPE VERT., respectively.

8. Depress ID switch and make necessary oscilloscope adjustments to position the trace on the oscilloscope. The trace should correspond to Figure B-11b.

B.5.3 DETECTION MODE

B.5.3.1 Channel Selection Test

1. Repeat step 1 through 5e. in section B.5.2.

2. Connect digital volt meter to the SCOPE VERT. on the OMSA.

3. Starting with Channel 1, record voltage for all channels and readings of AVERAGE AMPLITUDE display.

4. Depress DETECT. Switch (lamp on).

5. Select CHANNEL A BAND NO. starting with Channel 1.

6. Select CHANNEL B BAND NO. starting with Channel 35.

7. Connect DVM to CHANNEL A OUTPUT. The DVM should read within ±2% of the voltage recorded for Channel 1 in step (3).

8. Connect DVM for CHANNEL B OUTPUT. The DVM should read within ±2% of the voltage recorded for Channel 35 in step (3).

9. Steps(5)through(8)should be repeated for various combinations of CHANNEL A and CHANNEL B checking DVM readings against step(5)to verify proper channel addressing.

B.5.3.2 Threshold and Alarm Test

1. Select a channel number for CHANNEL A and set BAND NO. accordingly.
2. Take the number recorded from the AVERAGE AMPLITUDE (step 3, sec. B.5.3.1) for that channel and add $24_{(8)}$ to it and set this new number in CHANNEL A THRESHOLD register.
3. Repeat steps(1)and(2)for CHANNEL B except add $50_{(8)}$.
4. Reset any alarms.
5. Depress CAL.
6. Turn BAND SELECT to number in CHANNEL A BAND NO.
7. Increase drive voltage to LED until AVERAGE AMPLITUDE reads slightly greater than CHANNEL A THRESHOLD.
8. Depress DETECT. CHANNEL A ALARM RESET will light and cannot be reset by depressing ALARM RESET. Verify that CHANNEL B ALARM does not light.
9. Depress CAL.
10. Decrease drive voltage to LED until AVERAGE AMPLITUDE reads its original value.
11. Depress DETECT. switch and insure the alarm will reset.
12. Repeat step(1)substituting CHANNEL B for CHANNEL A.
13. Various combinations of CHANNEL A and CHANNEL B can be checked to verify proper operation with varying signal amplitudes.

B.6 WAVELENGTH CALIBRATION

B.6.1 INTRODUCTION

Only the horizontal deflection electronics of the OSMA image dissector require calibration. This calibration is done independently of the oil spill surveillance system.

The test set up is described in the Acceptance Tests in section B.5. For calibration, all but Channels 1 and 35 are blanked out on the slit mask. Care should be taken in aligning the slit mask to the horizontal and vertical deflection axes of the photocathode.

B.6.2 PROCEDURE

a. Before turning the OMSA power on, remove the top cover of the signal processor and the shield cover of the Image Dissector Electronics Module (IDEM).

b. Connect the SCOPE HORIZ. and SCOPE VERT. outputs of the OMSA to the X and Y inputs, respectively, of an oscilloscope.

c. Set the BAND SELECT to 22.

d. Connect a differential voltmeter (DVM) across the 10 ohm 1% resistors on the horizontal deflection coil driver board in the IDEM (see Figures B-12 and B-6).

e. Turn OMSA power on.

f. Depress LASER TRIGGER under MODE CONTROL until lamp is lit.

g. Depress CAL.

h. Adjust 1K potentiometer on the Bipolar Converter BD116 (Figure B-13) located in the OMSA signal processor section, until the DVM reads 0.0 $\pm$.02 volts.

i. Set BAND SELECT to 01.

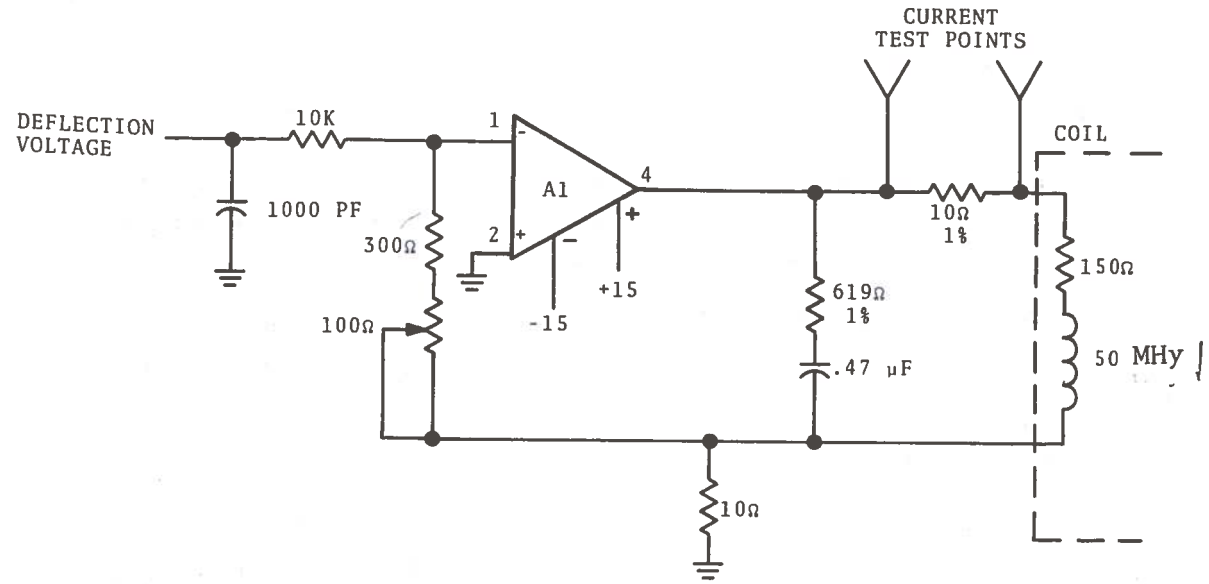

A1 - BURR-BROWN 3043/15

CURRENT: 11 MA @ +15V
6 MA @ -15V

Figure B-12. Circuit Diagram of the OMSA Horizontal Deflection Coil Driver

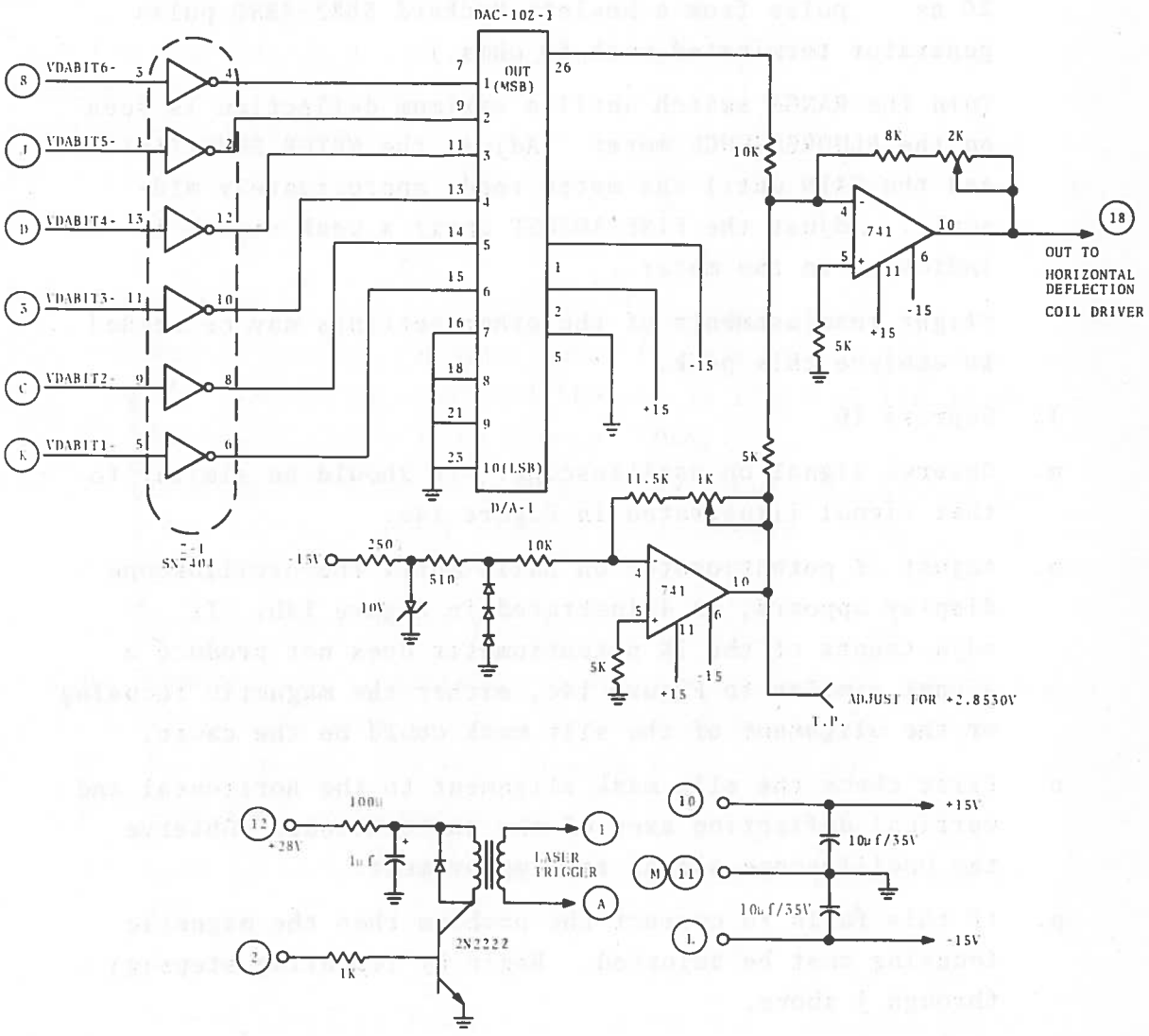

Figure B-13. Circuit Diagram of the Bi-Polar Converter

j. Adjust 2K potentiometer on BD 116 until the DVM reads approximately 170 millivolts.

k. Set METER SENSITIVITY to its full clockwise position and the GAIN to MAX.

Excite the LED with maximum safe power. (For the calibration done at MIT/CSDL the LED was driven by a 20 volt, 20 ns pulse from a Hewlett Packard 5082-4880 pulse generator terminated with 50 ohms.)

Turn the RANGE switch until a maximum deflection is seen on the FLUORESCENCE meter. Adjust the METER SENSITIVITY and the GAIN until the meter reads approximately mid-scale. Adjust the FINE ADJUST until a peak signal is indicated on the meter.

Slight readjustments of the other settings may be needed to achieve this peak.

l. Depress ID.

m. Observe signal on oscilloscope. It should be similar to that signal illustrated in Figure 14a.

n. Adjust 2K potentiometer on BD116 until the oscilloscope display appears, as illustrated in Figure 14b. If adjustments of the 2K potentiometer does not produce a signal similar to Figure 14c, either the magnetic focusing or the alignment of the slit mask could be the cause.

o. First check the slit mask alignment to the horizontal and vertical deflection axes of the photocathode. Observe the oscilloscope signal for improvement.

p. If this fails to correct the problem then the magnetic focusing must be adjusted. Begin by repeating steps (g) through j above.

q. Depress ID.

r. Again the signal on the oscilloscope will look similar to Figure B-14a. Adjust the 50 ohm potentiometer located on the Focus Coil Regulator in the IDEM. (see Figures

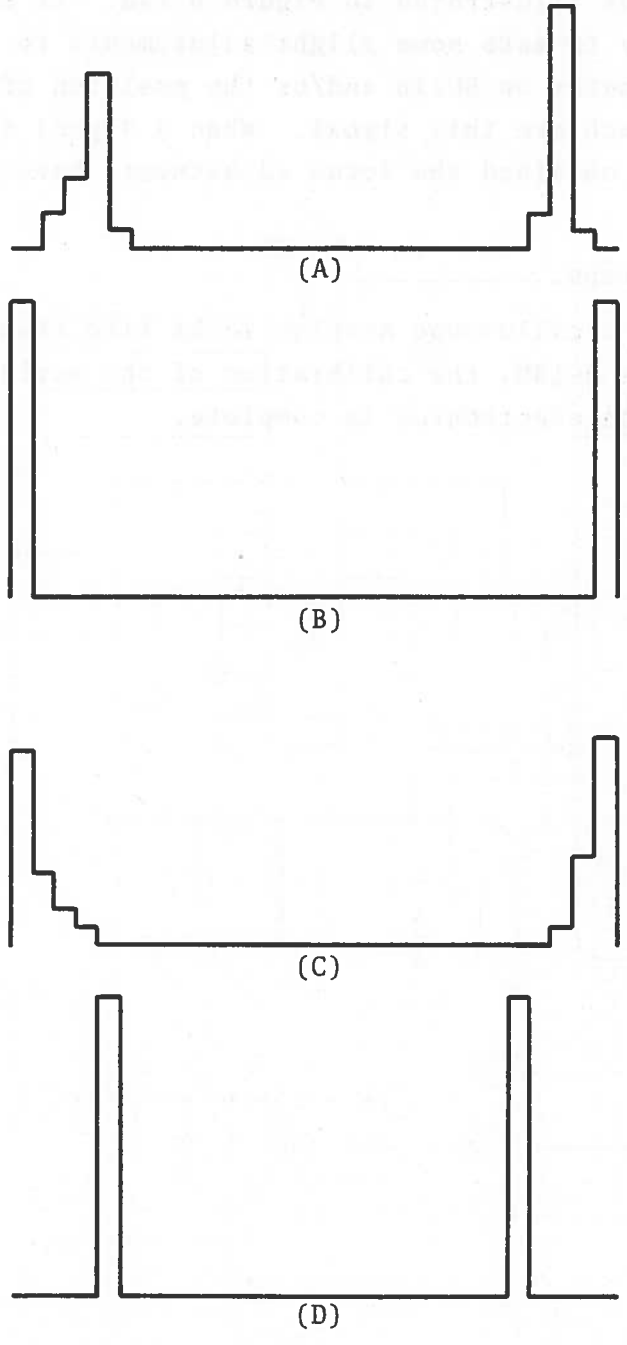

Figure B-14. Calibration Oscilloscope Displays

B-15 and B-6) until the signal on the oscilloscope appears as illustrated in Figure B-14d. It may be necessary to make some slight adjustments to the 2K potentiometer on BD116 and/or the position of the slit mask to achieve this signal. When a signal similar to B-14d is obtained the focus adjustments have been made properly.

s. Repeat steps.

t. When the oscilloscope display looks like that illustrated in Figure B-14b, the calibration of the horizontal deflection electronics is complete.

B.7 CIRCUIT DIAGRAMS

The main circuits of the OMSA are given in Figures B-15 through B-37. For more detail and printed circuit layouts see the U.S. Government Contract DOT-TSC-350 Report.

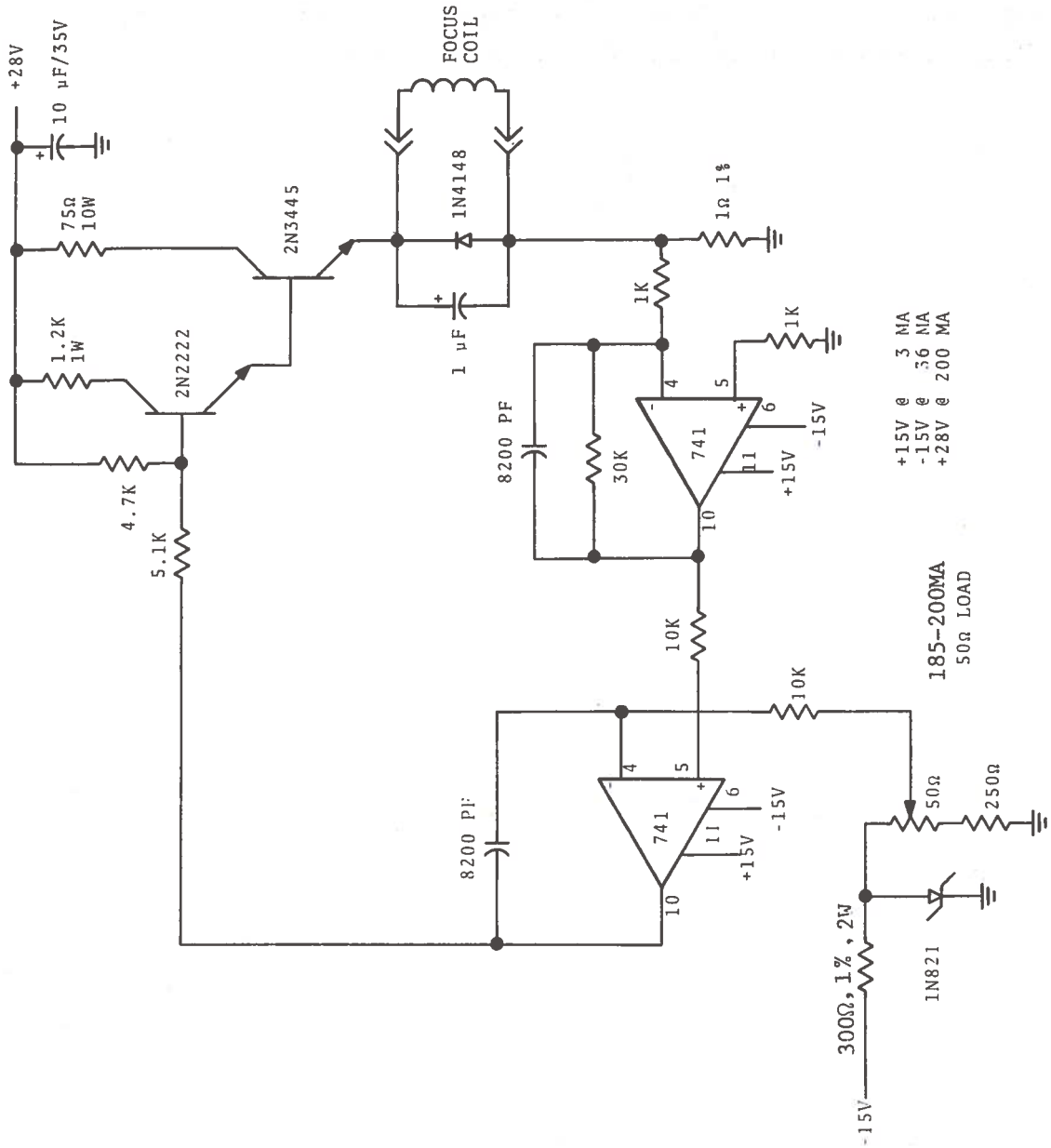

Figure B-15. Circuit Diagram, OMSA Focus Coil Regulator

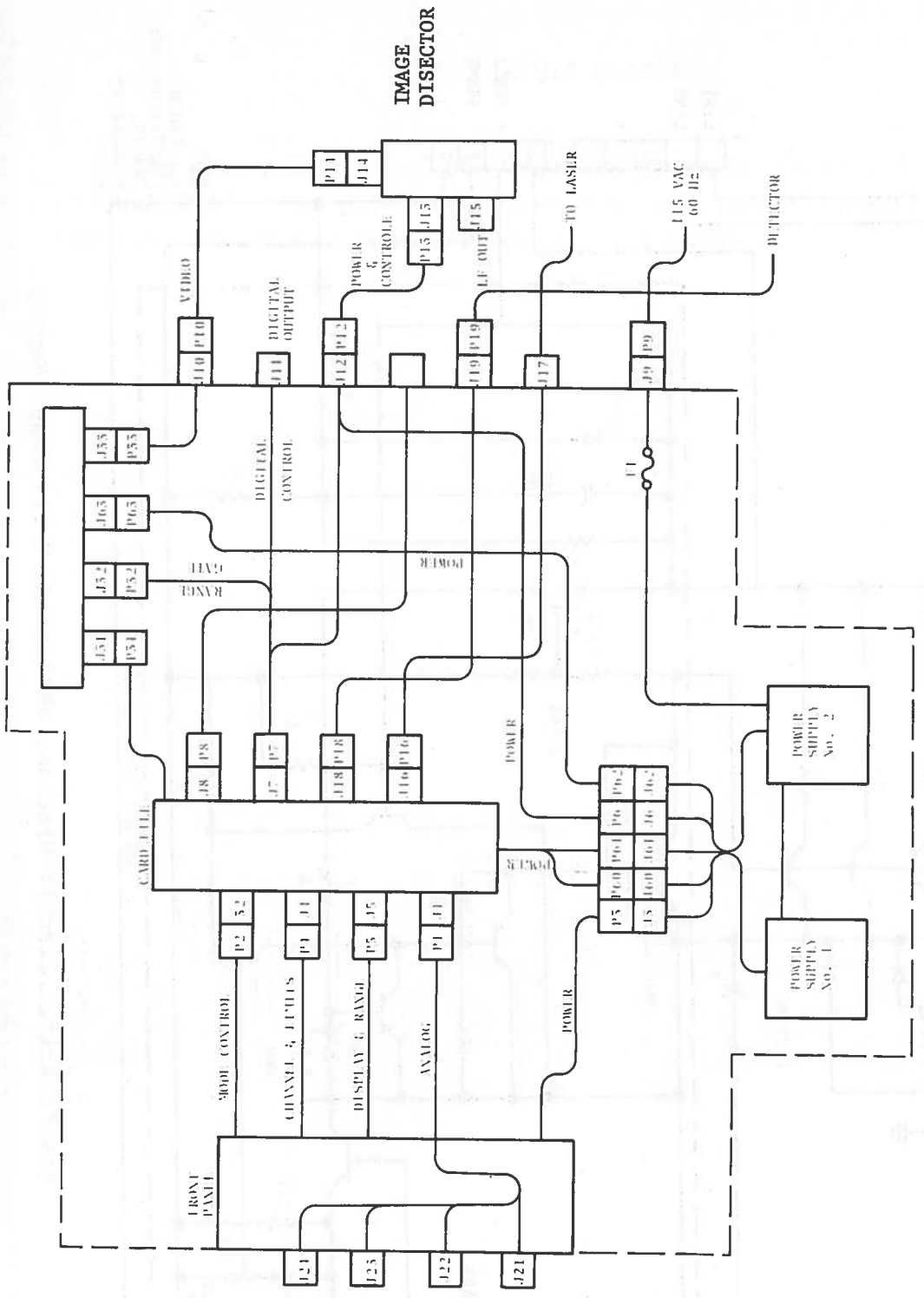

Figure B-16. Circuit Diagram, OMSA Subassemblies Interconnections

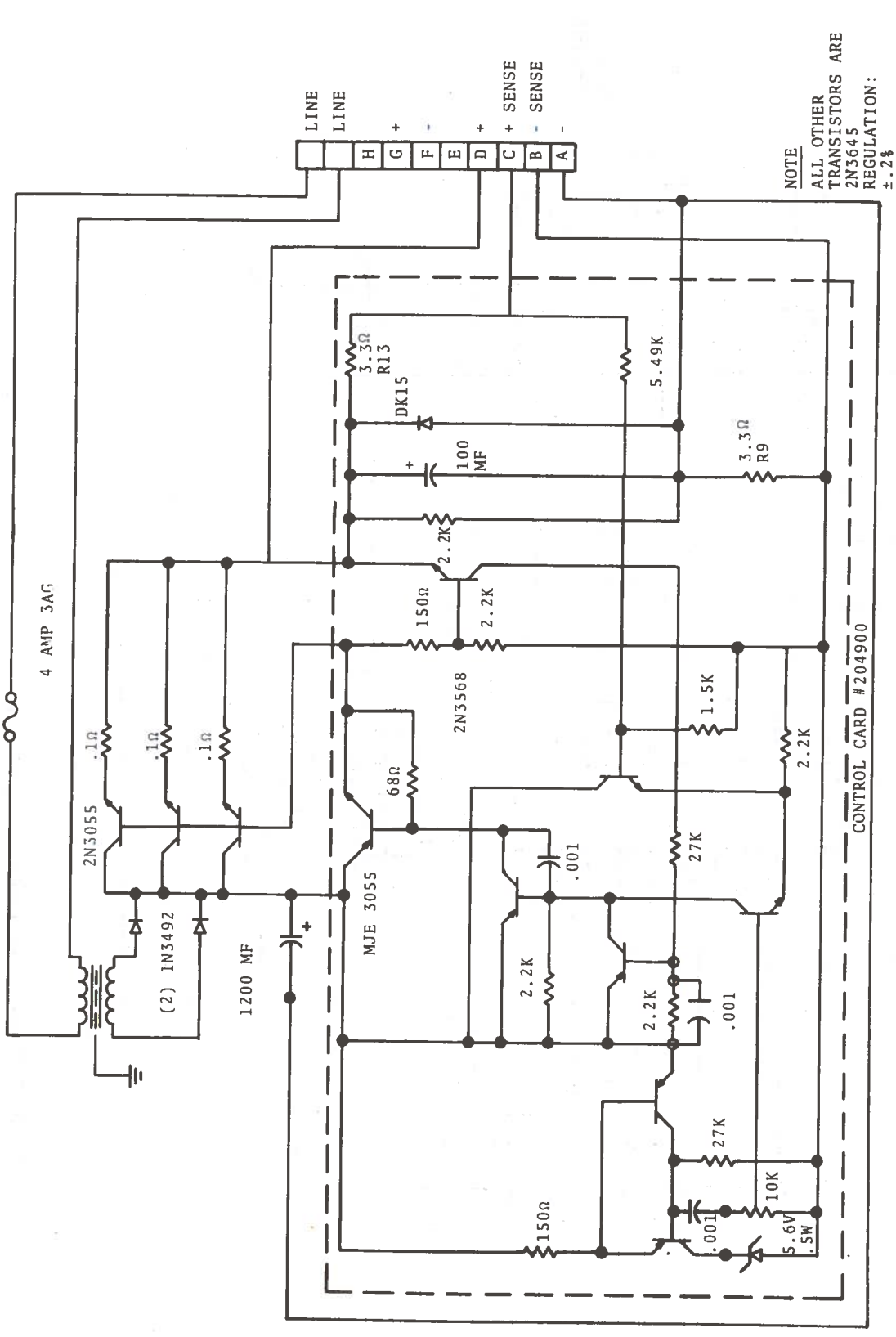

Figure B-17. Circuit Diagram, OMSA 18-28 Volts Power Supply

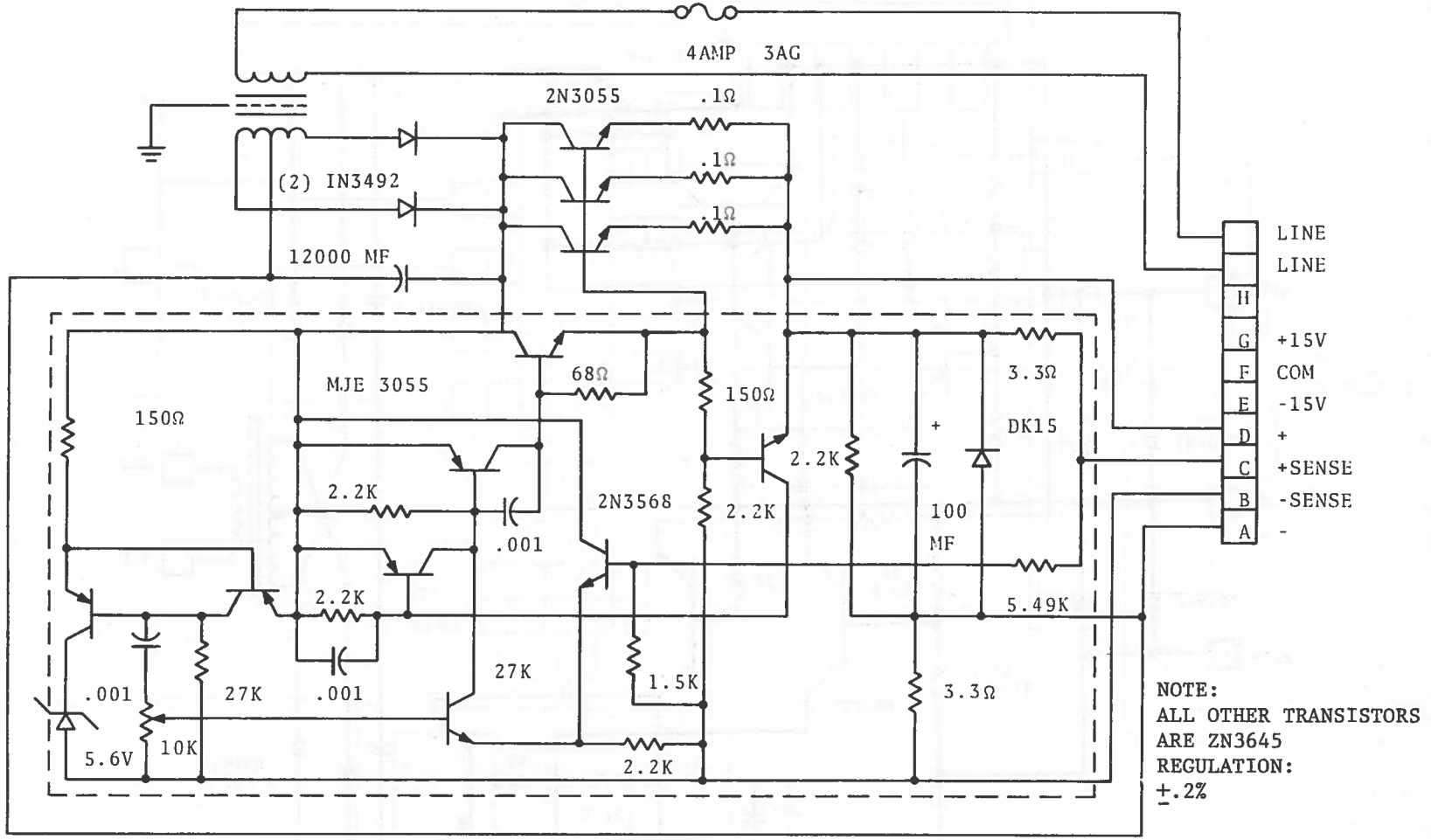

Figure B-18. Circuit Diagram, OMSA 5 Volt Power Supply

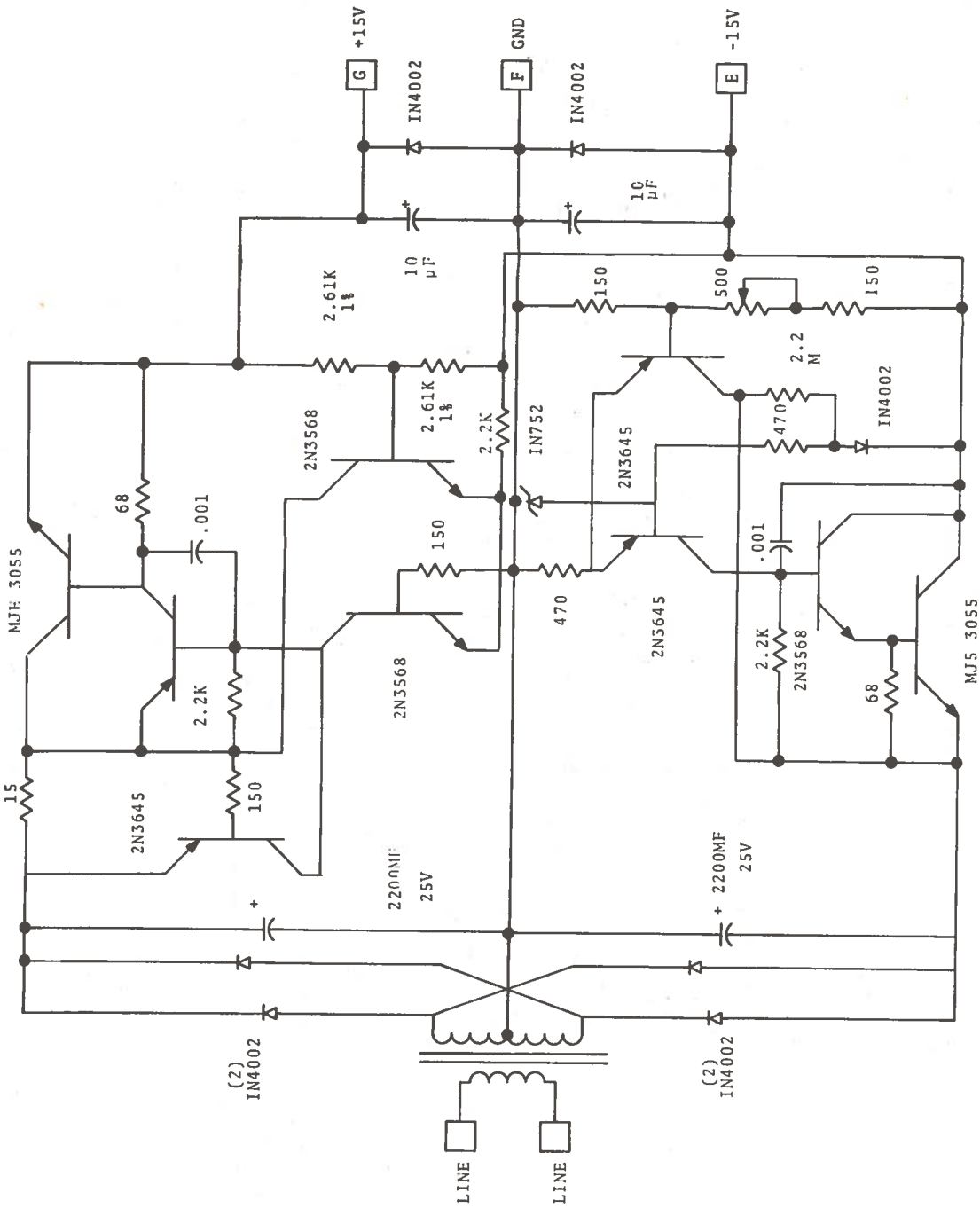

Figure B-19. Circuit Diagram, OMSA ±15 Volts Power Supply

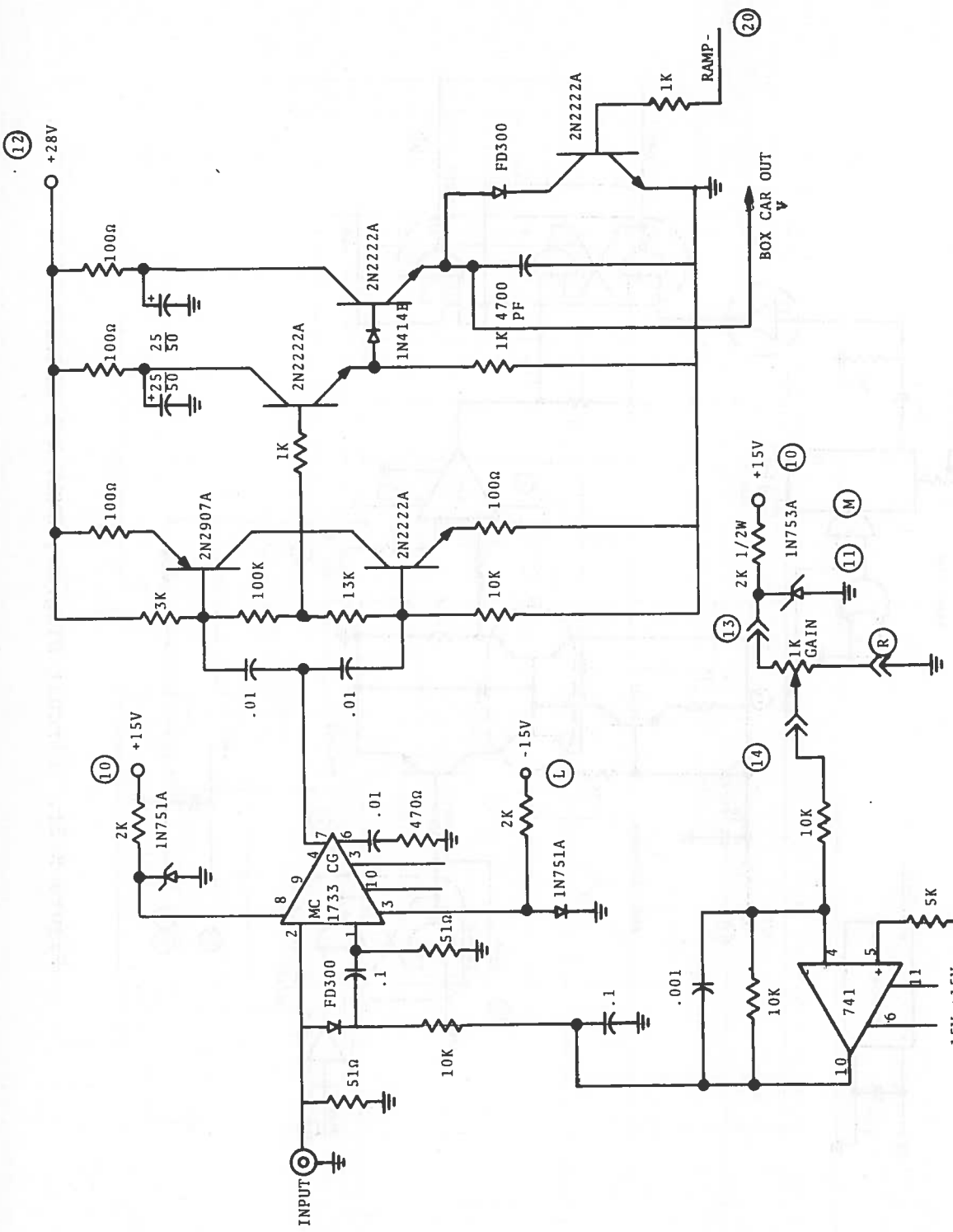

Figure B-20. Circuit Diagram, OMSA Video Amplifier and Peak Detectors

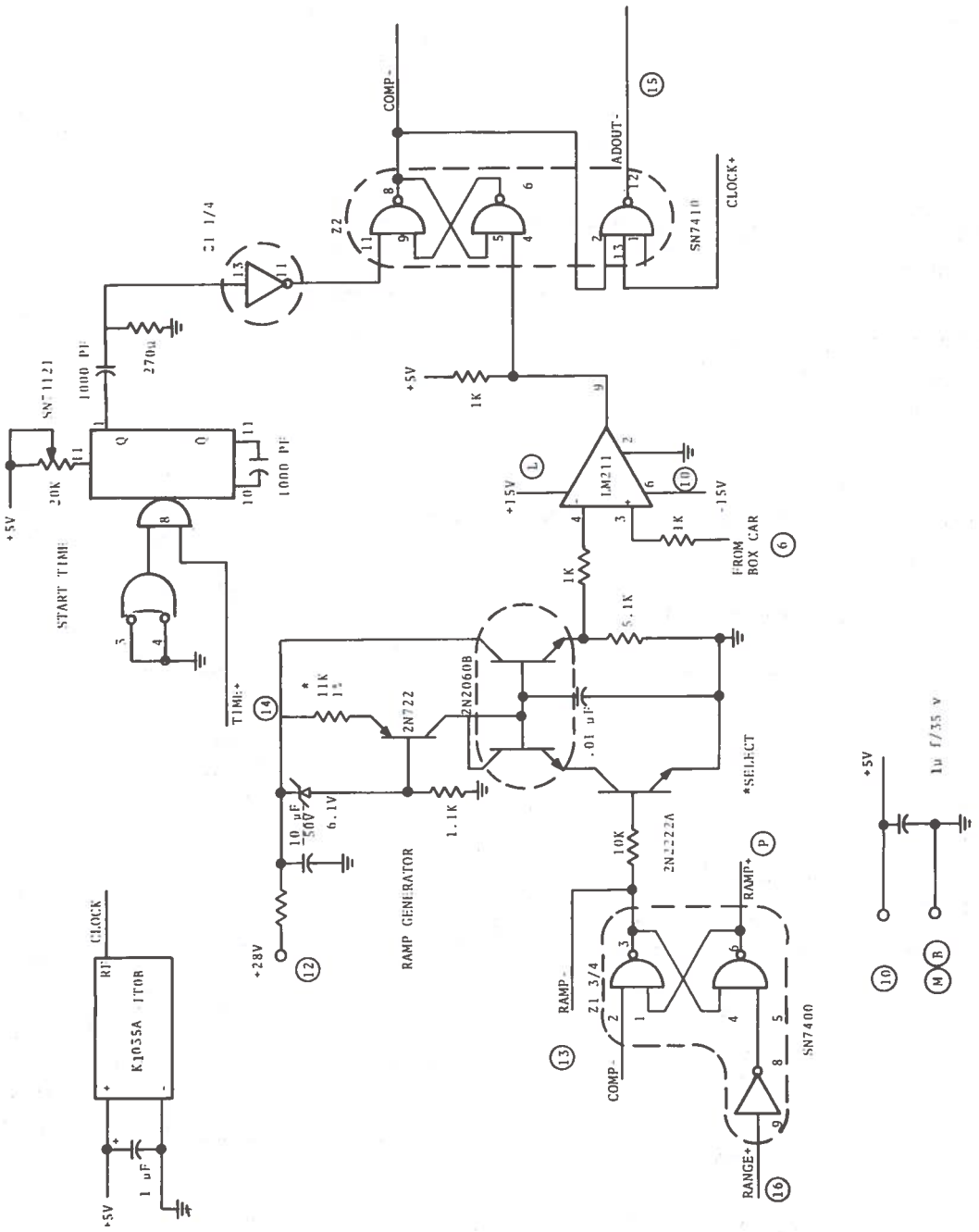

Figure B-21. Circuit Diagram, OMSA A/D Converter

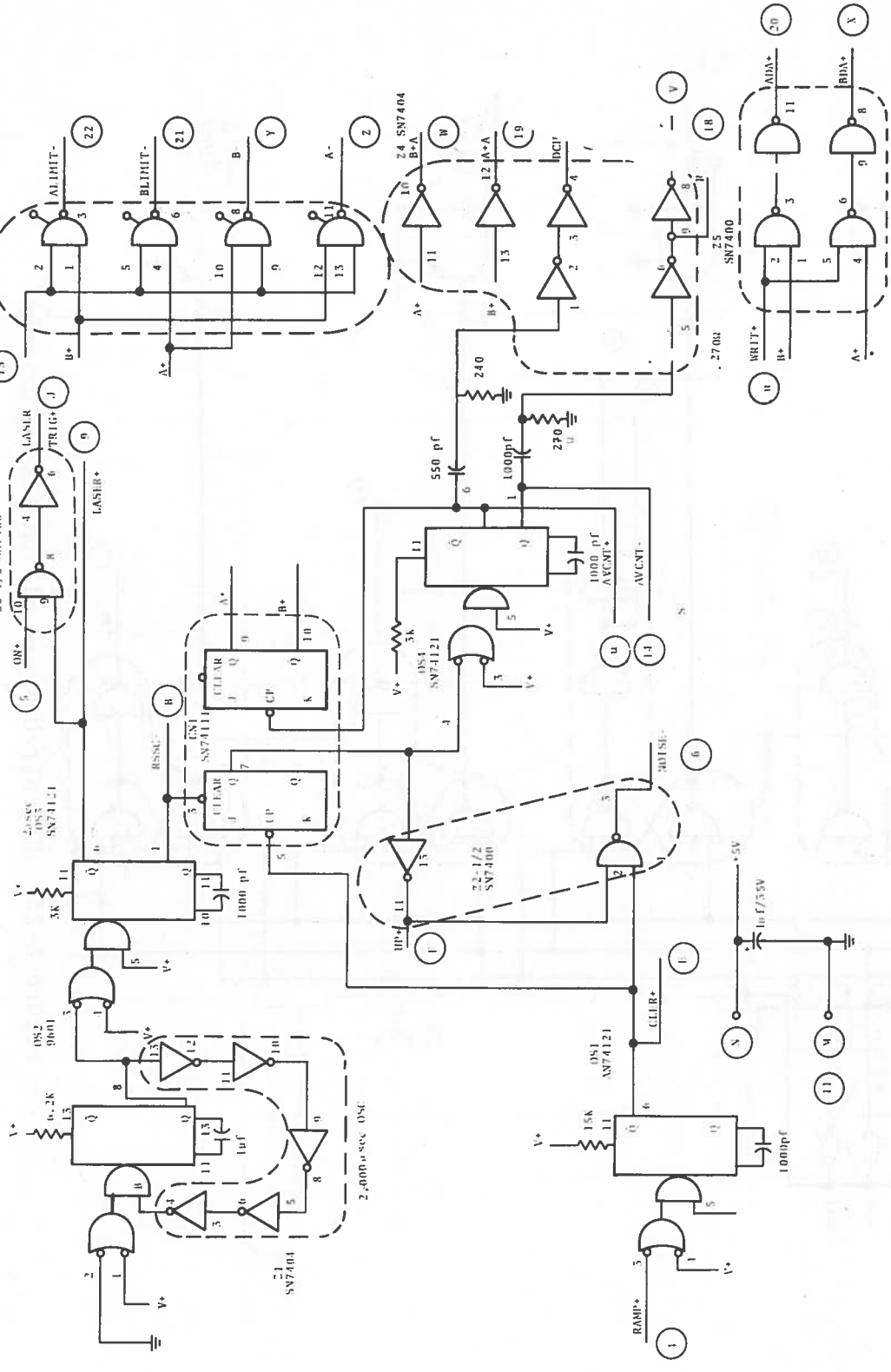

Figure B-22. Circuit Diagram, OMSA Timing Control

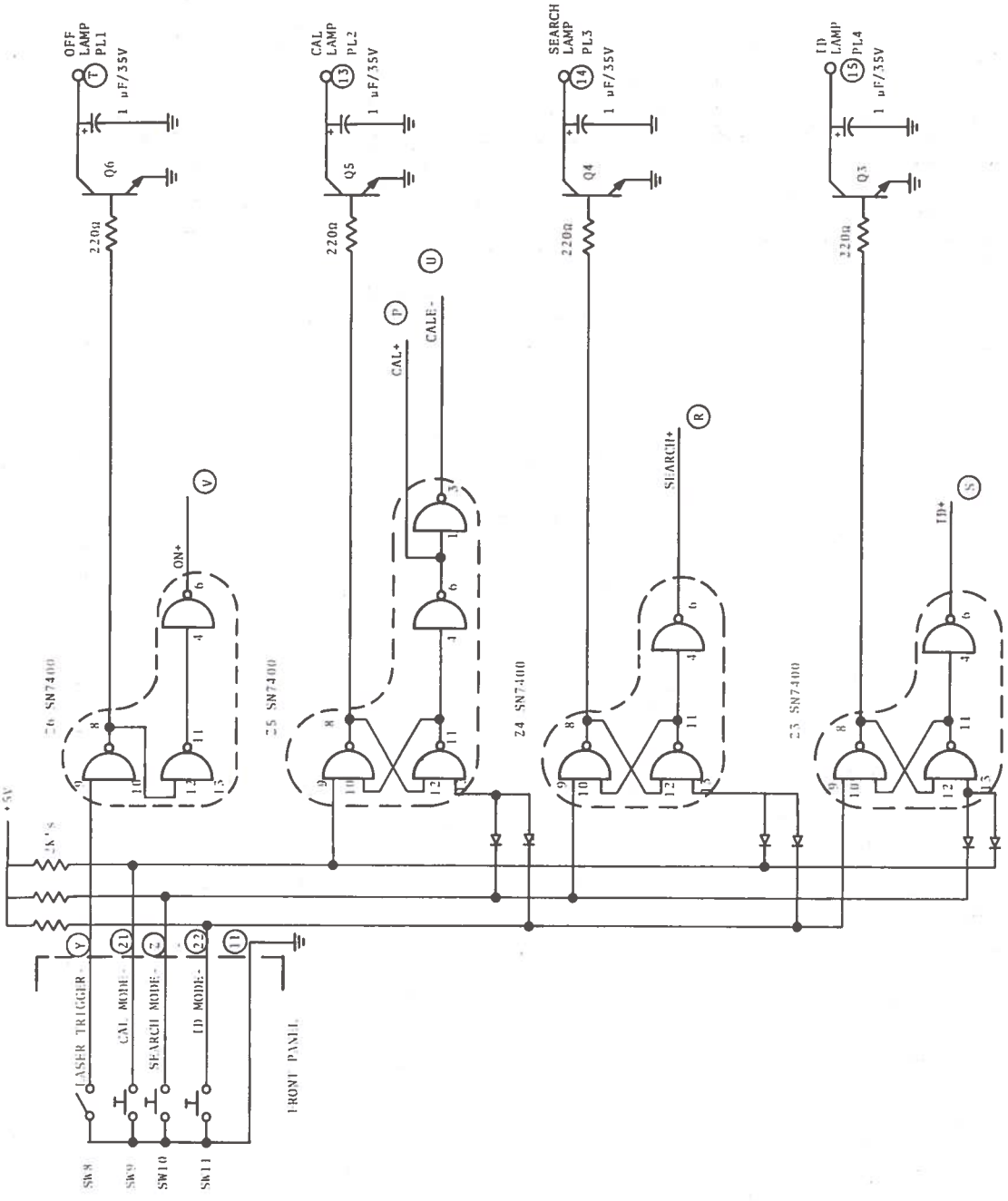

Figure B-23. Circuit Diagram, #1 OMSA Lamp Drivers

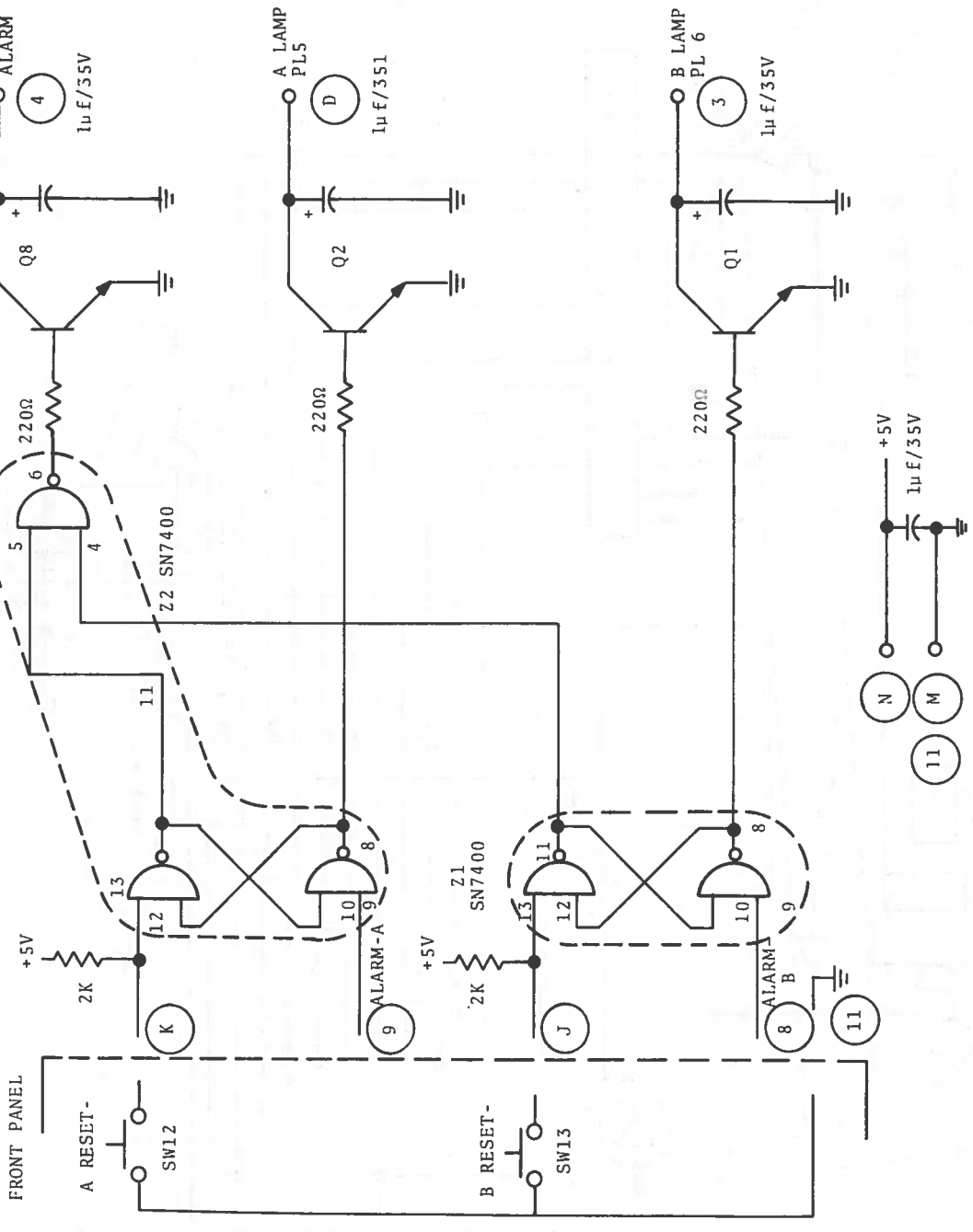

Figure B-24. Circuit Diagram,#2 OMSA Lamp Drivers

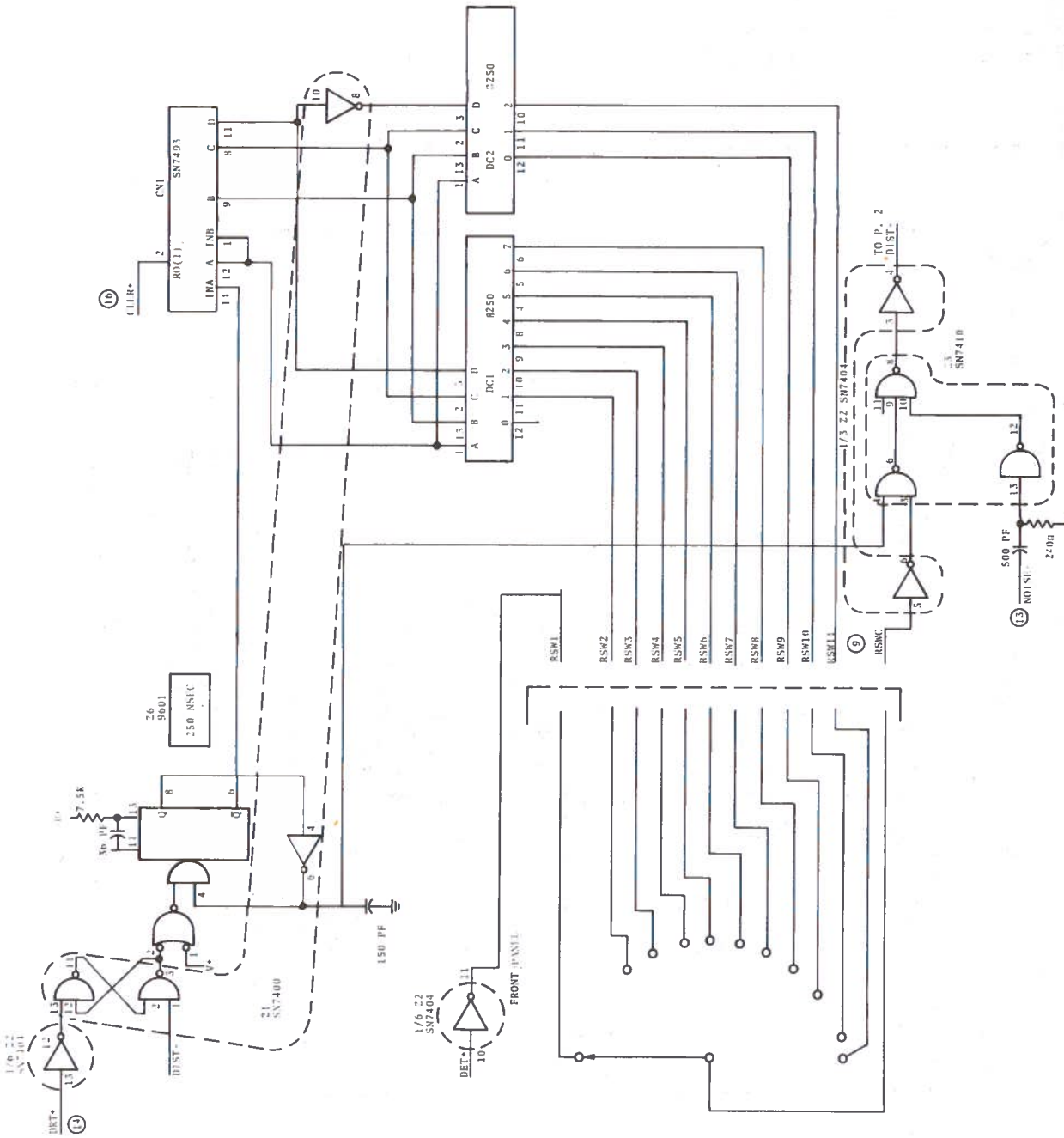

Figure B-25. Diagram, OMSA Range Circuit #1

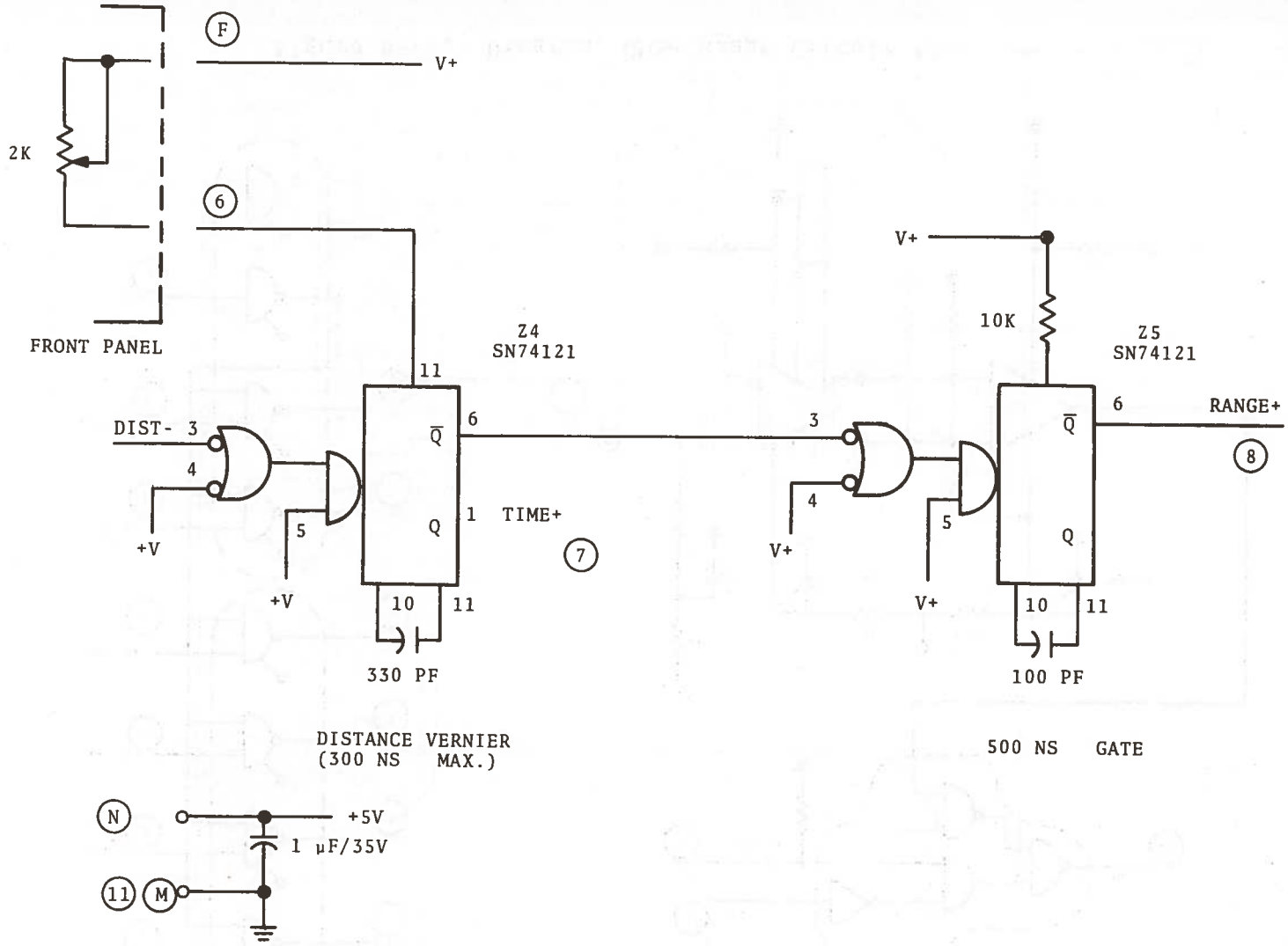

Figure B-26. Diagram, OMSA Range Circuit # 2

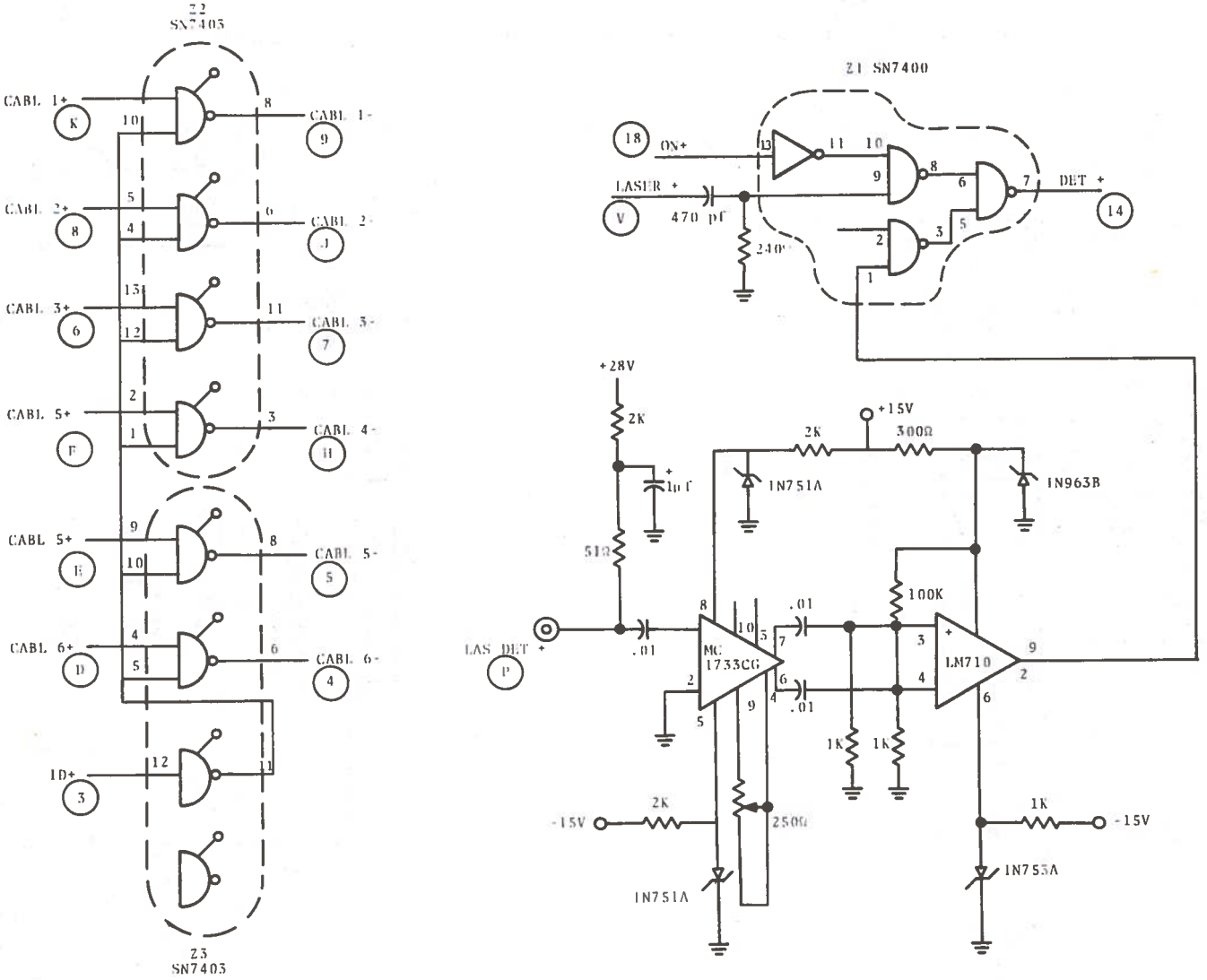

Figure B-27. Diagram, OMSA Range Circuit #3

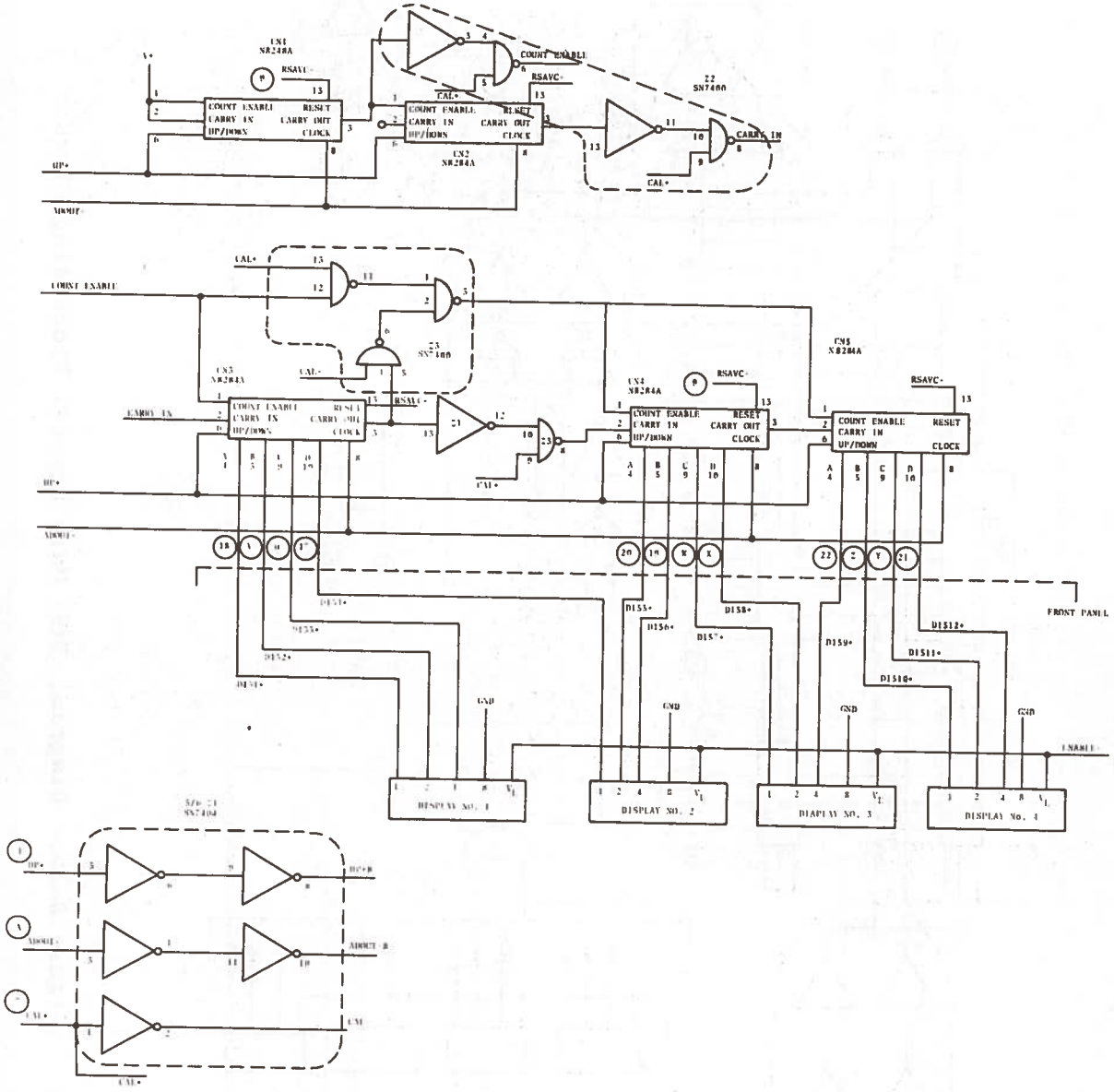

Figure B-28. Diagram, OMSA Average Counter Circuit

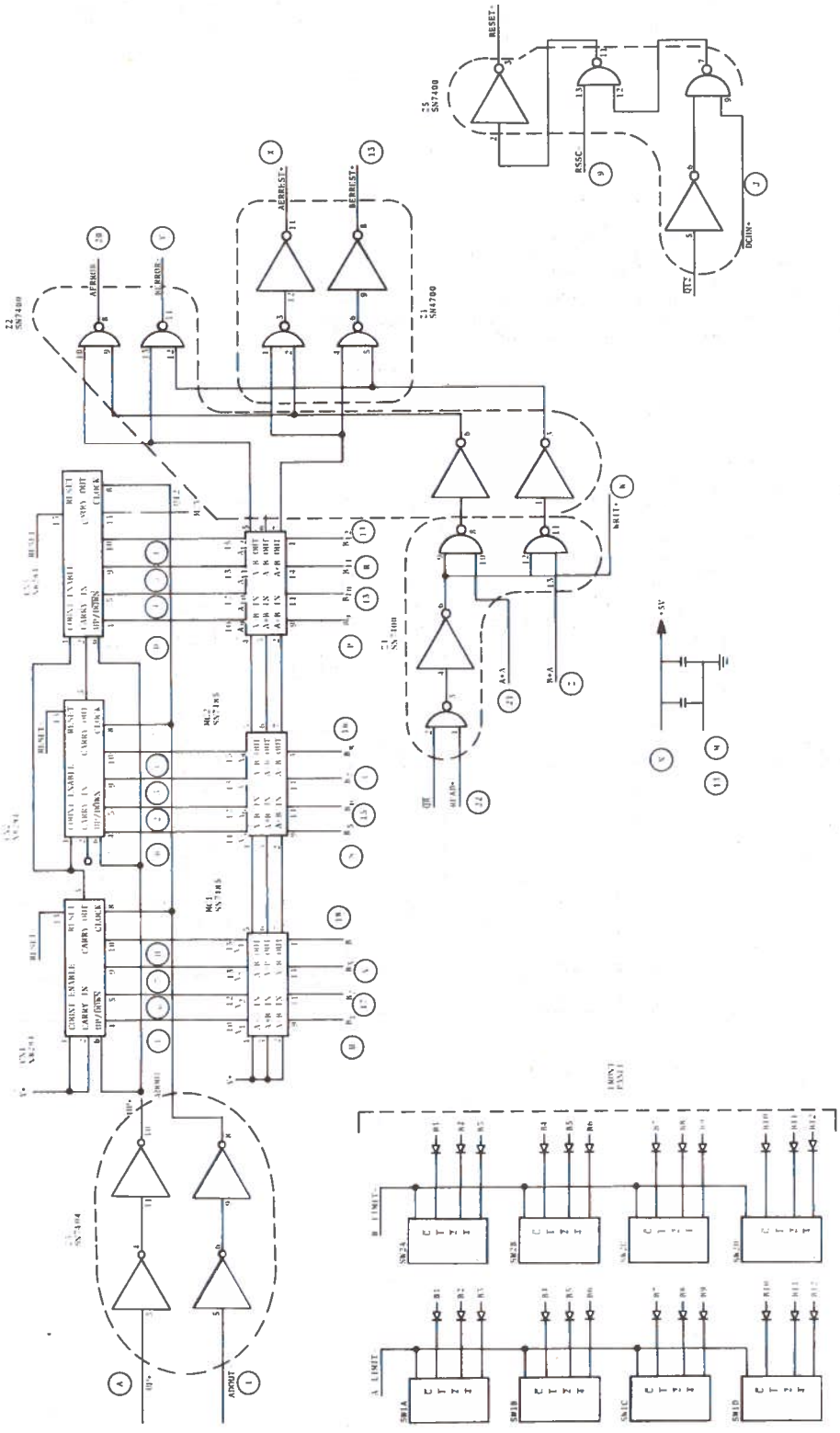

Figure B-29. Diagram, OMSA Main Digital Processing Circuit

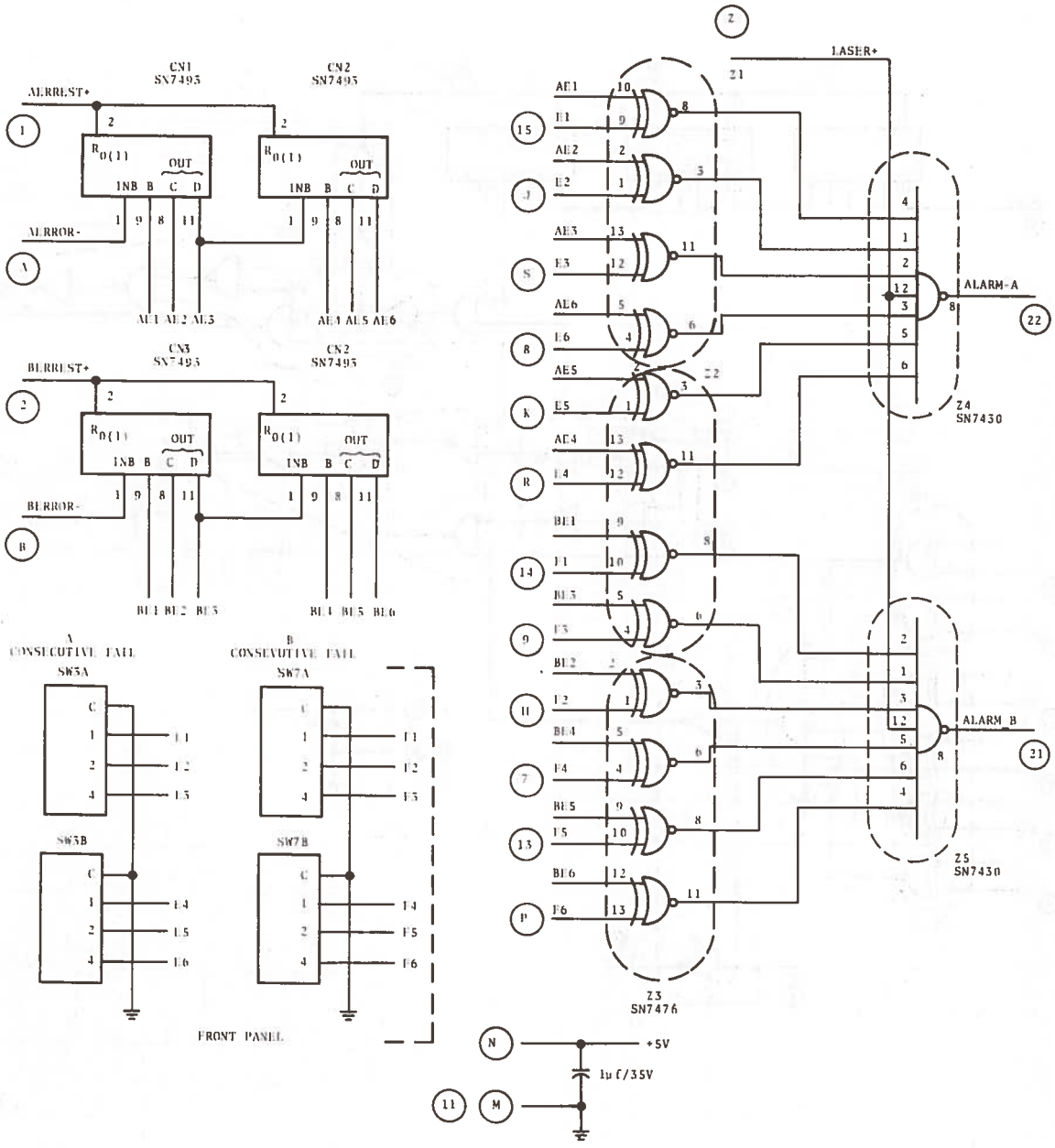

Figure B-30. Diagram, OMSA Alarm Trigger Circuit

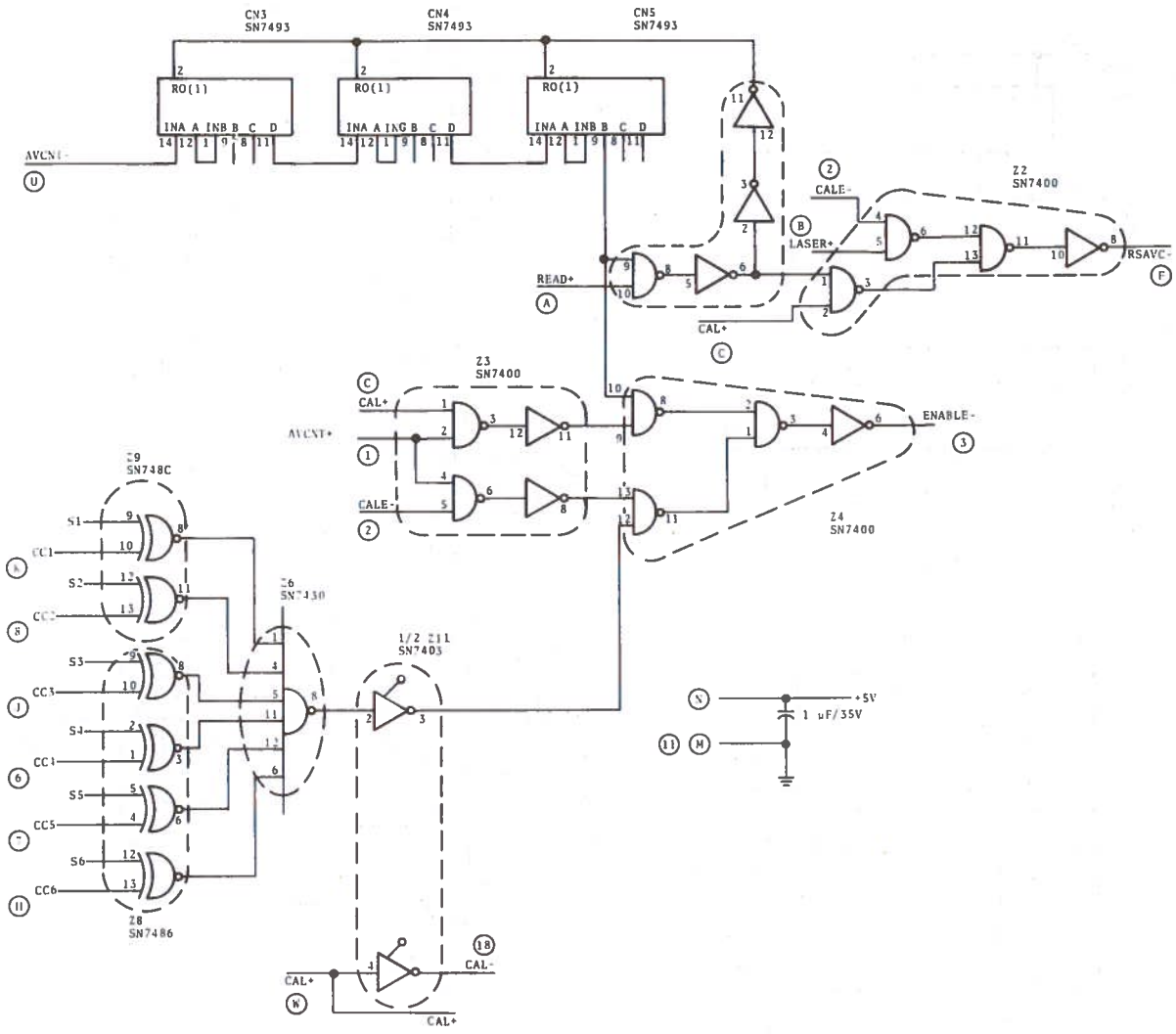

Figure B-31. Diagram, OMSA Channel Selection Circuit #1

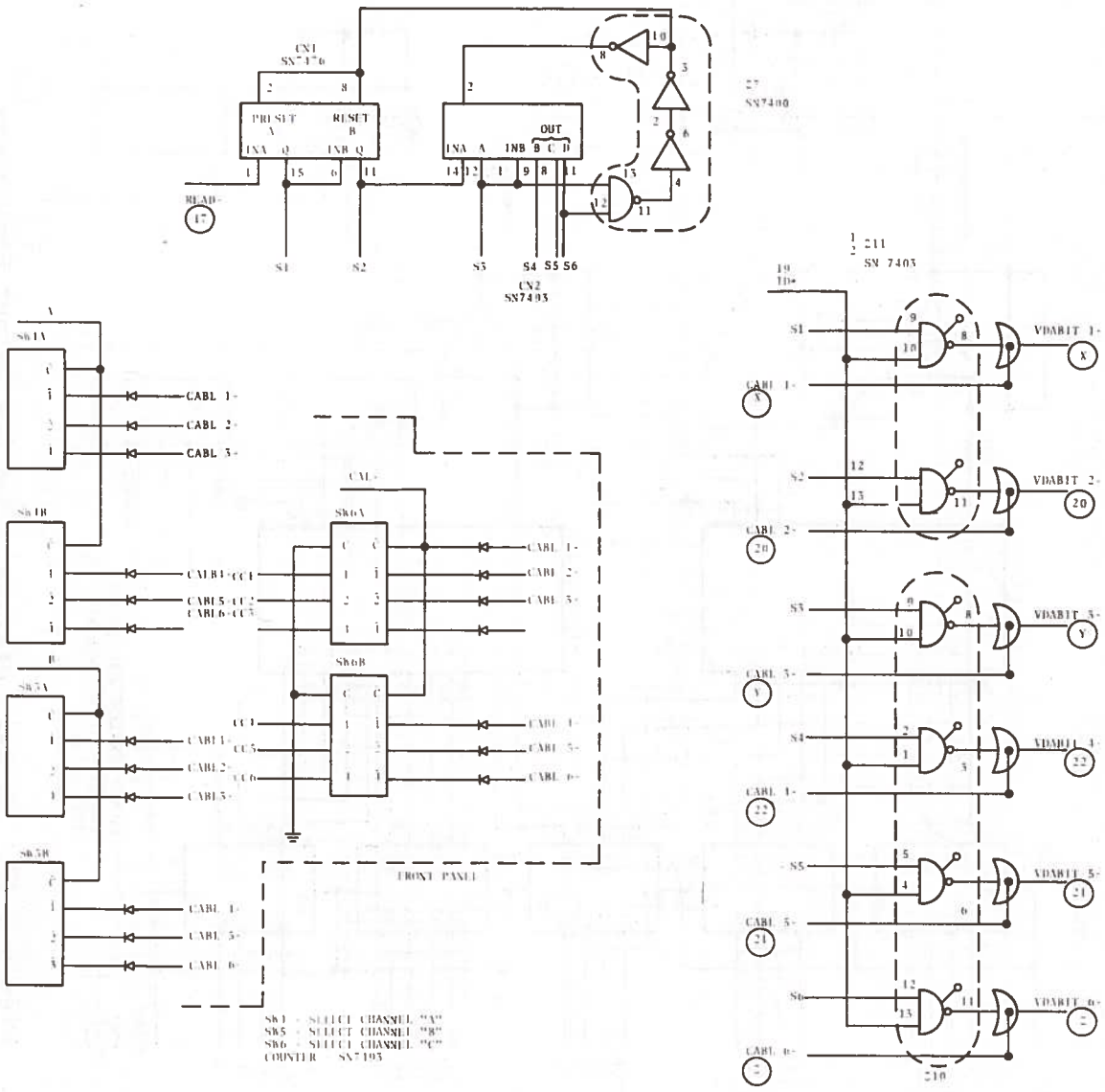

Figure B-32. Diagram, OMSA Channel Selector Circuit #2

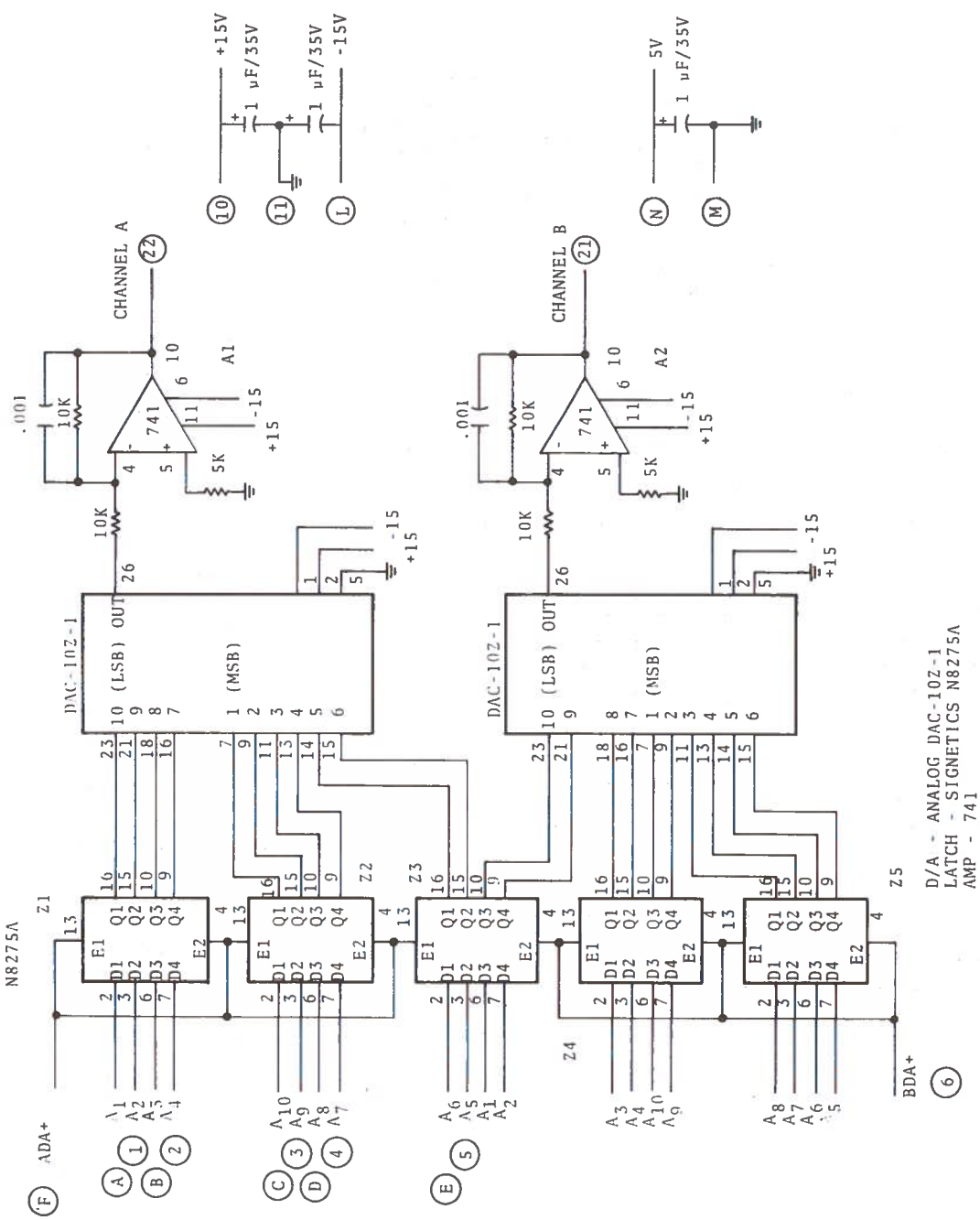

Figure B-33. Circuit Diagram, OMSA D/A Output Converters

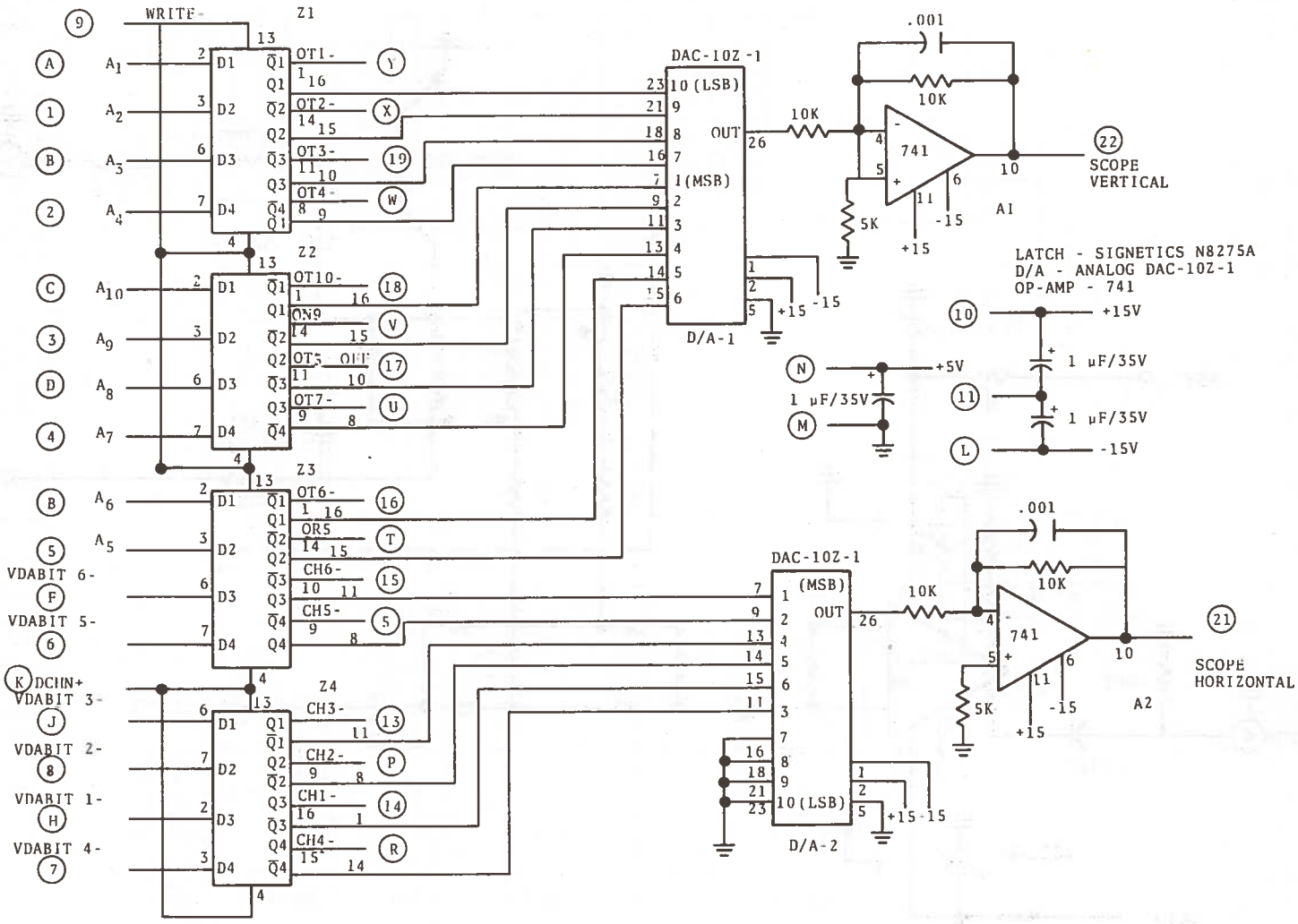

Figure B-34. Circuit Diagram, #2 OMSA D/A Output Converters

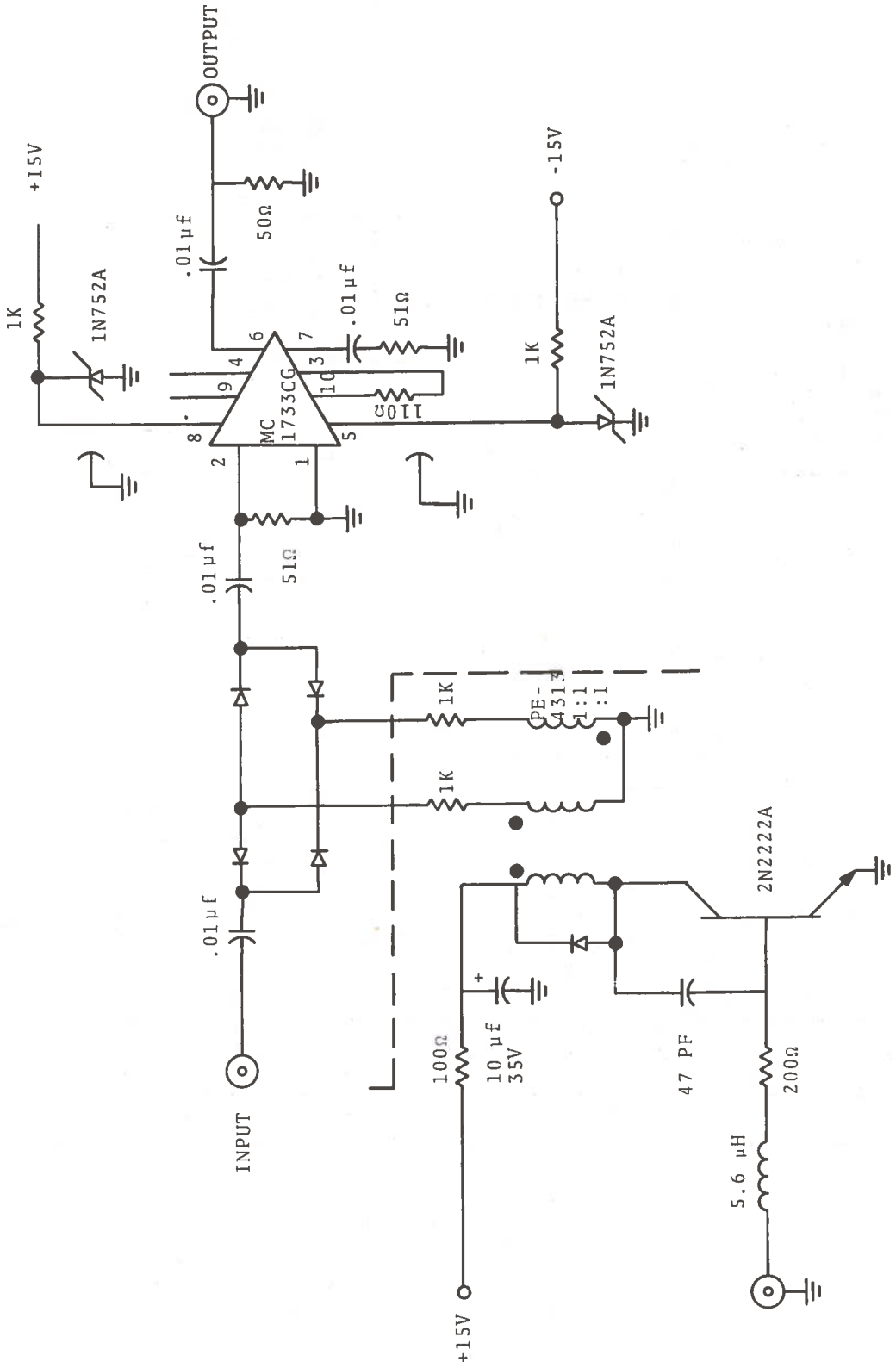

Figure B-35. Range Gate Circuit Diagram

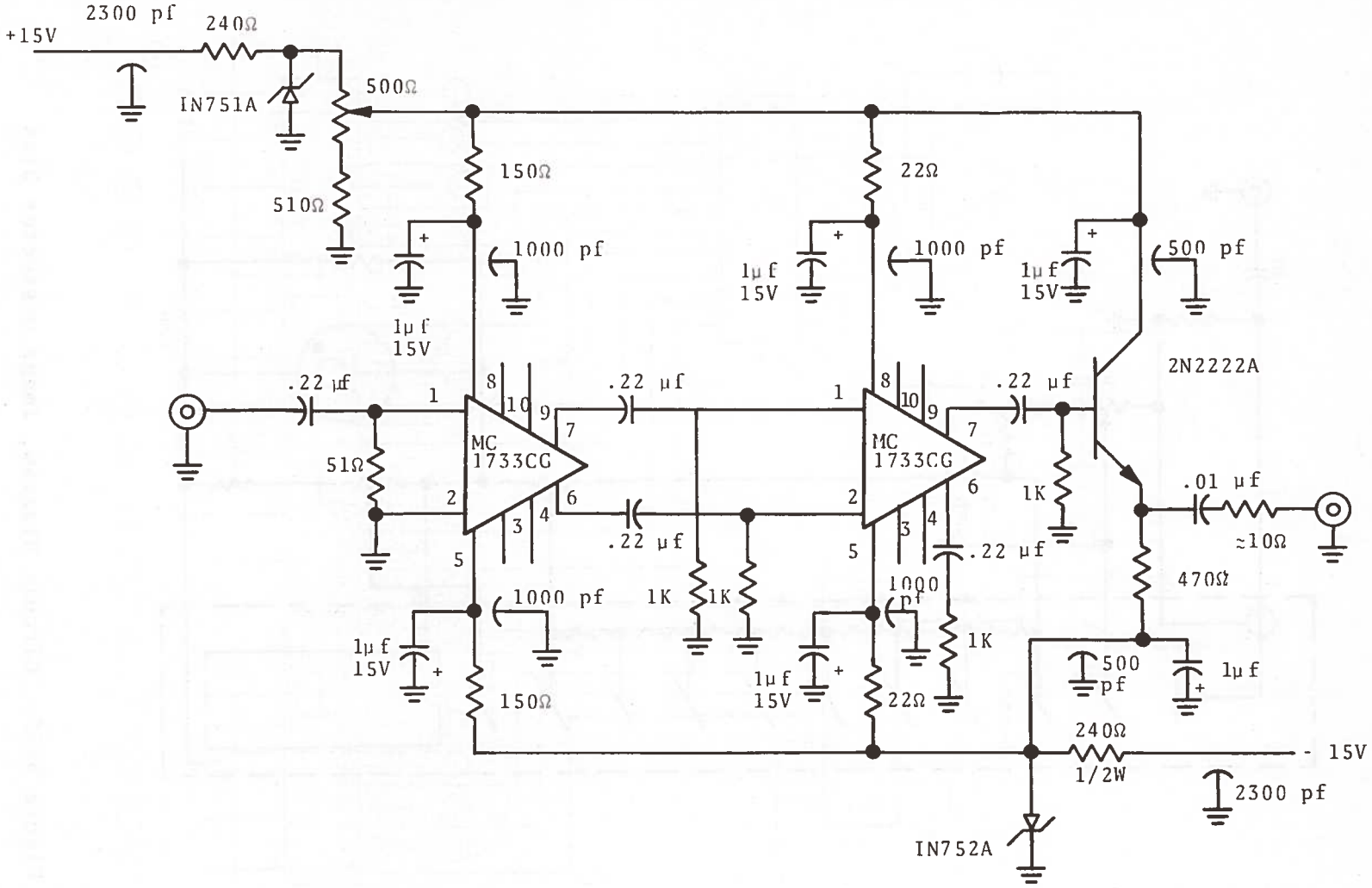

Figure B-36. Circuit Diagram, Video Preamplifier

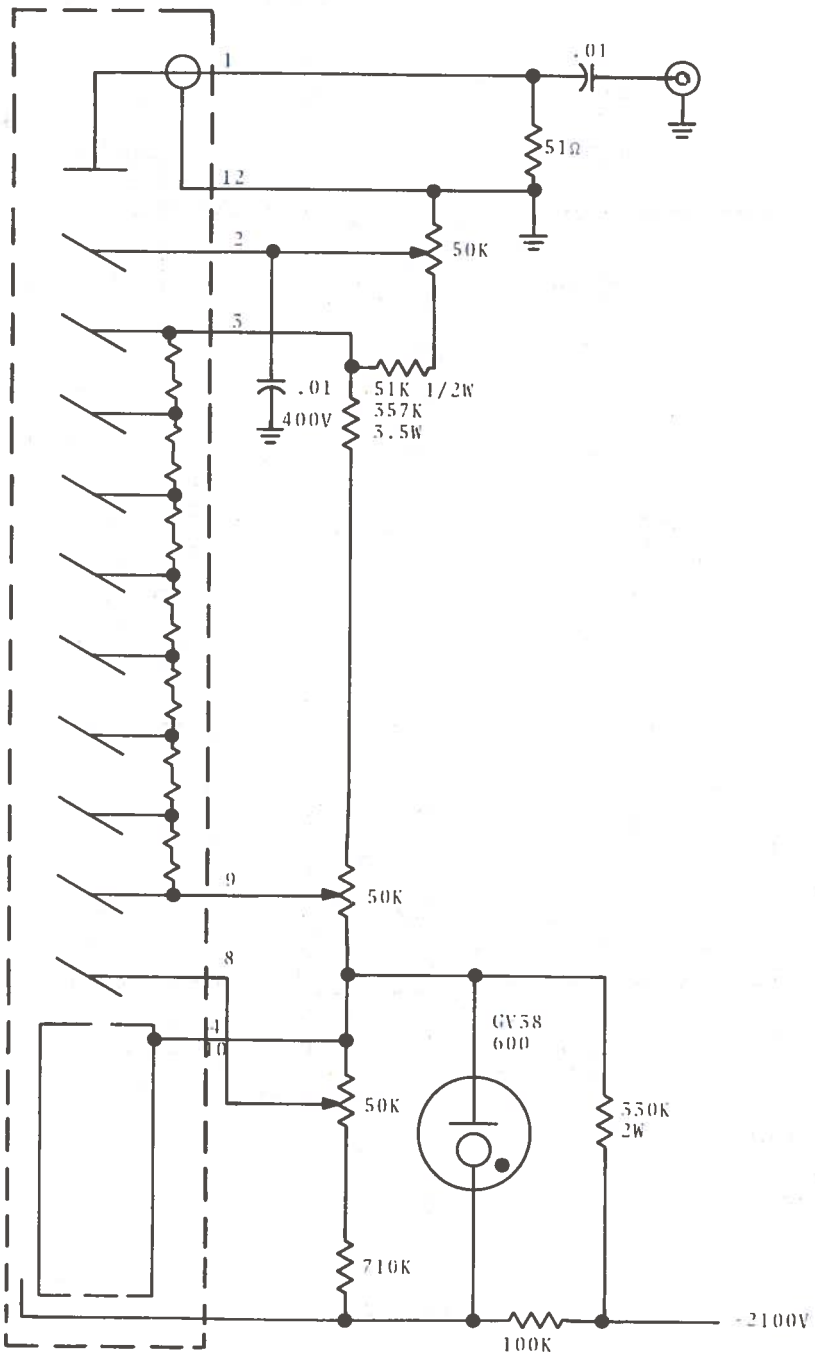

Figure B-37. Circuit Diagram, Image Dissecter Bias